



HAL
open science

Contribution to adaptative sliding mode, fault tolerant control and control allocation of wind turbine system

Xinyi Liu

► **To cite this version:**

Xinyi Liu. Contribution to adaptative sliding mode, fault tolerant control and control allocation of wind turbine system. Electric power. Université de Technologie de Belfort-Montbéliard, 2016. English. NNT : 2016BELF0295 . tel-01872262

HAL Id: tel-01872262

<https://theses.hal.science/tel-01872262>

Submitted on 11 Sep 2018

HAL is a multi-disciplinary open access archive for the deposit and dissemination of scientific research documents, whether they are published or not. The documents may come from teaching and research institutions in France or abroad, or from public or private research centers.

L'archive ouverte pluridisciplinaire **HAL**, est destinée au dépôt et à la diffusion de documents scientifiques de niveau recherche, publiés ou non, émanant des établissements d'enseignement et de recherche français ou étrangers, des laboratoires publics ou privés.

SPIM

Thèse de Doctorat



école doctorale sciences pour l'ingénieur et microtechniques
UNIVERSITÉ DE TECHNOLOGIE BELFORT-MONTBÉLIARD

Contribution to adaptive sliding mode, fault tolerant control and control allocation of wind turbine system



Xinyi LIU

SPIM

Thèse de Doctorat



école doctorale sciences pour l'ingénieur et microtechniques
UNIVERSITÉ DE TECHNOLOGIE BELFORT-MONTBÉLIARD

N° x x x

THÈSE présentée par

Xinyi LIU

pour obtenir le

Grade de Docteur de

l'Université de Technologie de Belfort-Montbéliard

Spécialité : **Automatique**

Contribution to adaptive sliding mode, fault tolerant control and control allocation of wind turbine system

Soutenue le 25 NOV 2016 devant le Jury :

Mohamed DJEMAI	Rapporteur	Professeur à l'Université Valenciennes et Hainaut-Cambrésis
Tarek AHMED-ALI	Rapporteur	Professeur à CNRS/l'Université Caen Basse-Normandie et ENSICAEN
Patrice WIRA	Examineur	Professeur à l'Université de Haute Alsace
Yacine CHITOUR	Examineur	Professeur à l'Université de Paris-Sud 11
Mickael HILAIRET	Examineur	Professeur à l'Université de Franche-Comté
Salah LAGHROUCHE	Directeur de thèse	Maître de Conférences (HDR) à l'Université de Technologie de Belfort-Montbéliard
Maxime WACK	Co-Directeur	Maître de Conférences (HDR) à l'Université de Technologie de Belfort-Montbéliard
Mohamed HARMOUCHE	Co-Directeur	Docteur ingénieur chez la société Actility

List of Publications

Peer-reviewed journal papers

1. Xinyi Liu*, M. Harmouche, S. Laghrouche, M. Wack, *A novel first order sliding mode algorithm for a wind turbine system*, International Journal of Emerging Electric Power Systems (IJEEPS), 2016, Accepted
2. R. Galvan-Guerra, Xinyi Liu*, S. Laghrouche, L. Fridman, M. Wack, *Fault Tolerant Control with Control Allocation for Linear Time Varying Systems: An Output Integral Sliding Mode Approach*, IET Control Theory & Applications, 2016, Accepted
3. Y. Zheng, J. Liu*, Xinyi Liu, D. Fang, L. Wu, *Adaptive Second-Order Sliding Mode Control Design for a Class of Nonlinear Systems with Unknown Input*, Mathematical Problems in Engineering, pp 1-7, (1), 2015, DOI: 10.1155/2015/319495
4. Xinyi Liu*, M. Harmouche, S. Laghrouche, M. Wack, *New adaptive first order sliding mode algorithm and its application for a wind energy conversion system*, IET Energy Conversion and Management, 2016, Under review
5. Xinyi Liu*, M. Harmouche, S. Laghrouche, M. Wack, *An adaptive HOSM controller for uncertain system and its application*, Energy Conversion and Management, 2016, Under review

Peer-reviewed international conference papers

1. Xinyi Liu*, M. Harmouche, S. Laghrouche, M. Wack, *A novel adaptive sliding mode controller for a wind energy conversion system with doubly fed induction machine*, The 4th International conference on renewable energy: generation and applications (ICREGA), Belfort, France, 2016

2. Xinyi Liu*, S. Laghrouche, M. Harmouche, R. Fellag, M. Wack, *Super twisting sliding mode MPPT control of an IM based wind energy conversion system*, 4th IEEE International Conference on Electrical Engineering (ICEE), Boumerdes, Algeria, 2015
3. Xinyi Liu*, S. Laghrouche, M. Wack, *MPPT control of variable speed wind generators with squirrel cage induction machines*, 4th Conference: Environmental Friendly Energies and Applications (EFEA), Paris, France, 2014

Acknowledgment

I would like to give my sincere gratitude to my supervisors Prof. Maxime Wack, Prof. Salah Laghrouche and Dr. Mohamed Harmouche, for the continuous support of my Ph.D study and research in Lab OPERA. Their patience, motivation, and immense knowledge, and their inspiring guidance during my thesis deserve the most appreciation and respect in my heart. Thanks for Prof. Leonid Fridman and Prof. Maurizio Cirrincione. It is really a great experience working with them. With their abundant research experience, they show me how to become an independent researcher.

I would further like to give my gratitude to the financial support from the program of China Scholarships Council (CSC). I would like also to thank to Université de Technologie de Belfort-Montbéliard (UTBM) so that I could do my thesis in such comfortable and inspiring environment.

Finally, I wish to take this opportunity to express my appreciation and thanks to all my friends for their emotional supports and research help. Especially, they are Biao Yin, Jiawei Zhu, Jianxing Liu, Binying Ye, Dongdong Zhao, Rosalba Galván-Guerra, Chariete Abderrahim, and Chen Zheng. I really cherish and engrave the friendship and all the beautiful memories with them. I would also like to express special thanks to my parents who provide me eternal love and supports. They encourage me to explore knowledge and teach me to be a person with responsibility. With all the love and faith, tomorrow is going to be better.

Contents

List of Publications	i
Acknowledgment	iii
Contents	iv
List of Figures	ix
General Introduction	1
0.1 Motivations	4
0.2 Contribution of the Thesis	7
0.3 Outline of the Thesis	8
1 Adaptive High Order Sliding Mode Control Design	11
1.1 State-of-the-art	12
1.2 Sliding Mode Control	13
1.2.1 Design of sliding Manifold	14
1.2.2 Control Design	15
1.3 Output Feedback Sliding Mode Control	17
1.3.1 Second Order Sliding Mode Definitions	18
1.3.2 Second Order Sliding Mode Dynamics	20
1.3.2.1 Relative Degree 1	20
1.3.2.2 Relative Degree 2	21
1.3.3 Second Order Sliding Mode Controllers	22
1.3.3.1 Super-Twisting Control Algorithm	23

1.3.3.2	Twisting Control Algorithm	23
1.3.3.3	Sub-Optimal Control Algorithm	25
1.4	High Order Sliding Mode Control	26
1.5	Adaptive Sliding Mode Control	28
1.5.1	Adaptive Twisting Algorithm	29
1.5.2	Adaptive first order algorithm of Plestan [1]	29
1.5.3	Adaptive Integral High Order Algorithm [2]	31
1.6	Conclusion	32
2	Modeling of Wind Energy Conversion System	33
2.1	System Configuration and Topology	33
2.2	WECS Modeling	35
2.2.1	Aerodynamics System Modeling	37
2.2.2	Transmission System Modeling	37
2.2.3	Doubly Fed Induction Generator Modeling	39
2.2.4	Space Vector Technique	41
2.2.5	Dynamic reduced order model of WECS	45
2.3	State of Arts of Control System	46
2.4	Conclusion	48
3	First order ASMC for Uncertain System and Application on WECS	51
3.1	Introduction	52
3.2	Theoretical study	54
3.2.1	Problem formulation	54
3.2.2	Idea behind the proposed controller	54
3.2.3	Main result	55
3.2.4	Discussion and comparison	57
3.2.5	Control objective	57
3.2.6	Adaptive sliding mode controller application	58
3.3	Simulation results	60
3.4	Conclusion	64
4	Adaptive HOSM Control for Uncertain System and Application on WECS	67
4.1	Introduction	67

4.2	Problem Formulation and Control Objective	68
4.3	Control design	70
4.3.1	First order controller	70
4.3.2	Stabilization of the $(r - 1)$ -th integral chain	74
4.3.3	Main Controller	76
4.3.4	Academic Example	77
4.4	Adaptive HOSM controller for WECS	80
4.4.1	System Configuration	80
4.4.2	Model of WECS	81
4.4.2.1	Aerodynamics	81
4.4.2.2	Gearbox and Shaft	82
4.4.2.3	Double Fed Induction Generator	82
4.4.2.4	Reduced Order Model	83
4.4.3	Control Objective and Controller Design	83
4.4.4	Simulation Results	85
4.5	Conclusion	91
5	Fault Tolerant Control with On-line Allocation for Linear Time Vary-	
	ing Systems	93
5.1	Introduction	94
5.2	Problem Formulation	95
5.2.1	Nominal System	97
5.3	Output Integral Sliding Mode Controller	97
5.4	States Reconstruction	99
5.5	Discussion: $u(t)$ reconstruction	101
5.5.1	Academic Example	103
5.6	FTC with on-line allocation of Wind Energy Conversion System	107
5.6.1	LPV Model of the Wind turbine system	108
5.6.2	Control Objective	110
5.6.3	Simulation Results	111
5.7	Conclusion	115
	Conclusion and Perspectives	119
	Appendices	123

Bibliography

125

List of Figures

Figure 0.1. Electrical energy conversion system	4
Figure 0.2. The power curve of WECS versus wind speed	5
Figure 1.1. Second order sliding mode trajectory	19
Figure 1.2. Super-twisting algorithm phase trajectory	24
Figure 1.3. Twisting algorithm phase trajectory	25
Figure 1.4. Sub-optimal algorithm phase trajectory	26
Figure 2.1. The configuration of variable speed wind energy conversion system .	34
Figure 2.2. Block scheme of a variable speed wind turbine model	36
Figure 2.3. Power coefficient C_p versus different wind speed	38
Figure 2.4. Turbine torque τ_t versus different wind speed and the maximum power point line	38
Figure 2.5. Ideal three-phase windings (stator and rotor) of the DFIG	39
Figure 2.6. DFIG electric equivalent circuit	40
Figure 2.7. Mechanical axis of the DFIG	41
Figure 2.8. WECS transformation to dq reference frame.	43
Figure 2.9. dq Model of the DFIM in synchronous coordinates.	44
Figure 2.10. PI based FOC Scheme	47
Figure 2.11. Wind energy conversion system	48
Figure 3.1. Behavior of adaptive gain K	56
Figure 3.2. Controller u and sliding variable s	56
Figure 3.3. Power coefficient versus tip-speed ratio in different pitch angle . . .	58
Figure 3.4. Control system block diagram	59

Figure 3.5. Controlled direct-axis current i_{rd}	60
Figure 3.6. Controlled quadrature-axis current i_{rq} of the rotor	61
Figure 3.7. Controlled mechanic rotation speed w_{mr}	61
Figure 3.8. Direct-axis controller u_{rd}	62
Figure 3.9. Quadrature-axis controller u_{rq}	62
Figure 3.10. Adaptive gain K_d of direct-axis controller u_{rd}	63
Figure 3.11. Adaptive gain K_q of quadrature-axis controller u_{rq}	63
Figure 3.12. Sliding variable s_d in case of the proposed algorithm	64
Figure 3.13. Sliding variable s_q in case of the proposed algorithm	64
Figure 3.14. Sliding variable s_d in case of Plestan et al. [1] algorithm	65
Figure 3.15. Sliding variable s_q in case of Plestan et al. [1] algorithm	65
Figure 4.1. Function $sat_\mu(s)$	70
Figure 4.2. Function $\frac{k_3}{1 - \frac{ s }{\epsilon}}$	71
Figure 4.3. Adaptive gain K	78
Figure 4.4. Controller u	78
Figure 4.5. Sliding variable s	79
Figure 4.6. States z_1 and z_2	79
Figure 4.7. System configuration	81
Figure 4.8. The controller U_d and U_q	85
Figure 4.9. The adaptive gain of U_d and U_q	86
Figure 4.10. The controller u_d and u_q	87
Figure 4.11. Sliding variable s_d and s_q	87
Figure 4.12. Integral chains of direct axis z_{d1} and z_{d2}	88
Figure 4.13. Integral chains of quadrature axis z_{q1} and z_{q2}	88
Figure 4.14. Rotor voltages u_{rd} and u_{rq}	89
Figure 4.15. Rotor currents i_{rd} and i_{rq} and rotor speed ω_r	89
Figure 4.16. Tracking performance of Q	90
Figure 4.17. Tracking performance of T	90
Figure 5.1. Nominal Behaviour of the Academic System	104
Figure 5.2. Additive Faults Reconstruction using a pseudoinverse methodology for the identified perturbation $v_{I,ap}(t)$	105

Figure 5.3.	Behaviour of the Academic System subject to additive faults in the absence of a fault tolerant control scheme: Nominal Behavior (red line), Faulty System (blue line)	105
Figure 5.4.	Behaviour of the Academic System subject to additive faults. OISM fault tolerant control scheme assuming the K value is completely reconstructed since the initial time: Nominal Behavior (red line), Faulty System (blue line)	106
Figure 5.5.	Behaviour of the Academic System subject to additive faults. OISM fault tolerant control scheme, K reconstructed with a pseudoinverse methodology: Nominal Behavior (red line), Faulty System (blue line)	107
Figure 5.6.	The configuration of the wind generation system	108
Figure 5.7.	The power coefficient C_p versus generator speed ω_r under different wind speed V	110
Figure 5.8.	The tracking performance of nominal PI controller without perturbation. The red dash lines are the reference values, and the blue solid lines are the real signals of speed and d/q currents.	112
Figure 5.9.	The faults in the actuators	112
Figure 5.10.	The tracking performance of nominal PI controller with perturbation. The red dash lines are the reference values, and the blue solid lines are the real signals of speed and d/q currents.	113
Figure 5.11.	The tracking performance of proposed controller with perturbation. The red dash lines are the reference values, and the blue solid lines are the real signals of speed and d/q currents.	113
Figure 5.12.	The observer performance of proposed structure. The red dash line are the real states, the blue solid line are the observed states	114
Figure 5.13.	The reconstructed perturbation ϕ_1 and ϕ_2	115
Figure 5.14.	The reconstructed faults K	116
Figure 5.15.	The reconstructed perturbation ϕ_1 and ϕ_2	116
Figure 5.16.	The tracking performance of proposed controller with reconstructed faults. The red dash lines are the reference values, and the blue solid lines are the real signals of speed and d/q currents.	117

General Introduction

Energy and sustainability are two major problems the world faces today. Renewable energy has been regarded as a promising means to solve these problems while smart grid is developed to improve energy efficiency, reliable and robust. The growth of distributed energy resources along with sustainable development, environmental issues are imposing new control challenges. Wind energy is an environment friendly, renewable and economical energy resource which has been regarded as an overwhelming competitor in the distributed generation.

The wind is a free, clean and renewable energy source on our planet. It has served mankind for centuries to pump water, grind grain, and move ships. Wind has been utilized as a source of power for thousands of years for such task as propelling sailing ships, grinding grain, pumping water, and powering factory machinery. In the United States the first wind electric systems were built in the late 1890s. By the 30s and 40s of last century, plenty of small-capacity, wind electric systems were in used in rural areas not served by the power grid. Since the oil shocks of the 70s of last century, which heightened awareness of our energy problems, the demand for renewable energy has been increasing rapidly during recent decades [3]. Within a decade or so, dozens of manufacturers installed thousands of new wind turbines. With the discovery of electricity and development of electric power, wind energy found new applications in human society in the form of providing clean and inexhaustible electric power in a wide range of scales and capacities. Nowadays, wind powered generation operates at variety of sizes between small residential and utility scales. Modern utility-scale wind power is the fastest growing energy sector in the world. It is becoming an important part in the national energy mix for many countries. The US continued to see growth and remains on top in total installed capacity followed by China and

Germany. Wind power is capable of becoming a major contributor to world's electricity supply over the next three decades, according to a report by the U.S Department of Energy.

It is well known that a wind turbine's efficiency is highly dependent on the operating conditions, such as wind speed, pitch angle and tip-speed ratio. In the aim to assure optimal operating conditions as well as to maximize the active power, parameter identification, diagnostics and feedback control are going to play an important role. The wind system is hard to obtain out, and the parametric varying be considered as uncertain system. Reliable measurements from the system are necessary to implement these designs. However it is not always possible to use sensors for measurements. Especially, in the conditions of gust inside the normal wind. Furthermore, available commercially sensors are too big and costly. Therefore, we have two kind of method to solve the uncertain bound problem. The first adaptive controller is a promising way to solve the uncertain bound problem. And state observer designs serve as a replacement for physical sensors, for obtaining the unavailable quantities and making feedback control implementable, are of great interest.

Sliding mode technique is known for its insensitivity to external disturbances, high accuracy and finite time convergence. Sliding mode observers have been widely used for fault reconstruction in the past two decades. Edwards *et al.* [4] proposed a fault reconstruction approach based on equivalent output error injection. In this method, the resulting residual signal can approximate the actuator fault to any required accuracy. Based on the work of [4], Tan *et al.* [5] proposed a sensor fault reconstruction method for well-modeled linear systems through the Linear Matrix Inequality (LMI) technique. This approach is of less practical interest, as there is no explicit consideration of disturbance or uncertainty. To overcome this, the same authors [6] proposed a FDI scheme for a class of linear systems with uncertainty, using LMI for minimizing the L_2 gain between the uncertainty and the fault reconstruction signal. Linear uncertain system models can cover a small class of nonlinear systems by representing nonlinear parts as unknown inputs. However, they will introduce too many unknown inputs which will make perfect or approximate decoupling difficult. Therefore, the study of nonlinear observer-based FDI has received considerable attention in the past few years. Jiang *et al.* [7] proposed a sliding mode observer based fault estimation approach for a class of nonlinear systems with uncertainties. Yan *et al.* [8] proposed a precise fault reconstruction scheme, based on equivalent output error injection, for a class of nonlinear systems with uncertainty. A sufficient condition based on LMI is

presented for the existence and stability of a robust sliding mode observers. The limitation is that requires a strong structural condition of the distribution associated with uncertainties. Later, this structural constraint was relaxed by the same authors [9], where the fault distribution vector and the structure matrix of the uncertainty are allowed to be functions of the system's output and input. However, all these works require that the bounds of the uncertainties and/or faults are *known*. Although in the work of [9], the requirement on the bound of uncertainty is removed, but it still needs to know the bound of the fault signal.

The idea of using a dynamical system to generate estimates of the system states was proposed by Luenberger in 1964 for linear systems [10]. In spite of the extensive development of robust control techniques, Sliding Mode Control (SMC) remains an efficiency solution for handling bounded uncertainties/disturbances and unmodeled dynamics in both control and estimation problems. From the practical point of view, a wind energy conversion system is a nonlinear dynamic plant, with multiple inputs, multiple outputs, variables strongly coupled, model uncertainty and external disturbances. Sliding mode techniques [11] known for its insensitivity to parametric uncertainty and external disturbance, are intensively studied and developed for control, estimation, Fault Tolerant Control (FTC) and Fault Diagnosis and Isolation (FDI) problems, existing in the wind power system. In particular, Higher Order Sliding Mode (HOSM) approaches are considered as a successful technique due to the following advantages [12]:

- Robustness with respect to parametric uncertainties;
- Possible to generate continuous output injection signals;
- Remove the conventional relative degree restrictions;
- Possible to offer 'chattering' attenuation.

The research filed of this thesis is 'Adaptive HOSM Design, Fault Tolerant Control and its Application to Wind Turbine Systems and Power Converters'. In general, this topic is of great importance and interest in industry and engineering, mainly for its economic and reliability reasons.

0.1 Motivations

Motivated by a large amount of important practical problems, in particular, wind power generation systems which have received great attention in the context of energy and pollution crises. Wind Energy Conversion System (WECS) with Induction Machine (IM), known as a high specific energy source is one of the most promising alternative energy sources due to high energy efficiency, low cost, ease of installation and environment friendly. Induction Machine is suitable for a wide variety of applications, from stationary power generations to electric automotive devices. Fig. 0.1 shows a typical system configuration

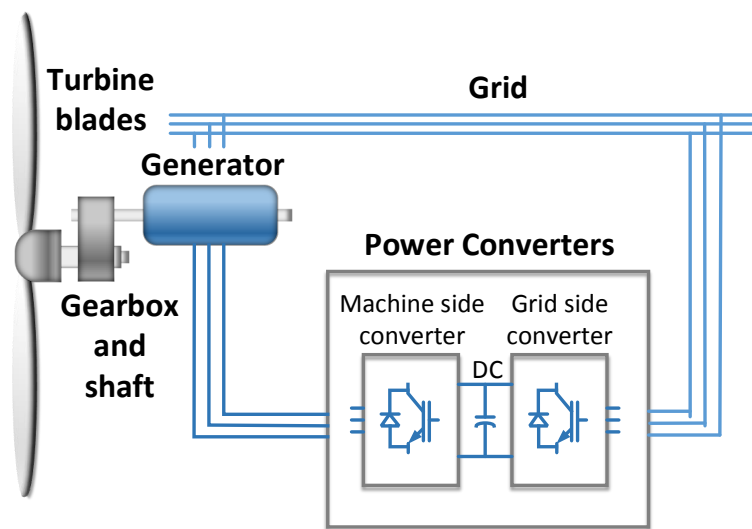


Figure 0.1. *Electrical energy conversion system*

which is general in industry. It consists of numerous interconnected components, i.e. wind turbine (horizon three blades mechanical device), an induction machine, we use doubly-fed induction generator (DFIG) here, a back-to-back converters (including a three-phase AC/DC rectifier, a three-phase DC/AC inverter, connected by a DC bus). The wind turbine is a mechanical device which can absorb kinetic energy from the wind, it is a high nonlinear and complex decoupled system. The gearbox and shaft increase the rotation speed given by the turbine, to adjust the rotation speed suitable for the generator. The DFIG can convert the energy from mechanical form into electrical form. The stator of DFIG is connected to the power grid directly and the rotor is connected to the power converters. The power converters are key components which deliver the power produced by energy sources, i.e. source grid, wind turbine generator. Fig. 0.1 shows a power electronics

topology of the wind energy conversion system which is a general configuration in industry.

Generally, there are four typical working regions which need different control policies according to various wind speed. The operation of a wind generator presents four typical working regions differentiated by upward wind speed, as shown in Fig. 0.2:

- Region I: below cut-in speed
- Region II: maximum generable power
- Region III: constant rated power
- Region IV: above cut-off speed

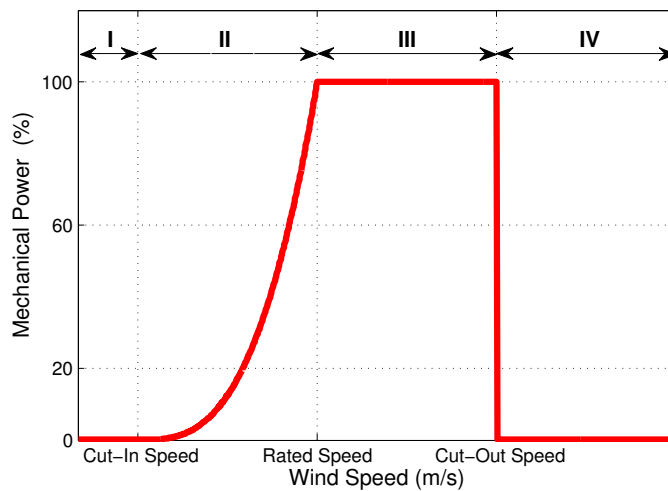


Figure 0.2. *The power curve of WECS versus wind speed*

The power characteristics of a wind turbine are defined by the power curve, which relates the mechanical power of the turbine to the wind speed. The power curve is a wind turbine's certificate of performance that is guaranteed by the manufacturer. The International Energy Association (IEA) has developed recommendations for the definition of the power curve. The recommendations have been continuously improved and adopted by the International Electrotechnical Commission (IEC). The standard, IEC61400-12, is widely accepted as a basis for defining and measuring the power curve.

The typical working regions are shown by power curve versus different wind speed in Fig. 0.2. As the wind speed grows up, the wind turbine (WT) shuts down and the system generates no power at beginning where it is called zero power region. When the wind speed reaches the cut-in speed and below the rated wind speed, the wind turbine works in the maximum power point tracking (MPPT) region. In this region, the speed of wind turbine is controlled by kinds of MPPT controllers to make sure that the wind turbine is operated at the optimal tip-speed ratio [13]. The tip-speed ratio (TSR) is defined by the wind turbine tip speed in proportion to the wind speed, and it plays a vital role in extracting the kinetic energy from wind to turbine shaft [14]. For all the wind turbines around the world, this is a common issue which also makes great challenge during the process of wind energy extracting process. On one hand, if the rotor of wind turbine rotates too slowly, most of the wind passes through the space between two blades without doing any work; on the other hand, if the rotor of wind turbine rotates too quickly, the area swept by the rotor will become impassable for the wind like a solid panel. Hence, there is an optimal tip-speed ratio for a certain wind turbine to get the maximum power. The third region is the constant power region, where the power is dynamically equal to the rated power as a result of varieties of mechanism control, like pitch control, stall control, or yaw control. In this region, the wind system is working in the rated condition. The last region is the cut-off region, where the wind speed is above the cut-off speed. The harmful wind is too strong to drive the wind system generating electricity, but to cause the electrical overloading and mechanical damage. The turbine shuts down in this region to protect for stranger winds. Most MPPT controllers require measuring wind speed [15][16] and wind turbine speed data in real-time. Therefore, time delay in measuring process would affect the control precision, which is an overshooting caused by delay. In practice, the anemometer is usually installed as a wind speed detector making the wind turbine operate at the optimal speed. Whereas, using anemometer would reduce the system's dynamic response and would also increase the costs of the equipment and maintenance. Moreover, since the turbine works in a three-dimension space, it makes the wind speed has a different distribution in the turbine rotating plane. Consequently, the effective wind speed (EWS) cannot be measured directly. So there is a need to design a sensor-less control system for wind system. However, previous EWS estimation works do not consist of the whole wind generator system [3][17]. In this thesis, we propose a method that the EWS estimation has been applied in the controller which cooperates with the wind turbine, the generator, and the converters.

This thesis builds a whole wind system with a MPPT controller based on adaptive sliding mode control. To get maximum power, only a variable speed wind turbine can be applied to this MPPT controller. We propose a method to estimate the optimal tip speed ratio. It is based on power balance equations which describes the relationship between the turbine torque and turbine speed versus the wind speed of the turbine rotor. Additionally, for safety reasons many systems require a fault tolerant control (FTC) for different types of faults. The faults in the actuators are very important since they may cause the control target is not reached or even worst a complete lost of stability. Normally, redundancy in actuators is used, but this requires the design of several control algorithms and a switching strategy in order to assure the correct controller is activated (see [18, 19, 20] and the reference therein for more information about fault tolerant control schemes). A FTC with a fixed control allocation (CA) using output integral sliding mode (OISM) is going to be proposed.

0.2 Contribution of the Thesis

In this thesis, we concentrate on the adaptive control and observation problems in the wind energy generation subsystem and power converters. First part, a novel Adaptive first order Sliding Mode (ASM) controller is developed for uncertain system. Second part, a High Order Sliding Mode (HOSM) controller is developed for uncertain system. Third part, Output Integral Sliding Mode (OISM) control and observer design for Linear Parameter Varying (LPV) system are addressed.

An adaptive controller are proposed for nonlinear system, and has been applied for the Wind Energy Conversion System (WECS) in order to Track the Maximum Power Point (MPPT) under the unknown of the WECS, with inside parameter varying and outside disturbance. Lyapunov-based adaptive first and high order sliding mode is developed to converge the sliding variables to a predefined region, which eliminate the chattering. The performance of the above two adaptive controllers are evaluated by comparison with other adaptation algorithm applied in a real time wind emulation system. The robustness against measurement noise and parameter variations is also validated simutanously.

An OISM is designed from available voltage inputs and supply manifold currents mea-

surements. The state estimation, parameter identification are performed simultaneously. The system states, i.e. direct and quadrature flux of the rotor are estimated successfully. This eliminates the need of an expensive flux sensor. The fault in actuators are considered in this study. It is reconstructed faithfully through analyzing the information, which is obtained on-line from comparisons between the measurements from the sensor installed in the real system and the outputs of the observer system.

The main contributions achieved in this thesis are:

- Lyapunov analysis demonstrates that the proposed adaptive-gain first order sliding mode algorithm establishes 'real' sliding mode without *a priori* knowledge of the upper bound of the fault signal, meanwhile, the gains of the proposed algorithm allow decreasing once the error converges to a predefined neighborhood exactly;
- The proposed adaptive-gain HOSM control algorithm are proved theoretically and the robustness of the proposed algorithm against parametric variation and measurement noise have also been validated;
- The proposed FTC strategy assures, by using only output information, theoretical exact compensation of the faults effects in the critical input channels (matched effects) and the minimization in the non-critical (unmatched) ones just after the initial time, allowing total failures of certain actuators. To guarantee theoretical exact reconstruction of the state vector right after the initial time a hierarchical observer using only the fault-free outputs is used.

0.3 Outline of the Thesis

This dissertation is organized into five major chapters. Chapter 1 provides adaptive high order sliding mode controller designs for uncertain systems. Chapter 2 describes the model of wind energy system. Chapter 3 provides the first order adaptive sliding mode controller design for WECS, which can be easily implemented in small wind turbine applications. Simulation results validate the advantages of the proposed controller. Chapter 4 presents an adaptive HOSM control for wind energy system. Comparison are made, simultaneously. The proposed method is validated by MATLAB simulation. Chapter 5 describes the FTC control based on LPV model and observer design for WECS. The performance variables,

flux of the stator and d-axis current of the rotor, are observed in order to realize fault tolerant control. Finally, some conclusions and future research directions are discussed.

Chapter 1

Adaptive High Order Sliding Mode Control Design

One of the most important problems is control under heavy uncertainty condition. While there are a number of sophisticated methods like adaptation based on identification and observation, or absolutely stability methods, the most obvious way to withstand the uncertainty is to keep some constraints by 'brutal force'. Indeed any strictly kept equality removes one 'uncertainty dimension'. The sliding mode approach is regarded as an efficient tool to design robust controllers for complex high order nonlinear dynamic plant operating under uncertain conditions. The research in this area was initiated in the former Soviet Union in 50th of last century [21]. And the sliding mode control methodology has subsequently received much more attention from the international control community within the last decades with the development of electronic technology.

Sliding mode control has found wide application in the areas of robust control, fault tolerant control (FTC), fault reconstruction in recent years. Their well known advantages are robustness and insensitivity to external disturbance. High order sliding mode control has better performance as compared with classical sliding mode based controller because their output is continuous and does not require filtering. Adaptive sliding mode controller does not need the knowledge of the uncertainties. However, insofar as we are aware, the adaptive sliding mode controllers can not guarantee the convergence region of the states. This chapter is going to present the traditional adaptive sliding mode controllers.

1.1 State-of-the-art

Robust finite time stability of uncertain nonlinear systems has become significant in practice. The uncertainties are assumed to be bound which is hard to obtain exactly while it affects the stability in many cases. The demand for renewable energy has been growing rapidly during last decade [22]. The control of wind energy conversion system (WECS) is mainly to focus on improving the utilization of the wind energy, which is known as maximum power point tracking (MPPT) technique [13]. A nonlinear model predictive control of WECS has been presented in [23] to promise the maximum power efficiency. [24] adopts a growing neural gas network-based field oriented controller (FOC) to obtain the optimal tip speed ratio as well as the active power. Sliding mode controllers of WECS have been presented in [25] [26]. However, all these controllers do not take into consideration of the bound of the wind speed and other perturbations. For the robustness, the coefficients of those controllers need to be tuned frequently, according to the varying disturbances and perturbations. As wind is an uncertain resource, the bound of the variation of wind speed affects the control of WECS. Robust control of WECS has become significant in both theory and practice. The uncertainties are assumed to be bounded physically. Moreover, the knowledge of the bound is hard to obtain exactly while it affects the precise control of WECS. It follows a challenge to design a robust controller of WECS, where the upper bound of the uncertainty is not requested. The desired controller might not require the knowledge of the uncertainties bound.

For the cases of unknown bounds, adaptive sliding mode (ASM) controllers have been presented in [27] [28] firstly. Huang et al. [29] develops an adaptive controller which ensure the convergence without the bound values. However, the algorithm can only increase the gain, which leads the gain over-estimation. Plestan et al. [1] proposes a new controller of a bounded uncertain system without the gain over-estimation. However, this algorithm has a drawback that it can not guarantee the sliding variable converge to a promised neighborhood. As for [30], the gain is adjusted properly to get a sufficient value to counteract the uncertainties, but the state still has overshooting around the neighborhood. Other works design an adaptive first or higher order sliding mode in [31, 32, 33, 2, 34, 35, 36, 37, 38]. An adaptive super twisting SM controller in [31] can continuously force the sliding variable and its first derivative to zero with unknown boundary. [32] presents an adaptive twisting SMC without gain over-estimation, which is a further development of [31]. [33] presents an

adaptive super twisting SM controller aiming to reduce chattering effect, and it is applied for an electro-pneumatic actuators system. An adaptive integral high order SM controller in [2] eliminates the need of knowledge about the upper bound of the uncertainties. The ASM controller in [39] converges a perturbed chains of integrators to a neighborhood of zero without the prior knowledge of the perturbation bound. [35] proposes a twisting ASM controller and observer with unknown boundaries. [36] develops high order ASM controller based on a first order ASM of unknown bound perturbed system. Discrete time ASM controller is considered in [37] which rejects the unknown bounded disturbance varying slowly with respect to the sample frequency. [38] is an advanced ASM controller of multi-input multi-output system.

1.2 Sliding Mode Control

The sliding mode approach is recognized as an efficient tool to design robust controllers for complex high order nonlinear dynamic plant operating under uncertain conditions. The 'sliding mode' phenomenon may appear in dynamic systems governed by ordinary differential equations with discontinuous state functions in the right hand sides.

The design methods for sliding mode control involving two independent subproblems of lower dimensions:

- design of the desired dynamics for a system of the $(n - m)$ th order by proper choice of a sliding manifold $s = 0$
- enforcing sliding motion in this manifold which is equivalent to a stability problem of the m th order system

Consider the nonlinear system, affine in the control, defined in the Brunovsky canonical form as

$$\left\{ \begin{array}{l} \dot{x}_1 = x_2 \\ \vdots \\ \dot{x}_2 = x_3 \\ \dot{x}_3 = \psi(x, t) + \varphi(x, t) + \gamma(x, t)u \\ y = x_1 \end{array} \right. \quad (1.1)$$

where $x \in X \subset \mathbb{R}$ is the state vector with X an open set of \mathbb{R}^n , and $u \in U \subset \mathbb{R}$ is the control input with U an open set of \mathbb{R} . The term y is a measured smooth output-feedback function. The nominal system dynamics are represented by $\psi(x, t)$, a known function defined on X . The functions $\varphi(x, t)$ and $\gamma(x, t)$ defined for $x \in X$, are sufficiently smooth but uncertain.

System 1.1 can be written in input-output terms as

$$y^{(n)} = \psi(\tilde{y}, t) + \varphi(\tilde{y}, t) + \gamma(\tilde{y}, t) u \quad (1.2)$$

where $\tilde{y} = \begin{bmatrix} y & \dot{y} & \dots & y^{(n-1)} \end{bmatrix}$. We assume that, the functions $\varphi(x, t)$ and $\gamma(x, t)$ are bounded by some positive constants $\bar{\varphi}$, γ_m and γ_M , such that

$$0 < \gamma_m \leq \gamma(x, t) \leq \gamma_M, |\varphi(x, t)| \leq \bar{\varphi} \quad (1.3)$$

Then we are dealing with the following differential inclusion

$$y^{(n)} \in \psi(\tilde{y}, t) + \begin{bmatrix} -\bar{\varphi} & \bar{\varphi} \end{bmatrix} + [\gamma_m, \gamma_M] u \quad (1.4)$$

where $\bar{\varphi}$ is the limit or bound of parameter uncertainty in the model, due to some possible simplification, unmodeled dynamics and/or external perturbation. The terms γ_m and γ_M represent the bounds of the uncertainty in the gain with respect to the controller u .

1.2.1 Design of sliding Manifold

Let $s(x, t) : X \times \mathbb{R}^+ \rightarrow \mathbb{R}$ be a measured smooth output-feedback function, and we assume that the control objective is to force s to zero. Here the function $s(x, t)$ is called sliding variable, and the set

$$S = \{x \in X \mid s(x, t) = 0\} \quad (1.5)$$

represents a sub-manifold of X of dimension $n - 1$, called the **sliding surface**.

Definition 1.2.1. *There exists an ideal sliding regime on S , if there exists a finite time T_s such that all solutions of System satisfy the condition $s(x, t) = 0$ for any time $t \geq T_s$.*

Definition 1.2.2. *Given the sliding variable $\sigma(x, t)$, the **real sliding surface** associated to 1.5 is defined as (with $\sigma > 0$)*

$$S^* = \{x \in X \mid |s(x, t)| < \delta\} \quad (1.6)$$

In this case, the dynamics of system 1.1 belong to a system of a dimension lower than the dimension of System (1.1). This autonomous system is called reduced system, and its dynamics are determined only by the choice of the sliding surface. For our example 1.1, the control objective is to force the output y to track a reference signal y_{ref} , which is a sufficiently smooth function. In other words, the objective is to ensure the convergence of the tracking error $e = y - y_{ref}$ to zero. One of the simplest sliding manifolds for this case is the hypersurface constructed from linear combination of the tracking error e and its higher time derivatives. We consider the following sliding variable

$$s(x, t) = e^{(n-1)} + l_{n-2}e^{(n-2)} + l_1\dot{e} + l_0e \quad (1.7)$$

with $l_i, i = 0, \dots, n-2$ are positive constants such that the polynomial

$$P(\theta) = \theta^{(n-1)} + l_{n-2}\theta^{(n-2)} + l_1\theta + l_0 \quad (1.8)$$

is Hurwitz. Therefore, after establishment of ideal sliding regime on S , the dynamics of the reduced system is determine by the stable associate differential equation

$$e^{(n-1)} + l_{n-2}e^{(n-2)} + l_1\dot{e} + l_0e = 0 \quad (1.9)$$

As a result, the tracking error e will converge to zero exponentially. In this section, we determined the dynamics of reduced system presented by the sliding surface. The next step is to tune a control law u , which forces the state trajectory of System 1.1 to reach the sliding surface in a finite-time, i.e to force sliding variable $s(x, t)$ to converge to zero in finite time.

1.2.2 Control Design

The control law u should be designed in such way that the trajectories of system 1.1 reach and stay on the sliding surface S in spite of perturbation and uncertainty. It should be remembered that the sliding variable $s(x, t)$ of Equation 1.8 is null on S . Consider the dynamics of $s(x, t)$ given as follow

$$s(x, t) \in \psi(\tilde{y}, t) + \begin{bmatrix} -\bar{\varphi} & \bar{\varphi} \end{bmatrix} + [\gamma_m, \gamma_M] u + \sum_{i=0}^{n-2} l_i e^{(i+1)} y_{ref}^{(n)} \quad (1.10)$$

The controller u should ensure a local attractivity to S in its neighborhood, i.e the trajectory of system 1.1 should be directed to S . A condition of stability of $s(x, t) = 0$, called condition of attractivity, should be satisfied by the controller. The well-known Lyapunov's

direct method requires a positive C radially-unbounded function $V(s)$, called Lyapunov Function, satisfying $V(0) = 0$ and $V(\infty) = \infty$. The function $V(s)$ represents a fictitious energy and give a global information of the System, and its time derivative \dot{V} gives an information of the stability of the system. If \dot{V} is negative for $s \neq 0$, then the system is asymptotically stable. One of the proposed Lyapunov function is the classical quadratic function

$$V(s) = \frac{1}{2} s^2 \quad (1.11)$$

The function $V(s)$ is clearly positive definite. Its time derivative should be negative to ensure the convergence of $s(x, t)$ to zero

$$\dot{V} = s\dot{s} \leq 0 \quad (1.12)$$

The previous condition (attractivity condition) ensures only the asymptotic convergence of s . Otherwise, for purpose of finite-time stability, a stronger condition needs to be imposed. In Classical Sliding Mode, a non-linear condition, called condition of η -attractivity, is used

$$\dot{V} = s\dot{s} < \eta|s|, \eta > 0 \quad (1.13)$$

Condition 1.13 is satisfied, if the controller u takes the form

$$u = -U \text{sign}(s) \quad (1.14)$$

where U is chosen sufficiently large to compensate the perturbation, uncertainty and the deviation between the system dynamics and Sliding variable dynamics. Usually, U is a sufficiently large constant. In order to satisfy Condition (1.12), U can be tuned as

$$U \geq \max_{x \in X} \left(\frac{1}{\gamma_m} \left(\left| \psi(x, t) + \sum_{i=0}^{n-2} l_i e^{(i+1)} - y_{ref}^{(n)} \right| + \bar{\varphi} + \eta \right) \right) \quad (1.15)$$

To summarize, we can describe the behavior of system in two steps:

- Reaching phase: It corresponds to the time $t \in [0, T_s]$. During this phase, the state trajectory converges to the sliding surface S .
- Sliding phase: It corresponds to the time interval $t \in [T_s, \infty]$, in which the state trajectories are confined to the sliding surface S . During this phase, the behavior of the system is entirely determined by the choice of the sliding surface.

In ideal Sliding Mode regime, the requested controller u should be able to switch at an infinite frequency. This is not possible in real life, due to the delay between the measurement and the generation of the command. This may cause the system to leave the sliding surface. Then, once the sign of the control is reversed order, the trajectories return on this surface and on the other side, and so on. This undesirable phenomena of oscillation around the sliding surface is called Chattering. One of the most effective methods to reduce chattering is the use of Higher Order Sliding Mode Control, which will be addressed in next Section.

1.3 Output Feedback Sliding Mode Control

Real systems are often suffered from disturbances and uncertainties which may affect the system performance greatly. Various control methods have been proposed in the literature [40, 41, 42]. HOSM control with properties of robustness with respect to uncertainties/perturbations and finite time convergence, has been proven to be effective to this problem [43, 44, 45, 46]. However, a lack of HOSM control is the use of sliding variables higher order derivatives. From a practical point of view, it decreases the interest in the presence of measurement noise. This motivated the development of output feedback SMC in order to remove this lack.

Two kinds of solutions are possible for the design of output feedback SMC. One solution is static output feedback using the available measurement information alone. A number of algorithms have been developed for robust stabilization of uncertain systems which are based on output feedback control schemes [47, 48, 49, 44]. In [47], a geometric condition is given to guarantee the existence of the sliding surface and the stability of the reduced order sliding motion. Edwards and Spurgeon [48] proposed an algorithm which is convenient for practical use. However, both of [47] and [48] require that the disturbance is matched, i.e. acts in the channels of the inputs. In many cases, the disturbance suffered by practical systems does not act in the input channel. Moreover, the system under consideration in [47, 48] is minimum phase and has relative degree one. In [44], an optimal version of the so-called 'twisting' algorithm has been provided which requires the derivative of sliding variable. The STA which requires no information of output time derivative was proposed by Levant [49], but it is restricted to the system with relative degree equal one with respect to the control input.

The other one consists in designing the controllers based on state observers or differentiators, such as High Gain Observers (HGOs) [50, 51, 52, 53, 54], SMOs [42, 55, 56, 57, 58, 59, 60]. Moreover, the performance of an observer-based sliding mode controller can be improved significantly by keeping the plant system and the observer system operating closely [56]. Khalil *et al.* [52] demonstrated that, under the hypothesis that a stabilizing globally bounded state feedback control is available, using a high gain observer one can recover the performance achieved under state feedback. Thus, a rather general nonlinear separation principle was established. The main drawbacks of HGOs are its sensitive to the measurement noise peaking effect with high gains. Especially, as the observer gain increases, the bandwidth of the observer is extended, exacerbating the presence of measurement noise. We should recall that asymptotic observers represent an issue which has not been entirely resolved in the realm of nonlinear systems, due to the lack of nonlinear separation principle. A robust exact differentiator [61] featuring finite time convergence was designed based on the STA [49]. Its implementation does not need the separation principle to be proved. These differentiators have been successfully applied in [62, 63, 64]. The stability analysis of HOSM output feedback control has been done by Levant [57]. In the following part, the design of observer based HOSM output feedback control will be introduced. For the sake of simplicity, we focus on single-input-single-output (SISO) systems.

1.3.1 Second Order Sliding Mode Definitions

Consider a discontinuous differential equation in the sense of Filippov [65]

$$\dot{x} = \nu(x), \quad (1.16)$$

where $x \in X \subset \mathbb{R}^n$ is the state vector, ν is a locally bounded measurable (Lebesgue) vector function. The equation can be replaced by an equivalent differential inclusion

$$\dot{x} \in \mathbb{V}(x), \quad (1.17)$$

If the vector-field ν is continuous almost everywhere, $\mathbb{V}(x)$ is the convex closure of the set of all possible limits of $\mathbb{V}(y)$ as $y \rightarrow x$, while $\{y\}$ are continuity points of ν . Solutions of the equation are defined as absolutely continuous functions $x(t)$, satisfying the differential inclusion almost everywhere [66].

Let a constrain function given by

$$s(t, x(t)) = 0, \quad (1.18)$$

where $s: \mathbb{R}^n \rightarrow \mathbb{R}$ is a sufficiently smooth function.

Definition 1.3.1. [66] Suppose that

- Successive total time derivatives s and \dot{s} are continuous functions of the system state variables. In other words, the discontinuity does not appear in the \dot{s} ;
- The set $s = \dot{s} = 0$ is non-empty and consists of Filippov's trajectories [66].

Then, the motion on the set $s = \dot{s} = 0$ is called a second sliding mode with respect to the constraint function s (Fig. 1.1).

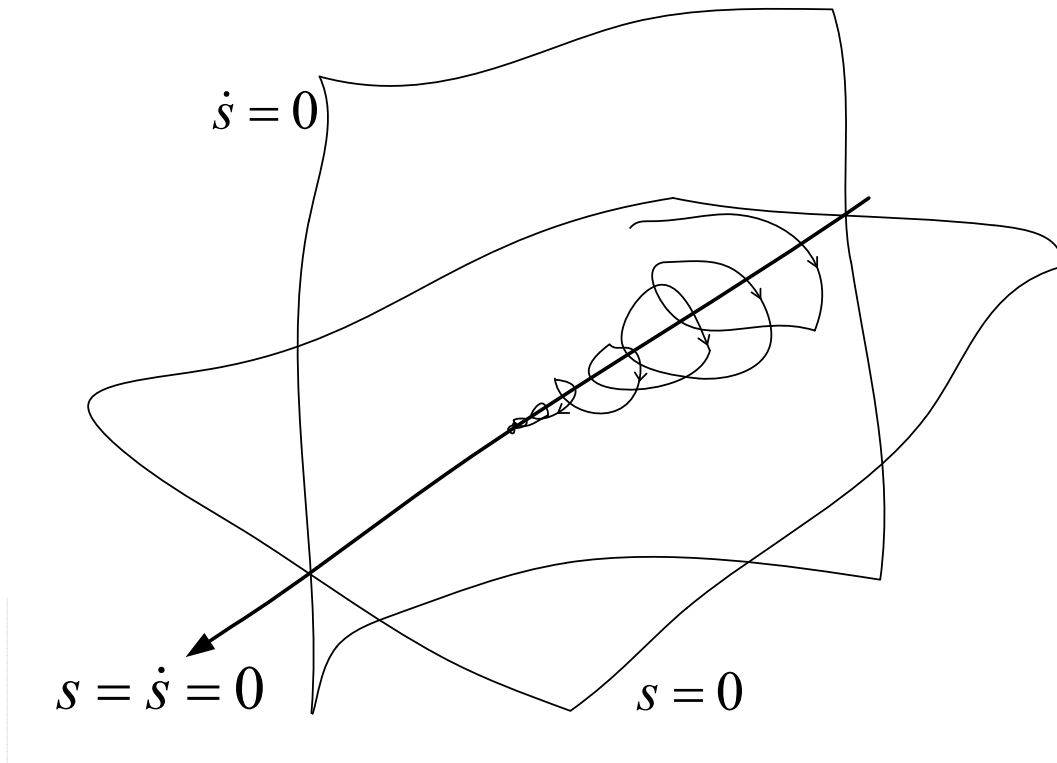


Figure 1.1. Second order sliding mode trajectory

1.3.2 Second Order Sliding Mode Dynamics

Consider the following nonlinear system [49]

$$\begin{aligned}\dot{x}(t) &= f(t, x(t), u), \\ s(t) &= s(t, x) \in \mathbb{R},\end{aligned}\tag{1.19}$$

where $x \in X \subset \mathbb{R}^n$ is the state vector, $u \in U \subset \mathbb{R}$ is the bounded control input, t is the independent variable time and f is a sufficiently smooth uncertain vector function. The control objective is to force the sliding variable and its time derivative $s(t)$ and $\dot{s}(t)$ to zero in finite time, i.e.

$$s(t) = \dot{s}(t) = 0.\tag{1.20}$$

Assume that the control task is fulfilled by its zero dynamics with respect to the sliding variable $s(t, x)$. By differentiating the sliding variable s twice,

$$\begin{aligned}\dot{s}(t) &= \frac{\partial}{\partial t} s(t, x) + \frac{\partial}{\partial x} s(t, x) f(t, x, u), \\ \ddot{s}(t) &= \underbrace{\frac{\partial}{\partial t} \dot{s}(t, x, u) + \frac{\partial}{\partial x} \dot{s}(t, x, u) f(t, x, u)}_{\varphi(t, x)} + \underbrace{\frac{\partial}{\partial u} \dot{s}(t, x, u)}_{\gamma(t, x)} \dot{u}(t).\end{aligned}\tag{1.21}$$

Depending on the relative degree [67] of the nonlinear SISO system (1.19), two cases are considered

- **Case a** : relative degree $r = 1$, i.e., $\frac{\partial}{\partial u} \dot{s} \neq 0$;
- **Case b** : relative degree $r = 2$, i.e., $\frac{\partial}{\partial u} \dot{s} = 0$, $\frac{\partial}{\partial u} \ddot{s} \neq 0$.

1.3.2.1 Relative Degree 1

In this case, the control problem can be solved by the classical first order SMC, nevertheless second order SMC can be used in order to avoid chattering. Shortly speaking, the time derivative of the control $\dot{u}(t)$ may be considered as the actual control variable. A discontinuous control $\dot{u}(t)$ steers the sliding variable s and its time derivative \dot{s} to zero, so that the plant control u is continuous and the chattering is avoided [49, 68].

The second time derivative \ddot{s} (1.21) is described by the following equation

$$\ddot{s} = \varphi(t, x) + \gamma(t, x) \dot{u}(t),\tag{1.22}$$

where $\varphi(t, x)$ and $\gamma(t, x)$ are some bounded functions. The following conditions are assumed [68]:

1. The control values belong to the set $U = \{u : |u| \leq U_M\}$, where $U_M = \text{constant} > 1$.
2. There exists $u_1 \in (0, 1)$ such that for any continuous function $u(t)$ with $|u(t)| > u_1$, there is t_1 , such that $s(t)u(t) > 0$ for each $t > t_1$.
3. There exist positive constants s_0 , K_m and K_M such that if $|s(t, x)| < s_0$, then

$$0 < K_m < \gamma(t, x) < K_M, \quad \forall u \in U, x \in X, \quad (1.23)$$

and the inequality $|u| > u_0$ entails $\dot{s}u > 0$.

4. There exists constant C such that within the region $|s(t, x)| < s_0$ the following inequality holds,

$$|\varphi(t, x)| \leq C, \quad \forall u \in U, x \in X. \quad (1.24)$$

Condition 2 means that there exists a proper control $u(t)$ forcing the sliding variable into a set for any initial value of state, given that the boundedness conditions on the sliding dynamics defined by conditions 3 and 4 are satisfied. It follows from (1.22), (1.23) and (1.24) that all solutions satisfy the differential inclusion

$$\ddot{s} \in [-C, C] + [K_m, K_M]\dot{u}(t), \quad (1.25)$$

1.3.2.2 Relative Degree 2

In this case, the control problem statement can be derived by considering the variable u as a state variable and \dot{u} as the actual control. Suppose the system dynamics (1.19) is affine in the control law, i.e.,

$$f(t, x(t), u) = a(t, x) + b(t, x)u, \quad (1.26)$$

where $a : \mathbb{R}^{n+1} \rightarrow \mathbb{R}^n$ and $b : \mathbb{R}^{n+1} \rightarrow \mathbb{R}^n$ are sufficiently smooth uncertain vector functions.

Eq. (1.21) can be rewritten as

$$\begin{aligned} \dot{s}(t) &= \frac{\partial}{\partial t}s(t, x) + \frac{\partial}{\partial x}s(t, x)a(t, x) + \frac{\partial}{\partial x}s(t, x)b(t, x)u = \frac{\partial}{\partial t}s(t, x) + \frac{\partial}{\partial x}s(t, x)a(t, x), \\ \ddot{s}(t) &= \frac{\partial^2}{\partial t^2}s(t, x) + \frac{\partial}{\partial x}s(t, x)\frac{\partial}{\partial t}a(t, x) \\ &+ \left[\frac{\partial^2}{\partial t \partial x}s(t, x) + a^T(t, x)\frac{\partial^2}{\partial x^2}s(t, x) + \frac{\partial}{\partial x}s(t, x)\frac{\partial}{\partial x}a(t, x) \right] \left[a(t, x) + b(t, x)u(t) \right] \\ &= \varphi(t, x) + \gamma(t, x)u(t). \end{aligned} \quad (1.27)$$

The following conditions are assumed [68]:

1.

$$\begin{aligned} \frac{\partial}{\partial x} s(t, x) b(t, x) &\equiv 0, \\ \left[\frac{\partial^2}{\partial t \partial x} s(t, x) + a^T(t, x) \frac{\partial^2}{\partial x^2} s(t, x) + \frac{\partial}{\partial x} s(t, x) \frac{\partial}{\partial x} a(t, x) \right] b(t, x) &\neq 0, \\ \forall t, u \in U, x \in X \end{aligned} \quad (1.28)$$

The differential equations (1.19, 1.26) with discontinuous right hand side admits solutions in the Filippov sense on the second sliding manifold $s = \dot{s} = 0$.

2. There exists $u_1 \in (0, 1)$ such that for any continuous function $u(t)$ with $|u(t)| > u_1$, there is t_1 , such that $s(t)u(t) > 0$ for each $t > t_1$.
3. There exist positive constants s_0 , K_m and K_M such that if $|s(t, x)| < s_0$, then

$$0 < K_m < \gamma(t, x) < K_M, \quad \forall u \in U, x \in X, \quad (1.29)$$

and the inequality $|u| > u_0$ entails $\dot{s}u > 0$.

4. There exists constant C such that within the region $|s(t, x)| < s_0$ the following inequality holds,

$$|\phi(x, u, t)| \leq C, \quad \forall u \in U, x \in X. \quad (1.30)$$

It follows from (1.23), (1.24) and (1.27) that all solutions satisfy the differential inclusion

$$\ddot{s} \in [-C, C] + [K_m, K_M]u(t), \quad (1.31)$$

1.3.3 Second Order Sliding Mode Controllers

In this part, the most well known second order sliding mode controllers are introduced, e.g., super-twisting Controller, twisting controller and sub-optimal controller. These controllers are insensitive to some model perturbations and external disturbances. Given that the expression for the sliding manifold is known, it is possible to design the constant parameters of the controllers [66].

1.3.3.1 Super-Twisting Control Algorithm

The STA was developed to control systems with relative degree one in order to avoid chattering in Variable Structure Control (VSC). The trajectories on the second sliding manifold are shown in Fig. 1.2

Consider the system (1.25), the control algorithm is defined [49]

$$\begin{aligned} u(t) &= u_1(t) + u_2(t), \\ \dot{u}_1(t) &= \begin{cases} -u, & \text{if } |u| > 1 \\ -\alpha \text{sign}(s), & \text{otherwise} \end{cases} \\ u_2(t) &= \begin{cases} -\lambda |s_0|^\rho \text{sign}(s), & \text{if } |s| > s_0 \\ -\lambda |s|^\rho \text{sign}(s), & \text{otherwise} \end{cases} \end{aligned} \quad (1.32)$$

where α, λ are positive constants and $\rho \in (0, 1)$. The sufficient conditions for the finite time convergence to the sliding manifold are

$$\alpha > \frac{C}{K_m}, \quad \lambda^2 \geq \frac{4C}{K_m^2} \frac{K_M(\alpha + C)}{K_m(\alpha - C)} \quad (1.33)$$

The STA does not need the evaluation of the sign of the time derivative of the sliding variable. For the choice $\rho = 1$, the origin is an exponentially stable equilibrium point. The choice $\rho = 0.5$ assures that the maximum real second order sliding is achieved. For $0 < \rho < 0.5$ the convergence to the origin is even faster. The choice $0 < \rho < 1$ assures the finite time convergence to the origin [49, 69].

1.3.3.2 Twisting Control Algorithm

This algorithm is characterized by a twisting around the origin, shown in Fig. 1.3 The finite time convergence to the origin of the plane is due to the switching of the control amplitude between two different values. The control amplitude switch at each axis crossing which requires the sign of the time derivative of the sliding variable \dot{s} .

In case the relative degree $r = 1$. Consider the system (1.25), the twisting algorithm is defined by the following control law [49]

$$\dot{u}(t) = \begin{cases} -u, & \text{if } |u| > 1 \\ -\alpha_m \text{sign}(s), & \text{if } s\dot{s} \leq 0, |u| \leq 1 \\ -\alpha_M \text{sign}(s), & \text{if } s\dot{s} > 0, |u| \leq 1 \end{cases} \quad (1.34)$$

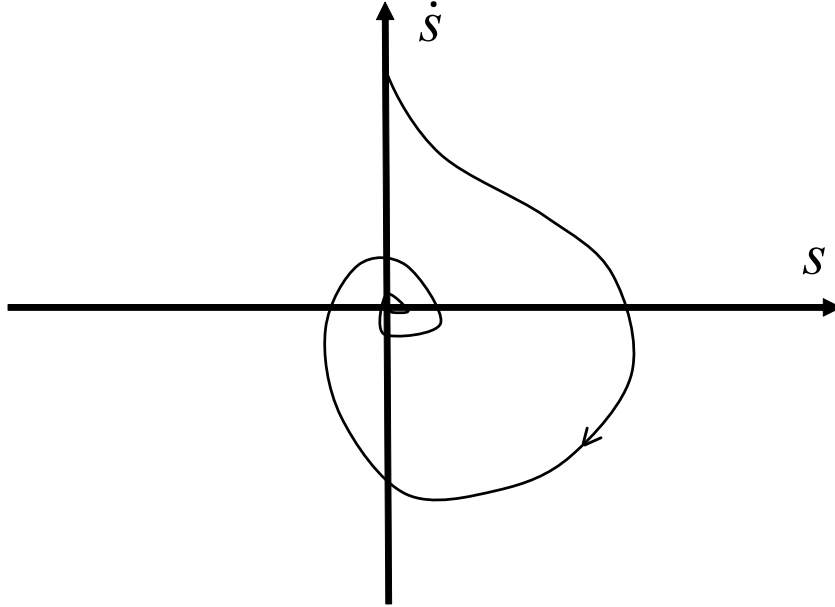


Figure 1.2. *Super-twisting algorithm phase trajectory*

where $\alpha_M > \alpha_m > 0$ and the sufficient conditions for the finite time convergence to the sliding manifold are

$$\alpha_m > \frac{4K_M}{s_0}, \quad \alpha_m > \frac{C}{K_m}, \quad K_m \alpha_M > K_M \alpha_m + 2C. \quad (1.35)$$

In case the relative degree $r = 2$. Consider the system (1.31), the twisting algorithm is defined by the following control law [57]

$$u = -r_1 \text{sign}(s) - r_2 \text{sign}(\dot{s}), \quad r_1 > r_2 > 0, \quad (1.36)$$

the sufficient conditions for the finite time convergence to the sliding manifold are

$$(r_1 + r_2)K_m > (r_1 - r_2)K_M + 2C, \quad (r_1 - r_2)K_m > C. \quad (1.37)$$

A particular case of the controller with prescribed convergence law [49, 66] is given by

$$u = -\alpha \text{sign}\left(\dot{s} + \lambda |s|^{\frac{1}{2}} \text{sign}(s)\right), \quad \alpha > 0, \quad \lambda > 0 \quad \text{and} \quad \alpha K_m - C > \frac{\lambda^2}{2}. \quad (1.38)$$

Controller (1.38) is close to a terminal sliding mode controller [70].

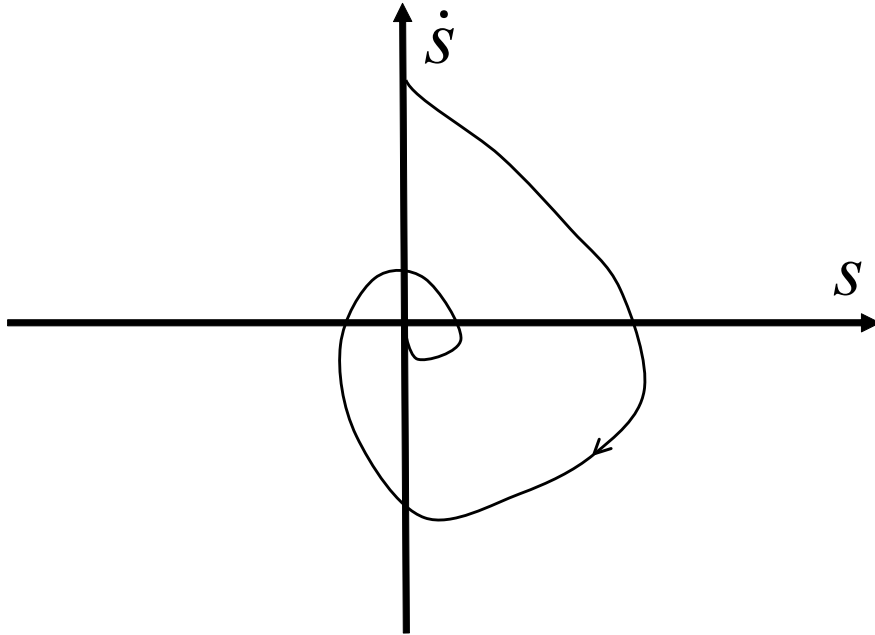


Figure 1.3. *Twisting algorithm phase trajectory*

1.3.3.3 Sub-Optimal Control Algorithm

The second order sliding mode controller was developed as a sub-optimal feedback implementation of the classical time optimal control for a double integrator [12]. This algorithm ensures the finite time convergence of s and \dot{s} to zero, confining the trajectories within limit parabolic arcs (including the origin). Both twisting and jumping (in which s and \dot{s} do not change sign) behaviors are possible (see Fig. 1.4). Unlike most SOSMC algorithms, sub-optimal control does not require continuous estimate of \dot{s} , only depends on upon the instances when the value of \dot{s} is zero.

Let the relative degree $r = 2$. Consider the system (1.31), the control algorithm is defined by the following control law [49, ?]

$$\begin{aligned} u(t) &= -\alpha(t)V_M \text{sign}\left(s - \frac{s^*}{2}\right), \\ \alpha(t) &= \begin{cases} \alpha^*, & \text{if } \left(s - \frac{1}{2}s^*\right)(s^* - s) > 0 \\ 1, & \text{otherwise} \end{cases} \end{aligned} \quad (1.39)$$

where s^* is the latter singular value of the function $s(t)$ which corresponds to the zero value of \dot{s} and α^* is a positive constant. The sufficient conditions for the finite time convergence

to the sliding manifold are

$$\begin{aligned} \alpha^* &\in (0, 1] \cap \left(0, \frac{3K_m}{K_M}\right), \\ V_M &> \max\left(\frac{C}{\alpha^* K_m}, \frac{4C}{3K_m - \alpha^* K_M}\right). \end{aligned} \quad (1.40)$$

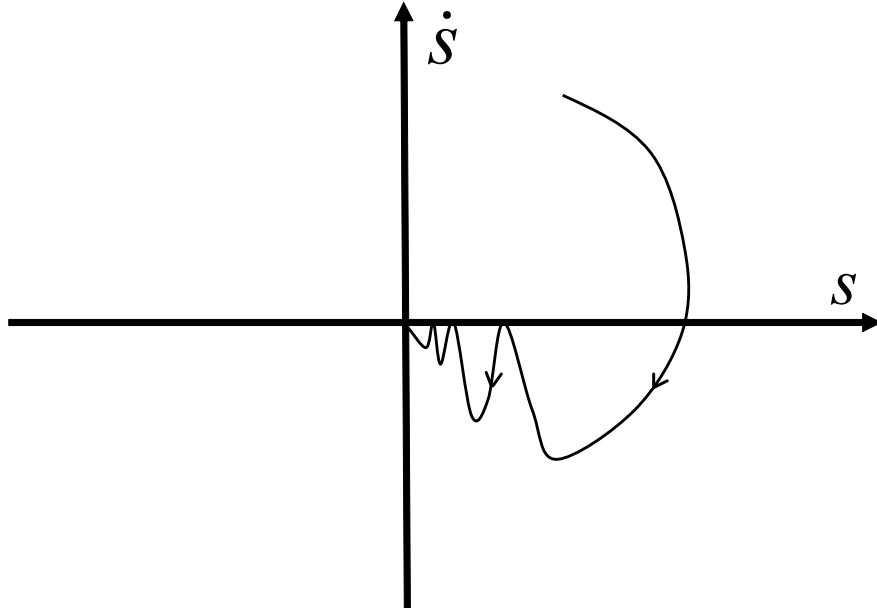


Figure 1.4. Sub-optimal algorithm phase trajectory

1.4 High Order Sliding Mode Control

A class of nonlinear dynamic system is considered as follows:

$$\begin{cases} \dot{x} = f(x) + g(x)u \\ y = s(x) \end{cases} \quad (1.41)$$

where $x \in \mathbb{R}_n$ are the state variables, $u \in \mathbb{R}_m$ is the control input, and $s(x) \in \mathbb{R}_m$ is the measured output function known as the sliding variable. It is assumed that $f(x)$ and $g(x)$ are smooth functions.

Definition 1.4.1. In system 1.41, the time derivatives of s , with \dot{s}, \dots, s^{r-1} are considered continuous. A set is called r th **order sliding set**, which is a non empty integral set in

the Filippov sense, if and only if

$$S^r = \{x | s(x, t) = \dot{s}(x, t) = \dots = s^{(r-1)}(x, t) = 0\} \quad (1.42)$$

the motion on S^r is called ***r*th order sliding mode** with respect to the sliding variable s .

The aim of the first order sliding mode control is to force the state trajectories to move along the sliding manifold $s(x) = 0$. In the higher order sliding mode control, the purpose is to move the states along the switching surface $s(x) = 0$ and to keep its $(r - 1)$ successive time derivatives viz \dot{s}, \dots, s^{r-1} to zero by using a suitable discontinuous control action. The *r*th order derivative of $s(x)$ satisfies the following equation:

$$s^r(x) = \varphi(x) + \gamma(x)u \quad (1.43)$$

where $\varphi(x) = L_f^r s(x)$ and $\gamma(x) = L_g L_f^r s(x)$. Here, L_f and L_g are the Lie derivatives of the smooth functions in 1.41. The corresponding sliding regularity condition has the form

$$\text{rank} \{ \nabla s_i, \dots, \nabla s_i^{(r_i-1)} | i = 1, \dots, m \} = r_1 + \dots + r_m \quad (1.44)$$

A sliding mode is called stable if the corresponding integral sliding set is stable.

Assumption 1. *Functions $\varphi(x)$ and $\gamma(x)$ are bounded uncertain functions, and without loss of generality, let also the sign of the control gain γ be constant and strictly positive. Thus, there exist $\gamma_m \in \mathbb{R}^+$, $\gamma_M \in \mathbb{R}^+$, $\bar{\varphi} \in \mathbb{R}^+$ such that*

$$0 < \gamma_m < \gamma < \gamma_M, |\varphi| \leq \bar{\varphi} \quad (1.45)$$

for $x \in X \subset \mathbb{R}^n$, X being a bounded open subset of \mathbb{R}^n within which the boundedness of the system dynamics is ensured.

The *r*th order sliding mode control of system 1.41 with respect to the sliding variable $s(x)$ can be expressed as

$$\begin{cases} \dot{z}_i = z_{i+1} \\ \dot{z}_r = \varphi(x) + \gamma(x)u \end{cases} \quad (1.46)$$

where $1 \leq i \leq r-1$, and $\begin{bmatrix} z_1 & z_2 & \dots & z_r \end{bmatrix}^T = \begin{bmatrix} s(x) & \dot{s}(x) & \dots & s^{r-1}(x) \end{bmatrix}^T$.

The objective of HOSM control is to design controllers for System 1.46 with respect to s , which is equivalent to the stabilization of System 1.43 to the origin, ideally in finite time. Since these controllers are to be discontinuous feedback laws $u = U(z)$, solutions of 1.46 need to be understood here in Filippov sense, defined as follows:

Definition 1.4.2. *A control algorithm is said to establish real sliding mode of order r with respect to s when for any local set of initial conditions and for any finite time interval $[t_1, t_2]$, there exist constants $1 \dots r$ such that for all $t > t_1$, the following inequalities are satisfied*

$$|s_1| \leq \Delta_1, |s_2| \leq \Delta_2, \dots, |s_r| \leq \Delta_r \quad (1.47)$$

1.5 Adaptive Sliding Mode Control

The sliding mode control is a very popular strategy for control of nonlinear uncertain systems, with a very large frame of applications fields. Due to the use of discontinuous function and high control gain, its main features are the robustness of closed-loop system and the finite-time convergence. However, its design requires the knowledge of uncertainties bound, which could be, by a practical point-of-view, a hard task; it often follows that this bound is over-estimated, which yields to excessive gain. Then, the main drawback of the sliding mode control, the well-known chattering phenomenon, is important and could damage actuators and systems. A first way to reduce the chattering is the use of a boundary layer: in this case, many approaches have proposed adequate controller gains tuning. A second way to decrease the chattering phenomenon is the use of higher order sliding mode controller. However, in these both control approaches, knowledge of uncertainties bound is required. As the objective is the not-requirement of the uncertainties bound, an other way consists in using adaptive sliding mode, the goal being to ensure a dynamical adaptation of the control gain in order to be as small as possible whereas sufficient to counteract the uncertainties/perturbations. As recalled previously, this problem is an exciting challenge for applications given that, in many cases, gains are also over-estimated, which gives larger control magnitude and larger chattering. In order to adapt the gain, many controllers based on fuzzy tools have been published; however, these papers do not guarantee the tracking performances. Control gain in [29] dynamics directly depends on the tracking error (sliding variable): the control gain is increasing since sliding mode is not established. Once it is the case, gain dynamics equals 0. The main drawback of this approach is the gain over-estimation with respect to uncertainties bound. Furthermore, this approach is not directly applicable, but requires modifications for its application to real systems: thus, the sign function is replaced by a saturation function whom the boundary layer width affects accuracy and robustness. Furthermore, no boundary layer width tuning methodology is provided. A method has been proposed in [71] in order to limit the switch-

ing gain must be mentioned. The idea is based on use of equivalent control: once sliding mode occurs, disturbance magnitude is evaluable and allows an adequate tuning of control gain. However, this approach requires the knowledge of uncertainties/perturbations bounds and the use of low-pass filter, which introduces signal magnitude attenuation, delay, and transient behavior when disturbances are acting. A gain-adaptation algorithm [72] is proposed by using sliding mode disturbance observer. The main drawback is that the knowledge of uncertainties bounds is required to design observer-based controller.

1.5.1 Adaptive Twisting Algorithm

The adaptation process in the controller consists of dynamically increasing the control gain $\alpha(t)$ such that the sliding variable and its derivative converge to the equilibrium point $s = \dot{s} = 0$ in the 2-sliding mode (2-SMC) in finite time regardless of the bounded perturbation with the unknown bound. Thereafter the gain $\alpha(t)$ starts to reduce. This gain reduction gets reversed as soon as the system trajectories again start deviating from the equilibrium.

The following Twisting control algorithm is considered

$$u = -\alpha(\operatorname{sgn}(x) + 0.5\operatorname{sgn}(y)) \quad (1.48)$$

where the adaptive gain $\alpha(t, x, y)$. For any initial conditions a real 2-sliding mode is established in the domain $M: \{x, y: N(x, y) \leq \eta\}, \eta > \mu$ in finite time via twist control with the adaptive gain

$$\dot{\alpha} = \begin{cases} \frac{\frac{\omega_1}{\sqrt{2\gamma_1}}}{\frac{1}{\gamma_1} - \frac{2ax^2 + |x|y^2}{|\alpha - \alpha^*|^3}} \operatorname{sgn}(N(x, y) - \mu) & \alpha \geq \alpha_{\min} \\ \chi & \alpha < \alpha_{\min} \end{cases} \quad (1.49)$$

with the establishment of the following conditions $\alpha > 2D$ and $0 < \gamma < \frac{4\sqrt{2}}{3}\sqrt{\alpha}(0.5\alpha - D)$, where $\gamma_1, \omega_1, \mu, \chi$ and α_{\min} are arbitrary positive constants, and α^* is a sufficiently large constant.

1.5.2 Adaptive first order algorithm of Plestan [1]

The controller of [1] displayed in this section does not estimate the boundary of perturbation and uncertainties. But, there is an eminent price to do that: the new strategy

guarantees a real sliding mode only. Consider the nonlinear uncertain system

$$\dot{x} = f(x) + g(x)u, \quad (1.50)$$

where $x \in X \subset \mathbb{R}$ is state vector, $u \in \mathbb{R}$ the control input. The $f(x)$ and $g(x)$ are bounded smooth uncertain functions. $f(x)$ contains unmeasured disturbances term and $g(x) \neq 0$ for $x \in X$.

The control objective consists in stabilize the continuous function $s(x, t)$. Suppose that s admits a relative degree 1 with respect to the controller u , and the derivation of the sliding variables as:

$$\begin{aligned} \dot{s} &= \frac{\partial s}{\partial t} + \frac{\partial s}{\partial x} \dot{x} \\ &= \underbrace{\frac{\partial s}{\partial t} + \frac{\partial s}{\partial x} f(x)}_{\varphi(x,t)} + \underbrace{\frac{\partial s}{\partial x} g(x)}_{\gamma(x,t)} \cdot u \\ &= \varphi(x, t) + \gamma(x, t)u \end{aligned} \quad (1.51)$$

The functions $\varphi(x, t)$ and $\gamma(x, t)$ are supposed to be bounded and satisfy the following assumptions

$$0 < \gamma_m \leq \gamma(x, t) \leq \gamma_M, \quad |\varphi(x, t)| \leq \varphi_M, \quad (1.52)$$

where γ_m , γ_M and φ_M are unknown positive constants.

Definition 1.5.1. Consider the non-empty real sliding surface S^* given by 1.6, and assume that it is locally an integral set in the Filippov sense. The corresponding behavior of system 1.51 on 1.6 is called **real sliding mode** with respect to the sliding variable $s(x, t)$.

Consider the following controller

$$\dot{K} = \begin{cases} \bar{K}|s(x, t)| \operatorname{sign}(|s(x, t)| - \varepsilon) & \text{if } K > \mu \\ \mu & \text{if } K \leq \mu \end{cases} \quad (1.53)$$

with $K(0) > 0$, $\bar{K} > 0$, $\varepsilon > 0$ and $\mu > 0$ very small. The parameter μ is introduced in order to get only positive values for K . Given the nonlinear uncertain system 1.51 with the sliding variable $s(x, t)$ dynamics 1.51 controlled by 1.51, there exists a finite time $t_F > 0$ so that a real sliding mode is established for all $t \geq t_F$, i.e. $|\sigma(x, t)| < \sigma$ for $t \geq t_F$, with

$$\delta = \sqrt{\varepsilon^2 + \frac{\psi_M^2}{K\Gamma_m}} \quad (1.54)$$

In conclusion, s converges to the domain $|s| \leq \delta$ in a finite time, but could be sustained in the bigger domain $|s| \leq \delta$. Therefore, the real sliding mode exists in the domain $|s| \leq \delta$.

1.5.3 Adaptive Integral High Order Algorithm [2]

Consider the system which is represented by the SISO integrator chain as

$$\left\{ \begin{array}{l} \dot{z}_1 = z_2 \\ \dot{z}_2 = z_3 \\ \vdots \\ \dot{z}_r = \varphi(z) + \gamma(z)u + \Delta(z, t) \end{array} \right. \quad (1.55)$$

The control objective is to drive the states of 1.55 to $z = \mathbf{0}$ at the fixed finite time

Theorem 1. *Let $k_1, k_2, \dots, k_n > 0$ be such that the polynomial $\phi(\lambda) = \lambda^n + k_n \lambda^{n-1} + \dots + k_2 \lambda + k_1$ is Hurwitz. For system 1.55, there exists a value such $\varepsilon \in (0, 1)$ that for every $\varepsilon \in (1 - \varepsilon, 1)$, the origin is a globally stable equilibrium in finite time under the feedback*

$$\omega_{nom}(z) = -k_1 \text{sgn} z_1 |z_1|^{\alpha_1} - k_2 \text{sgn} z_2 |z_2|^{\alpha_2} - \dots - k_n \text{sgn} z_n |z_n|^{\alpha_n} \quad (1.56)$$

where, $\alpha_1, \alpha_2, \dots, \alpha_n$ satisfy $\alpha_{i-1} = \frac{\alpha_i \alpha_{i+1}}{2\alpha_{i+1} - \alpha_i}$, $i = 2, \dots, n$ with $\alpha_{n+1} = 1$

Consider an integral sliding surface

$$s(z) = z_n - z_n(0) - \int \omega_{nom}(z) dt \quad (1.57)$$

The initial condition of the system is defined by $z_n(0)$. The nominal control ω_{nom} ensures the convergence of the chain of integrators in finite time as given in Theorem 1.

Using the constant plus proportional reaching law yields

$$\dot{s} = -\rho_1 s - \rho_2 \text{sgn}(s) \quad (1.58)$$

where $\rho_1 \geq 0$, $\rho_2 > \Delta(z, t)$ to satisfy the reaching law condition, the control is obtained as

$$\dot{u} = -\bar{\gamma}(z)^{-1} \{ \varphi(z) + \dot{\gamma}(z)u - \dot{\omega}_{nom} + \kappa(\dot{z}_n - \dot{\omega}_{nom}) + \rho_1 s + \rho_2 \text{sgn}(s) \} \quad (1.59)$$

The parameter ρ_2 will be estimated by using the adaptation law

$$\rho_2 = \nu \|s\| \quad (1.60)$$

where ν is a positive constant.

1.6 Conclusion

In this chapter, we discuss the ASM control design for uncertain nonlinear systems. Firstly, we introduced traditional first order sliding mode design for uncertain systems. Then the first order design strategies were extended to a class of high order systems. However, the choice of the algorithms gains depends on the knowledge of boundary of uncertainties. Therefore, an adaptive-gain SOSM algorithm was proposed without *a priori* requiring the knowledge of the boundary of uncertainty, meanwhile, the gains of the algorithm stop increasing when the observation error converges to zero exactly.

In the next chapter, a complex nonlinear system, i.e., wind energy conversion system (WECS) will be presented. Adaptive control design and FTC will be concerned for this system in the subsequent chapters.

Chapter 2

Modeling of Wind Energy Conversion System

Wind energy has been regarded as an environmentally friendly alternative energy source which has attracted much attentions [13]. Many initiatives have been launched to improve the utilizing of wind power in electricity generation [73]. Subsequent interest in wind systems expanded in the support of utility grid, more reliable and relatively cost declined [74]. This section is organized as follow. the model of wind power systems are briefly discussed in 2.2. The configuration of the system has been presented in 2.1. The traditional control methods have been introduced in 2.3. Finally, the conclusion has been given in 2.4

2.1 System Configuration and Topology

A wind energy conversion system (WECS) is composed of several parts to achieve kinetic-to-electric energy conversion. Wind generator is mechanical and electrical device that convert the kinetic energy of wind into mechanical energy and are under intensive development in the past few years as they are regarded as an efficient carbon free electricity production technology. It forces electric flow through an external electrical device. For wind power applications, fixed speed wind turbine is mostly operated with a squirrel cage induction generator (SCIG) and a multiple stage gearbox during the 1980s and 1990s. That fact that the rotor circuit of an SCIG is not accessible can be changed if the rotor circuit is wound and made accessible via slip rings. Permanent magnet synchronous

generators (PMSG) are becoming increasingly popular because of their ability to reduce failures in the gearbox and lower maintenance problems. However, the price of PMSG is very expensive. Since the late 1990s, most wind turbines, in which the power level was increased to 1.5 MW and above, have adopted variable speed operation because of the grid requirement for power quality. For these variable speed applications, doubly fed induction generators (DFIG) are commonly used together with a multi stage gearbox and power electric converters. The DFIG typically operates about 30% above and below synchronous speed, sufficient for most wind speed conditions. It also enables generator-side active power control and grid-side reactive power control. The reduced-capacity converter is less expensive and requires less space, which makes the DFIG WECS popular in today's market. The common topology adopting the DFIG generator for wind power applications is shown in Fig. 2.1.

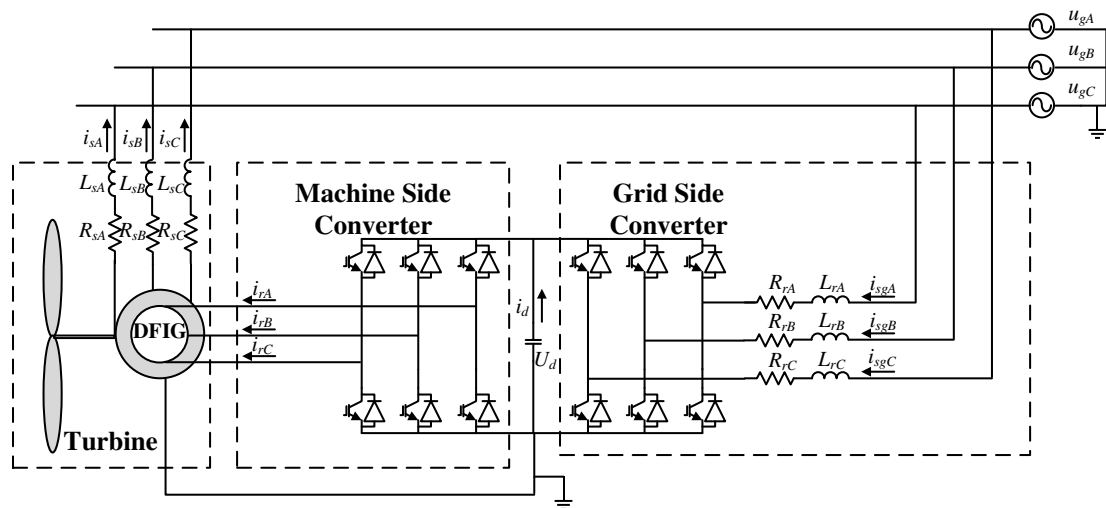


Figure 2.1. The configuration of variable speed wind energy conversion system

The side view of a typical wind turbine is shown in Fig. 2.1. There are several variants to this layout of components, particularly for wind turbine with DFIG. Nonetheless, the figure serves as a general reference to locate and describe the different parts in modern wind turbines [75][76]:

- Wind turbine, which is an instrument capturing wind energy by blades and convert-

ing the wind kinetic power to mechanical power.

- Gearbox, which is a transmission device to adapt the rotation speed for the generator.
- Generator, which converts the power from mechanical form into electricity form. The stator of the generator is connected to the grid directly, while the rotor is interfaced with the grid through a power converter system with reduced power capacity.
- Converters, which is used as an interface connecting the DFIG rotor and the power grid.

Variable-speed wind turbines can achieve maximum energy conversion efficiency over a wide range of wind speeds. The turbine can continuously adjust its rotational speed according to the wind speed. In doing so, the tip speed ratio, which is the ratio of the blade tip speed to the wind speed, can be kept at an optimal value to achieve the maximum power conversion efficiency at different wind speeds. To make the turbine speed adjustable, the wind turbine generator is normally connected to the utility grid through a power converter system. The converter system enables the control of the speed of the generator that is mechanically coupled to the rotor (blades) of the wind turbine. The main advantages of the variable-speed turbine include increased wind energy output, improved power quality, and reduced mechanical stress. The main drawbacks are the increased manufacturing cost and power losses due to the use of power converters. Nevertheless, the additional cost and power losses are compensated for by the higher energy production. Furthermore, the smoother operation provided by the controlled generator reduces mechanical stress on the turbine, the drive train and the supporting structure. This has enabled manufacturers to develop larger wind turbines that are more cost-effective. Due to the above reasons, variable-speed turbines dominate the present market. This case has been studied on variable-speed turbine topology. The following section focuses on the wind energy generation system mathematics model.

2.2 WECS Modeling

The proposed wind turbine model with control scheme is composed of the following systems, shown in Fig. 2.2:

- Aerodynamic model, evaluates the turbine torque τ_t as a function of wind speed v and the turbine angular speed ω_t

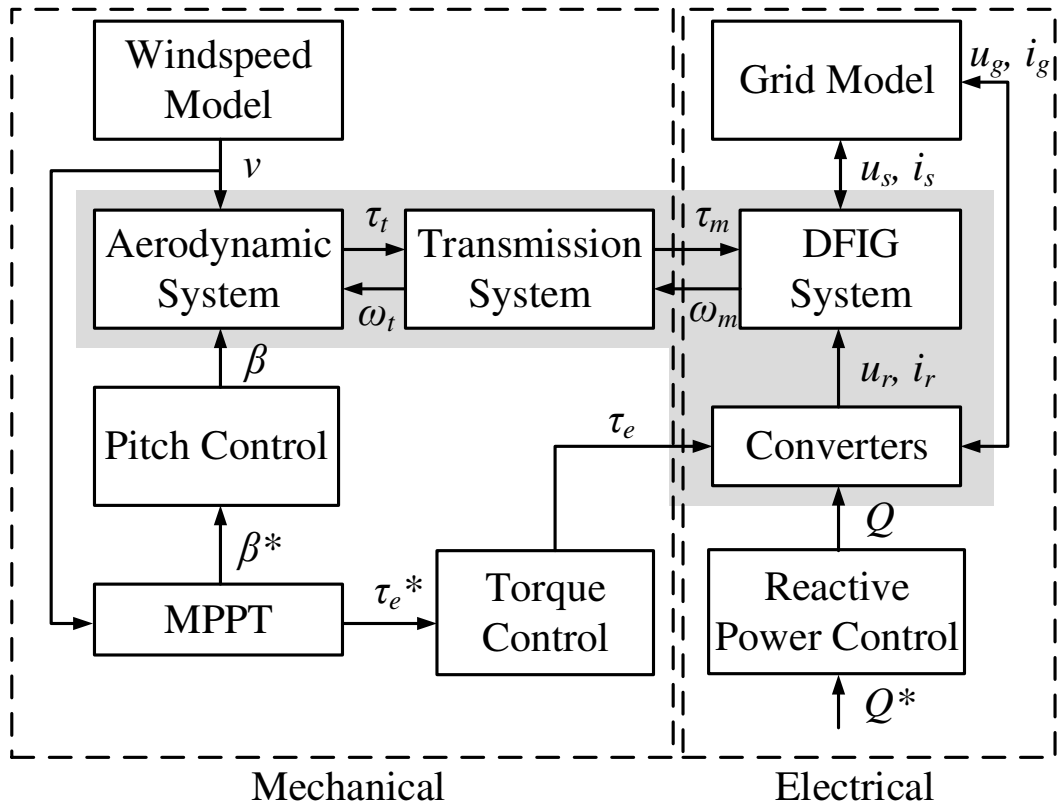


Figure 2.2. Block scheme of a variable speed wind turbine model

- Pitch system, evaluates the pitch angle β dynamics as a function of pitch reference β^*
- Mechanical system, evaluates the generator speed ω_t and turbine angular speed ω_m as a function of turbine torque τ_t and generator torque τ_m
- Electrical machine and power converters transform the generator torque into a grid current as a function of voltage grid
- Control system, evaluates the generator torque, pitch angle and reactive power references as a function of wind speed and grid voltage

2.2.1 Aerodynamics System Modeling

The system of variable wind turbine with the power converters is a high order, high non-linear and complex coupled system. The aerodynamic power P_a in watt can be extracted from the wind turbine is

$$P_a = 0.5\pi\rho r^2 C_p(\lambda, \beta) v^3 \quad (2.1)$$

where, r is the blade radius of turbine blades (m), v is the wind velocity (m/s), ρ is the air density of the area (kg/m^3). πr^2 is the area swept by the turbine blades. As a result, $\pi r^2 v \rho$ is the mass of the air passing through the turbine swept area in a unit time. Consequently, $0.5\pi r^2 v^3 \rho$ is the kinetic energy of the wind at the velocity v in a unit time.

As a matter of fact, it is impossible to obtain all the kinetic energy from the wind. Therefore a power coefficient C_p can be represented to describe the percentage of the wind power by utilizing the following equation

$$C_p(\lambda, \beta) = c_1 \left(\frac{c_2}{\lambda_i} - c_3 \beta - c_4 \right) e^{-\frac{c_5}{\lambda_i}} + c_6 \lambda \quad (2.2)$$

$$\lambda = \frac{v_{tip}}{v} = \frac{\omega_t r}{v} \quad (2.3)$$

$$\frac{1}{\lambda_i} = \frac{1}{\lambda + 0.08\beta} - \frac{0.035}{\beta^3 + 1} \quad (2.4)$$

where, c_1 to c_6 are parameters designed by the turbine installation, ω_t is the angular speed of the turbine blades (rad/s), λ is the tip-speed ratio defined as the ratio between the turbine blades tip speed $v_{tip} = \omega_t r$ and wind speed v in (2.3). β is the pitch angle (deg). C_t is the turbine torque coefficient, which defined as

$$C_t = C_p / \lambda \quad (2.5)$$

As shown in Fig. 2.3, the C_p grows up according various wind speed and has an unique peak point.

2.2.2 Transmission System Modeling

The torque produced by the turbine and the mechanic torque delivered by the gearbox is

$$\tau_t = \frac{P_a}{\omega_t} = \frac{\pi\rho r^2 C_p(\lambda, \beta) v^3}{2\omega_t} \quad (2.6)$$

$$\tau_t = k_{gb} \tau_m, \omega_{mr} = k_{gb} \omega_t \quad (2.7)$$

where, k_{gb} is the gearbox ratio. τ_t represents the aerodynamic torque in the turbine

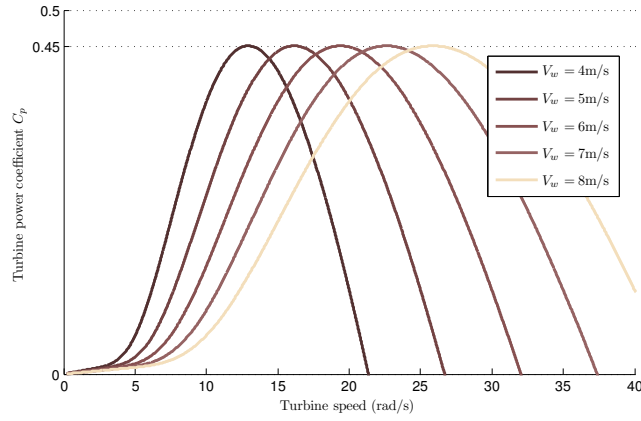


Figure 2.3. Power coefficient C_p versus different wind speed

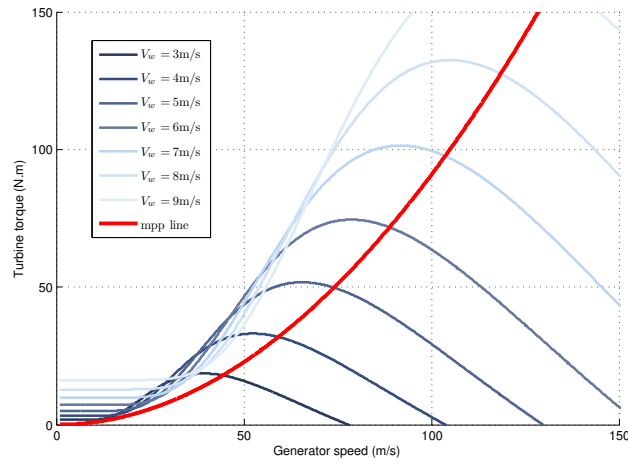


Figure 2.4. Turbine torque τ_t versus different wind speed and the maximum power point line

side. τ_m and ω_{mr} are the mechanic torque and mechanical speed of the generator in the machine side, respectively. Or in the form using the torque coefficient C_t :

$$\tau_m = \frac{\tau_t}{k_{gb}} = \frac{\pi \rho r^3 C_t(\lambda, \beta) v^2}{2k_{gb}} \quad (2.8)$$

Fig. 2.4 shows the curves of turbine torque versus different wind speed with maximum power point line.

2.2.3 Doubly Fed Induction Generator Modeling

The dynamic and steady-state model of the DFIG is introduced, which consists of the differential equations to describe the electromagnetic dynamic of the stator and rotor in synchronous frame as Fig. 2.5 shows. The effects of slotting have been neglected. It is assumed that the permeability of the iron parts is infinite and the flux density is radial in the air-gap. And for simplicity in the notation, the time dependence of the magnitudes will be omitted in the following sections. In subsequent sections, the magnitudes and parameters of the rotor are always referred to the stator. The simplified and idealized DFIG model can be described as three windings in the stator and three windings in the rotor, as illustrated in Fig. 2.5.

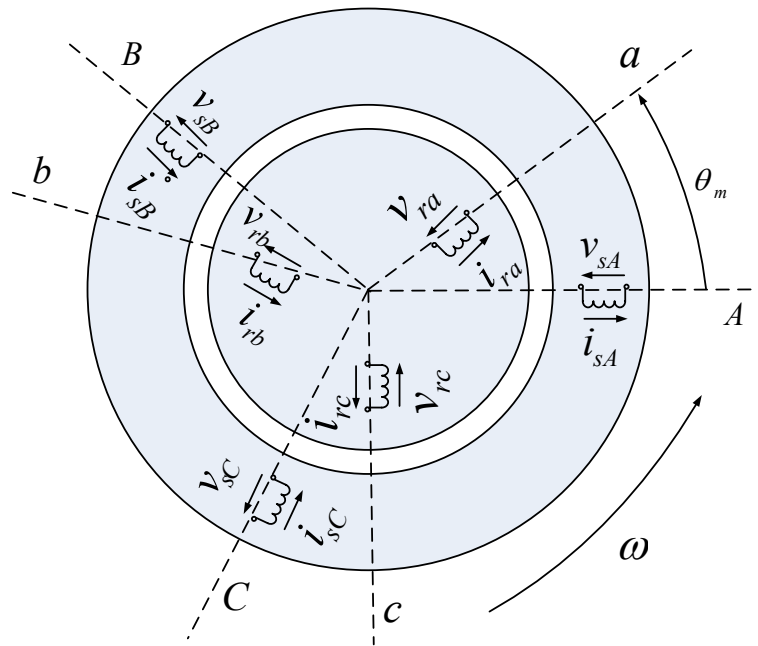


Figure 2.5. Ideal three-phase windings (stator and rotor) of the DFIG

These windings are an ideal representation of the real machine, which helps to derive an equivalent electric circuit, as shown in Fig. 2.6. Under this idealized model, the instantaneous stator voltages, current, and fluxes of the machine can be described by the

following electric equations:

$$v_{sA} = R_s i_{sA} + \frac{d\psi_{sA}}{dt} \quad (2.9)$$

$$v_{sB} = R_s i_{sB} + \frac{d\psi_{sB}}{dt} \quad (2.10)$$

$$v_{sC} = R_s i_{sC} + \frac{d\psi_{sC}}{dt} \quad (2.11)$$

where R_s is the stator resistance; i_{sA} , i_{sB} , and i_{sC} are the stator currents of phases A, B, and C; v_{sA} , v_{sB} , and v_{sC} are the applied stator voltages; and ψ_{sA} , ψ_{sB} , and ψ_{sC} are the stator fluxes. The stator side electric magnitudes, at steady state, have a constant

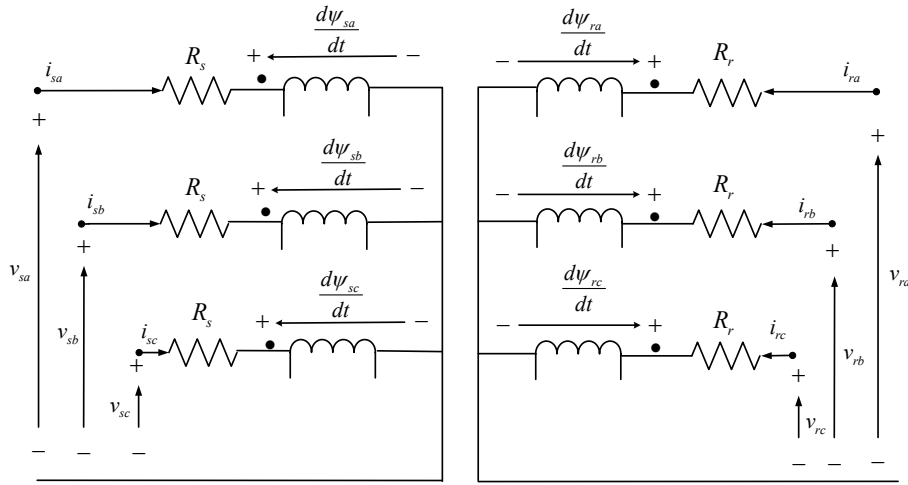


Figure 2.6. DFIG electric equivalent circuit

sinusoidal angular frequency θ_m , the angular frequency imposed by the grid. Similarly, the rotor magnitudes are described by

$$v_{ra} = R_r i_{ra} + \frac{d\psi_{ra}}{dt} \quad (2.12)$$

$$v_{rb} = R_r i_{rb} + \frac{d\psi_{rb}}{dt} \quad (2.13)$$

$$v_{rc} = R_r i_{rc} + \frac{d\psi_{rc}}{dt} \quad (2.14)$$

where R_r is the rotor resistance referred to the stator; i_{ra} , i_{rb} , and i_{rc} are the stator referred rotor currents of phases a , b , and c ; v_{ra} , v_{rb} , and v_{rc} are the stator referred rotor voltages; and ψ_{ra} , ψ_{rb} , and ψ_{rc} are the rotor fluxes. Under steady state operating conditions, the rotor magnitudes have constant angular frequency, ω_r . Assuming a general DFIG built with different turns in the stator and rotor, all parameters and magnitudes of

the rotor are referred to the stator. It was indicated that the relation between the stator angular frequency and the rotor angular frequency is

$$\omega_r + \omega_m = \omega_s \quad (2.15)$$

where ω_r is the electrical angular frequency of the machine. Similarly, ω_m is the mechanical angular speed, related to the electrical frequency by means of a pair of poles p_r :

$$\omega_r = p_r \omega_m \quad (2.16)$$

Hence, the rotor variables (voltages, currents, and fluxes) present a pulsation or that varies with the speed. And the electromagnetic torque τ_e generated by the DFIG shown in Fig.

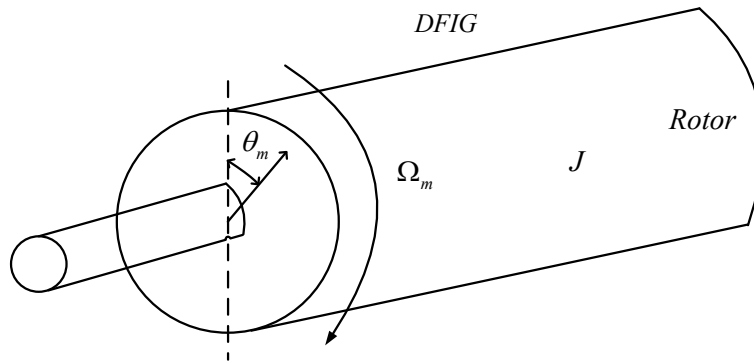


Figure 2.7. Mechanical axis of the DFIG

2.7 mathematically represented by the following equation:

$$\tau_e - \tau_m = J \frac{d\omega_m}{dt} \quad (2.17)$$

where J is equivalent inertia of the mechanical axis, τ_m express external torque applied to the mechanical axis, here it is the torque from the gearbox. ω_m is mechanical rotational speed. From the mechanical model, it is possible to derive the electric rotational speed ω_m and the angle θ_m .

2.2.4 Space Vector Technique

By assuming a symmetrical three-phase operation in sinusoidal steady-state, whereby currents, voltages, and flux linkages are sinusoids and form a positive sequence, then, for example, the instantaneous stator currents, if I_s is the rms value of the current and ω is its angular frequency and t the time, can be expressed as follows:

$$i_s(t) = |i_s| e^{j\omega t} = I_s e^{j\omega t} \quad (2.18)$$

where j is the imaginary unit, $a = e^{j2\pi/3}$ is the complex operator that makes a vector rotate $2\pi/3$ rad in the counter-clockwise direction, $|i_s|$ is the amplitude of the stator current space-vector.

Because of the earlier emphasized physical meaning, the space-vector quantity has been historically defined with reference to the AC electric machine currents. Its application can, however, be extended to any three-phase time-varying quantity, being it not related to electric machines. Given therefore a set of three-phase quantities $x_A(t)$, $x_B(t)$, and $x_C(t)$, the corresponding space-vector could be defined in this way:

$$x(t) = k [x_A(t) + ax_A(t) + a^2x_A(t)] = |x| e^{j\alpha x} = x_D(t) + jx_Q(t) \quad (2.19)$$

where $x_D(t)$ and $x_Q(t)$ are, respectively, the instantaneous values of the sD and sQ components of the stator current space-vector corresponding to the real and imaginary components of the space-vector in the complex plane.

Let $x(t) = x_D(t) + jx_Q(t)$ be a generic space-vector. It should be remarked that its direct and quadrature components $x_D(t)$ and $x_Q(t)$ can be directly computed from the three-phase variables $x_A(t)$, $x_B(t)$, and $x_C(t)$ and vice versa. The transformation from the three-phase into the biphas variables is called 3/2 transformation, or DQ transformation, while that from the biphas into the three-phase variables is called 2/3 transformation. Both these transformations are linear and depend on the constant factor k in the definition of the space-vector 2.19.

A nonlinear transformation is needed to retrieve the space-vector $x^g = x_x^g + jx_y^g$ expressed in this generic reference frame rotating at the speed ω_g from the corresponding $x(t) = x_D(t) + jx_Q(t)$ expressed in the stationary reference frame:

$$x^g = x_x^g + jx_y^g = xe^{-j\theta_g} \quad (2.20)$$

Decomposing 2.20 in its real and imaginary components, it is possible to compute x_x^g , x_y^g starting from the corresponding components in the stationary reference frame x_D , x_Q as

$$\begin{aligned} x_x^g &= x_D \cos(\theta_g) + x_Q \sin(\theta_g) \\ x_y^g &= -x_D \sin(\theta_g) + x_Q \cos(\theta_g) \end{aligned} \quad (2.21)$$

where the θ_g implies the chosen space vector direction, which has the infinite reference frame. Hence, in Fig. 2.8, the transformation from abc into the dq reference frame is

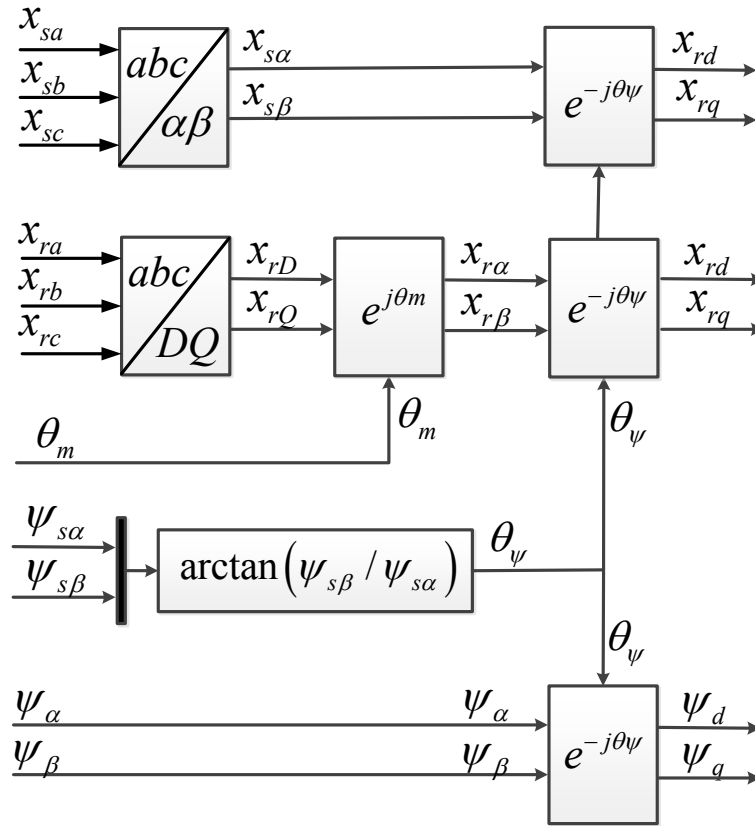


Figure 2.8. WECS transformation to dq reference frame.

illustrated. The x notation represents voltages or currents. For the rotor voltages and currents, only a rotational transformation is required. However, for stator voltages and currents, rotational and Clarke transformations become necessary. Finally, for both stator and rotor fluxes, the DQ components are calculated by means of the rotational transformation. In this case, the DQ reference frame rotates at ω angular frequency. The space vectors referred to this DQ rotating frame also rotate but at different speed, that is, or angular frequency.

Consequently, by applying these last transformations in Fig. 2.8, the space vector diagrams of Fig. 2.6 are converted to the space vector diagrams of Fig. 2.9. In this case, the dq reference frames rotate at θ_m electric pulsation, θ_ψ which denotes stator flux direction, so the space vectors referred to this dq rotating frame are stationary. This leads to constant dq components of the space vector projections, due to this rotating dq axis.

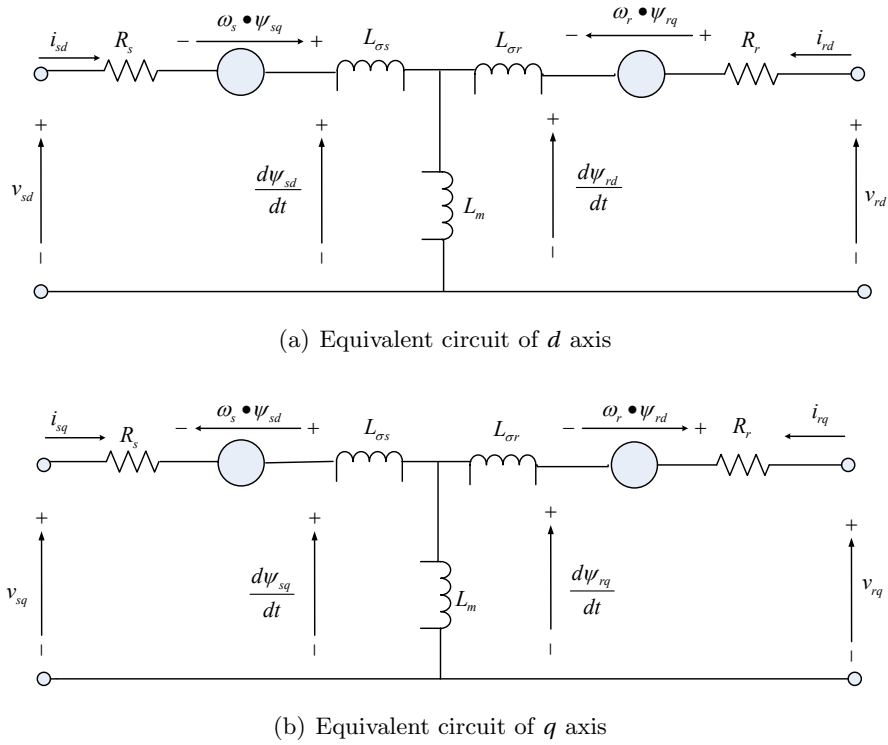


Figure 2.9. dq Model of the DFIM in synchronous coordinates.

Then, it is possible to derive DQ to dq components, from the calculated abc components, without needing a different model of the machine. So, by simply using reference frame transformations, the behavior of the machine is inferred in DQ and dq reference frames.

The fact that the rotor circuit of DFIG is not accessible can be changed if the rotor circuit is wound and made accessible via slip rings, which offers the possibility of controlling the rotor circuit so that the operational speed range of the generator can be increased in a controlled manner.

The dynamic and steady-state model of the DFIG is introduced, which consists of the differential equations to describe the electromagnetic dynamic of the stator and rotor in

synchronous dq frame as follows:

$$\dot{\psi}_{sd} = -R_s i_{rd} + \omega_L \psi_{sq} + v_{sd} \quad (2.22)$$

$$\dot{\psi}_{sq} = -R_s i_{rq} - \omega_L \psi_{sd} + v_{sq} \quad (2.23)$$

$$\dot{\psi}_{rd} = -R_r i_{rd} + (\omega_L - \omega_r) \psi_{rq} + v_{rd} \quad (2.24)$$

$$\dot{\psi}_{rq} = -R_r i_{rq} - (\omega_L - \omega_r) \psi_{rd} + v_{rq} \quad (2.25)$$

$$\psi_{sd} = L_s i_{sd} + L_m i_{rd} \quad (2.26)$$

$$\psi_{sq} = L_s i_{sq} + L_m i_{rq} \quad (2.27)$$

$$\psi_{rd} = L_r i_{rd} + L_m i_{sd} \quad (2.28)$$

$$\psi_{rq} = L_r i_{rq} + L_m i_{sq} \quad (2.29)$$

where the variables, the direct components and quadrature components are represented as d and q for short. The i_{sd} and i_{sq} are stator current viewed from rotating reference of dq parts. Similarly, i_{rd} and i_{rq} are rotor currents. ψ_{sd} and ψ_{sq} are stator flux linkages. ψ_{rd} and ψ_{rq} are rotor flux linkages. L_s , L_r and L_m are the stator, the rotor and the mutual inductance. R_s and R_r are the resistance of the stator and rotor. ω_L is the frequency of the grid.

The mechanical part of the DFIG also has been transferred, generator rotor electrical angular speed ω_r equals $p_r \omega_{rm}$, where p_r is the number of the pole pairs of the generator.

$$\tau_e = \frac{3 L_m}{2 L_s} p_r (\psi_{sq} i_{rd} - \psi_{sd} i_{rq}) \quad (2.30)$$

$$\dot{\omega}_r = p_r \dot{\omega}_m = \frac{p_r}{J} (\tau_t - \tau_e) \quad (2.31)$$

2.2.5 Dynamic reduced order model of WECS

When the system is working in the nominal region, the q-axis of the reference frame is aligned with the stator flux vector. Assuming that the d-axis of the stator reference frame is aligned with the stator flux spatial vector, the stator flux dynamic equations can be rewritten as follows. When the system is working in the nominal region, the q-axis of the reference frame is aligned with the stator flux vector. The stator flux dynamic equations

can be rewritten as follows:

$$\begin{aligned}
 \psi_{sd} &= V_L/\omega_L \\
 \psi_{sq} &= 0 \\
 \dot{\psi}_{sd} &= 0 \\
 \dot{\psi}_{sq} &= 0
 \end{aligned} \tag{2.32}$$

By replacing 2.32 into 2.22–2.29 state equations of the WECS can be expressed as follows,

$$\text{with } x = \begin{bmatrix} i_{rd} & i_{rq} & \omega_r \end{bmatrix}, u = \begin{bmatrix} v_{rd} & v_{rq} \end{bmatrix},$$

$$\dot{x}_1 = -\frac{L_s R_r}{L_{eq}^2} x_1 + (\omega_L - x_3) x_2 + \frac{L_s}{L_{eq}^2} u_{rd} \tag{2.33}$$

$$\dot{x}_2 = -\left(\frac{L_m V_L}{\omega_L L_{eq}^2} + x_1\right)(\omega_L - x_3) - \frac{L_s R_r}{L_{eq}^2} x_2 + \frac{L_s}{L_{eq}^2} u_{rq} \tag{2.34}$$

$$\dot{x}_3 = \frac{\rho \pi r^3 C_p v^2 k_{gb} p_r^2}{2J\lambda} + \frac{3L_m V_L p_r^2}{2JL_s \omega_L} x_2 \tag{2.35}$$

where, $L_{eq}^2 = L_r L_s - L_m^2$.

2.3 State of Arts of Control System

Scalar control of Induction Machines (IM), although yet successfully employed in industry, is not adoptable for those application requiring high dynamic performance (e.g., servo drives, flying shears, rolling mills, robotic manipulators). The open-loop control of the magnetic flux linkage, typical of scalar control, makes the generation of the rated electromagnetic torque of the machine basically impossible at very low and zero speed. Field oriented control (FOC shown in Fig 2.10) of IM drives was introduced almost 30 years ago, but it has been intensively studied and over the last few years, becoming nowadays the industrial standard as far as high-performance IM drives are concerned. Its development has been a significant breakthrough in the field of control of electrical drives with IM since it has permitted the use of this kind of motor for applications where only DC motors offered adequate dynamic performance. FOC permits the IMs to be controlled with dynamic performance comparable with that achievable with DC motor drives, but without the drawbacks caused by the brushes.

speed of rotation around the longitudinal axis of the blades has a bandwidth much greater than that of the control of the angle itself. Given these last two observations, the most standard approach is to represent the loop control, the rate of change of pitch angle, and a linear system of first order containing the main dynamics of the actuator (hydraulic or electric). In fact, when modeling the pitch control, it is very important to model the rate of change of this angle. Indeed, given the effort sustained by the blades, the variation of the pitch must be limited. It is limited to about during normal operation and 20 for emergencies. Regulation of the blade angle is modeled as shown in Fig. 2.11, by a PI controller that generates a reference rate of change of pitch; this reference is limited and a first order system gives the dynamic behavior of speed control of pitch variation. The pitch angle itself is then obtained by integrating the variation of the angle. Pitch control is normally used for large wind turbines. During normal operating conditions with the wind speed in the range from 3 to 15m/s, the pitch angle is set at its optimal value to capture the maximum power from the wind. When the wind speed becomes higher than the rated value, the blade is turned out of the wind direction to reduce the captured power. The blades are turned in their longitudinal axis, changing the pitch angle through a hydraulic or electromechanical device located in the rotor hub attached to a gear system at the base of each blade. As a result, the power captured by the turbine is kept close to the rated value of the turbine.

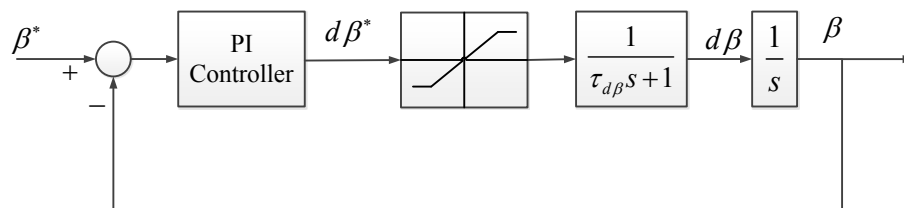


Figure 2.11. *Wind energy conversion system*

2.4 Conclusion

In this chapter, we introduced the system configuration and topology of the wind energy conversion system. And the system has been modeled in electrical and mechanical parts. Space vector of induction machine has been introduced in order to decouple and simplify the DFIG model. Finally, a traditional field oriented control has been designed for the

system. In the following chapter, an advanced adaptive control of the system will be designed based on first order sliding mode control.

Chapter 3

First order ASMC for Uncertain System and Application on WECS

Robust finite time stability of uncertain nonlinear systems has become significant in practice. The uncertainties are assumed to be bound is hard to obtain exactly while it affects the stability in many cases. The call for renewable energy has been growing rapidly during last decade [22]. Wind energy regarded as an environmental friendly alternative energy has attracted much attentions of industry and academy. The main control objective of a wind energy conversion system (WECS) is focus on improving the utilization of the wind energy, which is famously emerged as maximum power point tracking (MPPT) technique [13]. A sensorless control for small WECS has been presented in [77] to promise the maximum power efficiency. [78] adopts a neural network based field oriented controller (FOC) to obtain the optimal tip speed ratio as well as the active power. However, all these controllers do not take consideration of the bounds of the wind speed and other perturbations. As a result, their positive gains of the controllers have to be chosen carefully, as a large value to overcome the perturbations. Sliding mode controllers of WECS have been presented in [25] and [26]. However, the gains of the controllers are fixed. For the robustness, the coefficients of those controllers need to be tuned frequently, according to the varying disturbances and perturbations in practice. As wind is an uncertain resource, the bound of the variation of wind speed affects the stability of WECS. Robust control of WECS has become significant in both theory and practice. The uncertainties are assumed to be bounded physically. Moreover, the knowledge of the bound is hard to obtain exactly while

it affects the precise control of WECS. It follows a challenge to design a robust controller of WECS, where the upper bound of the uncertainty is not requested. The desired controller might not require the knowledge of the uncertainties bound.

The chapter is organized as follows. In section 3.1, the state of arts of adaptive sliding mode control has been discussed. In section 3.2, the theory of a new sliding mode algorithm is introduced, and the mathematical model of the WECS is discussed, and the proposed controller is applied to regulate the WECS. Section 3.3 gives simulation results of the WECS conducted by the controller in MATLAB SIMULINK. Also a comparison algorithm is given to validate the better dynamic performance of the proposed scheme. At last, section 3.4 draws the conclusion.

3.1 Introduction

For the cases of unknown bounds, adaptive sliding mode (ASM) controllers have been presented in [27] [28] firstly. Huang et al. [29] develops an adaptive controller which can work without the bound values. The controller of [29] need not to know the bound of uncertainties, or other disturbances comprised in the system. The gain of the controller is dynamically tuned in order to ensure the convergence of a sliding variable. However, the algorithm can only increase the gain, which leads the gain over-estimation. An important design goal for an adaptive controller is to ensure a dynamical adaptation of the control gain as small as possible. In order to adaptive the gain, many controllers have been published [79]. However, methods proposed in those papers can not guarantee the tracking performances. Furthermore, the gain dynamics equals to zero, when the sliding variable converges to zero. It leads the controller stop working. As the boundary layer width affects accuracy and robustness, boundary layer width tuning methodology is provided in [79]. However, this approach requires the knowledge of uncertainties and disturbances. One of the adaptive sliding mode controller proposed in [1] (by Plestan et al.) must be mentioned to solve the problems above. Plestan et al. [1] present a novel controller of a bounded uncertain system without the problem of gain over-estimation. However, this algorithm is not able to guarantee the sliding variable converge to an exact neighborhood. As for [30], the gain is adjusted properly to get a sufficient value to counteract the uncertainties, but the state still has overshooting around the neighborhood. Other works design an adaptive first or higher order sliding mode in [31, 32, 33, 2, 34, 35, 36, 37, 38].

A super twisting ASM controller in [31] can continuously force the sliding variable and its first derivative to zero with unknown boundary. [32] presents an adaptive twisting SMC without gain over-estimation, which is a further development of [31]. [33] presents a super twisting ASM controller aiming to reduce chattering effect, and it is applied for an electro-pneumatic actuators system. An integral high order ASM controller in [2] eliminates the need of knowledge about the upper bound of the uncertainties. The ASM controller in [39] converges a perturbed chains of integrators to a neighborhood of zero without the prior knowledge of the perturbation bound. [35] proposes a twisting ASM controller and observer with unknown boundaries. [36] develops high order ASM controller based on a first order ASM of unknown bound perturbed system. Discrete time ASM controller is considered in [37] which rejects the unknown bounded disturbance varying slowly with respect to the sample frequency. [38] is an advanced ASM controller of multi-input multi-output system. However, the common drawback for all these works is that the insurance of forcing the sliding variable inside the neighborhood of zero does not exist.

In our approach, the sliding variable converges to a predefined neighborhood without any overshooting. According to the knowledge of authors, it is the first work attributing this performance. This approach has been studied in this thesis for first order system. Our future objective is to generalize this first step for arbitrary order.

As recalled previously, this problem is a challenge for some applications, when the sliding mode is achieved. But its adaptive gain is overestimated after reaching of its sliding mode.

In this chapter, we present Lyapunov-based adaptive first order sliding mode controller of WECS. The advantage is that in the case where the bound of the uncertainty is unknown, the controller is able to converge the sliding variable to a predefined neighborhood of the origin and never get out of it. Additionally, it presents interest to develop the application of the proposed algorithm, which is an ideal option to control the uncertain WECS operating in perturbed environments. This new adaptive controller results following attractive characteristics:

- Insurance of convergence to a predefined neighborhood of zero without any overshooting
- Rapid adaptation dynamically responses to the error

3.2 Theoretical study

In this section, the theory of the algorithm is studied with the proof based on Lyapunov analysis. Additionally, the BH algorithm is compared with the similar work of Plestan et al. [1].

3.2.1 Problem formulation

Recall the classical problem formulation presented in [1].

The control objective is to stabilize the continuous function $s(x, t)$. Suppose that s has a relative degree 1 with respect to the controller u , and the derivation of the sliding variables as:

$$\begin{aligned} \dot{s} &= \frac{\partial}{\partial x} [s] [f(x) + g(x)u] \\ &= \underbrace{\frac{\partial s}{\partial t} + \frac{\partial s}{\partial x} f(x)}_{\varphi(x,t)} + \underbrace{\frac{\partial s}{\partial x} g(x)}_{\gamma(x,t)} \cdot u \\ &= \varphi(x, t) + \gamma(x, t) u \end{aligned} \quad (3.1)$$

The functions $\varphi(x, t)$ and $\gamma(x, t)$ are supposed to be bounded and satisfy the following assumptions

$$0 < \gamma_m \leq \gamma(x, t) \leq \gamma_M, \quad |\varphi(x, t)| \leq \varphi_M, \quad (3.2)$$

where γ_m , γ_M and φ_M are unknown positive constants.

Remark 1. *In our study, we don't use any assumptions for the time derivative of $\varphi(x, t)$ and $\gamma(x, t)$.*

3.2.2 Idea behind the proposed controller

The controller has an objective to force the sliding variable s to a neighborhood of zero $|s| \leq \varepsilon$ for some positive predefined ε . Our idea consists of forcing s in finite time to a smaller neighborhood defined by $|s| \leq \varepsilon/2$ by increasing the gain as in [1]. Then the controller forces s to remain in the predefined neighborhood ($|s| \leq \varepsilon$) for all consecutive time by creating some unreachable edge on $|s| = \varepsilon$.

3.2.3 Main result

Consider the following controller

$$u = -K(s, t) \cdot \text{sign}(s), \quad (3.3)$$

where K is the adaptive gain defined as

$$\begin{aligned} \dot{K} &= k_1 \quad \text{until } |s| < \frac{\varepsilon}{2}, \\ K &= \frac{\varepsilon \bar{K}}{\varepsilon - |s|} \quad \text{later,} \end{aligned} \quad (3.4)$$

with $K(0)$, \bar{K} and k_1 are arbitrary positive constants.

Then there exist a finite time T and a constant $\bar{\varepsilon} < \varepsilon$, such that

$$\begin{aligned} \text{(i)} \quad & \forall t \geq T, |s| \leq \max(0, \bar{\varepsilon}), \\ \text{(ii)} \quad & \limsup |u| \leq \max(\bar{K}, \frac{\varphi_M}{\gamma_m}). \end{aligned} \quad (3.5)$$

Proof. The proof is given in two steps.

First step: Convergence of s to $|s| \leq \varepsilon/2$.

We assume first that the initial condition of s satisfies $|s| > \varepsilon/2$, then the adaptive gain can be defined by $\dot{K} = k_1$. In this case the convergence is evident.

Second step: s remains in $|s| \leq \varepsilon$.

We assume now that the initial condition in this phase satisfies $|s| \leq \varepsilon/2$, and we proof that for all next time that $|s| \leq \varepsilon$.

Consider the Lyapunov Function $V = \frac{1}{2}s^2$, then its time derivative can be given as follows

$$\begin{aligned} \dot{V} &= s(\varphi + \gamma u) \\ &= s \cdot \varphi - s \cdot \gamma \cdot \frac{\bar{K} \cdot \text{sign}(s)}{\varepsilon - |s|} \\ &\leq |s| \cdot \bar{\varphi} - \frac{|s| \cdot \gamma_m \cdot \bar{K} \cdot \varepsilon}{\varepsilon - |s|} \\ &= -\frac{|s|}{\varepsilon - |s|} \cdot (\gamma_m \cdot \bar{K} \cdot \varepsilon - \bar{\varphi} \cdot \varepsilon + |s| \cdot \bar{\varphi}) \end{aligned} \quad (3.6)$$

It's easy to get that $\dot{V} < 0$, for $\max(0, \bar{\varepsilon}) < |s| < \varepsilon$, where

$$\bar{\varepsilon} = \varepsilon \left(1 - \frac{\gamma_m \bar{K}}{\bar{\varphi}} \right). \quad (3.7)$$

This proves the item (4.10 (i)).

As the adaptive gain K is monotonous for $s \in (0, \varepsilon)$, then by simple computation one gets that

$$\limsup |u| \leq \max(|u|_{(s=0)}, |u|_{(s=\varepsilon)}). \quad (3.8)$$

This ends the proof. □

In order to illustrate the theory, we fix our objective to force s to $|s| \leq \varepsilon = 0.2$. We consider the following simulations in Fig. 3.1 and Fig. 3.2.

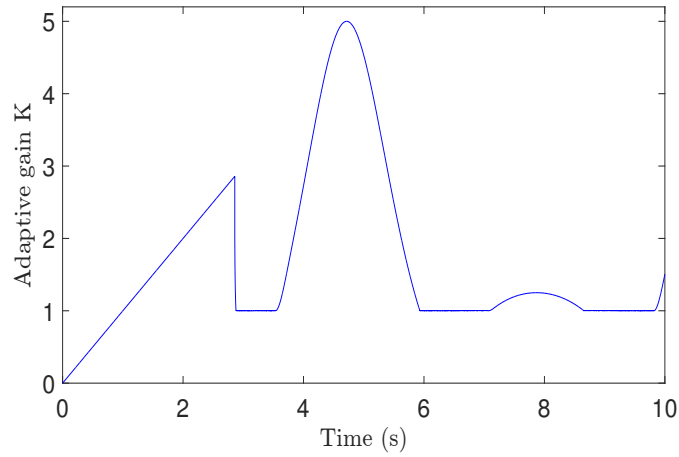


Figure 3.1. Behavior of adaptive gain K

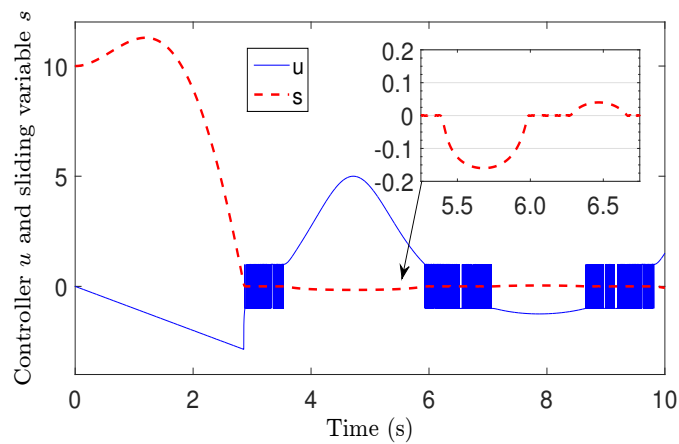


Figure 3.2. Controller u and sliding variable s

The adaptive gain $K(t)$ will increase and it forces the sliding variable s to converge to a small neighborhood of zero ($|s| \leq 0.1$) in around 3 second. Then it will force s to remain in $|s| \leq \varepsilon = 0.2$ for all subsequent time.

3.2.4 Discussion and comparison

In the study of [1], the neighborhood of convergence is defined by $|s| \leq \bar{\varepsilon}_p$, where $\bar{\varepsilon}_p$ is defined as

$$\bar{\varepsilon}_p = \sqrt{\varepsilon^2 + \frac{\varphi_M^2}{\bar{K}\gamma_m}} \quad (3.9)$$

Clearly, $\bar{\varepsilon}_p > \varepsilon$ means that the neighborhood of convergence is greater than the required. In addition it can not be estimated as φ_M and γ_m are unknown.

Otherwise, in our result we get

$$\bar{\varepsilon} = \varepsilon \left(1 - \frac{\gamma_m \bar{K}}{\bar{\varphi}} \right) < \varepsilon. \quad (3.10)$$

We can ensure the convergence for predefined region. To our best knowledge, it is the first work that get such a result.

3.2.5 Control objective

As the Fig. 3.3 shows that the power coefficient curves have the unique maximum point $C_{p\max}$, which are related to the optimal tip-speed ratio λ_{opt} . A limit on the amount of the power that can be captured from the wind is known as the Betz Limit which is approximately 59.3% of the attainable kinetic power. Considering the imperfection of the turbine, this value will drop. Fig. 3.3 depicts the relationship of C_p versus λ curve, the maximum value of C_p is 0.4953 ($C_{p\max} = 0.4953$), and the respective λ_{opt} is 7.2.

The control problem addressed in this thesis is to regulate the torque and the reactive power as follows:

$$\begin{aligned} e_Q &= Q(t) - Q_{ref}(t) < \varepsilon_d \\ e_\tau &= \tau_e(t) - \tau_{opt}(t) < \varepsilon_q \end{aligned} \quad (3.11)$$

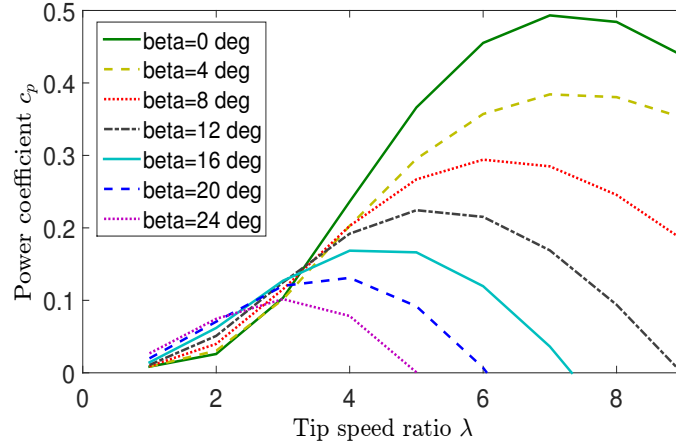


Figure 3.3. Power coefficient versus tip-speed ratio in different pitch angle

The torque developed by the machine and the reactive power injected by the system into the grid can be written as:

$$Q = \frac{3}{2} V_L \left(\frac{L_m}{L_s} i_{rd} - \frac{V_L}{L_s \omega_L} \right) \quad (3.12)$$

$$\tau_e = -\frac{3}{2} \frac{L_m V_L}{L_s \omega_L} p_r i_{rq} \quad (3.13)$$

For the turbine torque given in (4.46-4.46), to achieve MPPT objective, the torque could be rewritten as:

$$\tau_{opt}(t) = \frac{P_{max}}{\omega_t} = \frac{1}{2} \rho \pi r^5 C_{pmax} \frac{\omega_r^2 p_r^2}{\lambda_{opt}^3 k_{gb}^3} \quad (3.14)$$

To simplify the expression, a coefficient k_{opt} describing the relationship between torque and rotor speed is defined as:

$$k_{opt} = \frac{1}{2} \rho \pi r^5 \frac{C_{pmax}}{\lambda_{opt}^3} \quad (3.15)$$

3.2.6 Adaptive sliding mode controller application

Define the sliding variables equal to the errors of the control variables:

$$s_d(t) = e_Q = Q(t) - Q_{ref}(t) \quad (3.16)$$

$$s_q(t) = e_\tau = \tau_e(t) - \tau_{opt}(t) \quad (3.17)$$

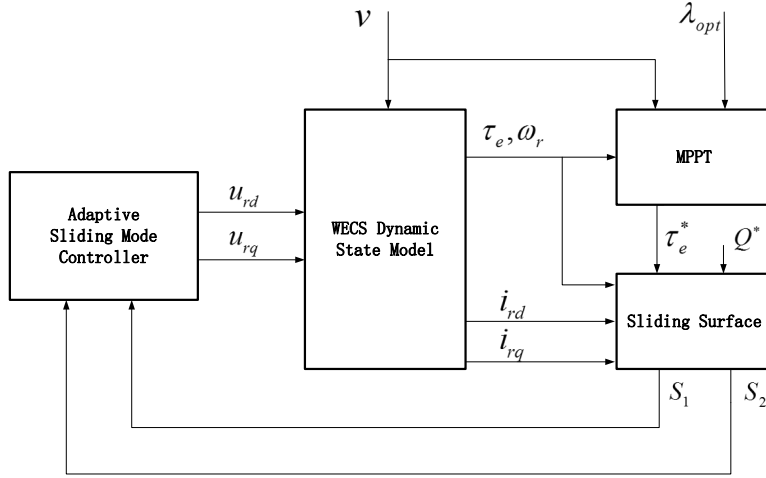


Figure 3.4. Control system block diagram

The control objective is to steer the variables $s = [s_d, s_q]$ and its first time derivative \dot{s} to a predefined region ε in finite time. From (4.61-3.17), we have:

$$s_d(x) = \frac{3}{2} V_L \left(\frac{L_m}{L_s} i_{rd} - \frac{V_L}{L_s \omega_L} \right) - Q_{ref}(t) \quad (3.18)$$

$$s_q(x) = -\frac{3}{2} \frac{L_m V_L}{L_s \omega_L} p_r i_{rq} - \frac{k_{opt}}{p_r^2 k_{gb}^3} \omega_r^2 \quad (3.19)$$

The first order derivative of sliding variables \dot{s}_d and \dot{s}_q are:

$$\dot{s}_d = \underbrace{-\frac{3}{2} \frac{L_m R_r V_L}{L_{eq}^2} x_1 + \frac{3}{2} \frac{L_m V_L}{L_s} (\omega_L - x_3) x_2}_{\varphi_d} - \underbrace{\frac{\partial}{\partial x} Q_{ref}}_{\varphi_d} + \underbrace{\frac{3}{2} \frac{L_m V_L}{L_{eq}^2} u_{rd}}_{\gamma_d} \quad (3.20)$$

$$\begin{aligned}
\dot{s}_q = & \underbrace{\frac{3}{2} \left(\frac{L_m^2 V_L^2 p_r}{L_s \omega_L^2 L_{eq}^2} + \frac{L_m V_L p_r}{L_s \omega_L} x_1 \right)}_{\varphi_q} (\omega_L - x_3) \\
& - \underbrace{\frac{k_{opt}}{k_{gb}^3} \left(\frac{\rho \pi r^3 C_p v^2 k_{gb}}{J \lambda} + \frac{3 L_m V_L}{J L_s \omega_L} x_2 \right)}_{\varphi_q} x_3 \\
& + \underbrace{\frac{3 L_m V_L R_r p_r}{2 L_{eq}^2 \omega_L} x_2}_{\varphi_q} - \underbrace{\frac{3 L_m V_L p_r}{2 L_{eq}^2 \omega_L} u_{rq}}_{\gamma_q}
\end{aligned} \tag{3.21}$$

The control diagram of the system is shown in Fig. 3.4. The block of MPPT control provides optimal value of the torque, the sliding mode surface is generated by the states. Finally, the proposed controller gives rotor voltages to the system.

3.3 Simulation results

The implementation of the wind turbine aerodynamics, generator dynamics, and sliding mode control architecture in SIMULINK are shown from Fig. 3.5 to Fig. 3.13. The wind speed model is generated by a test function, which is able to produce varying degrees of wind speed variations. This particular wind speed function is chosen to demonstrate the effectiveness of the controller design because of its highly time-varying, and the wide range.

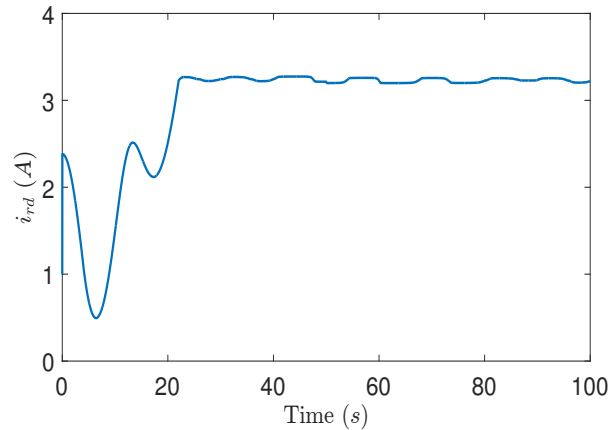


Figure 3.5. Controlled direct-axis current i_{rd}

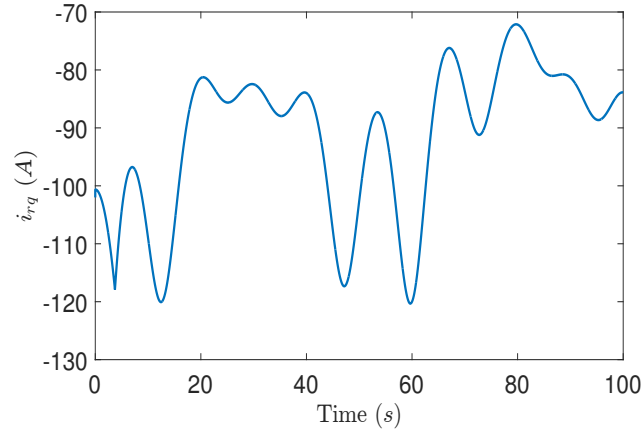


Figure 3.6. Controlled quadrature-axis current i_{rq} of the rotor

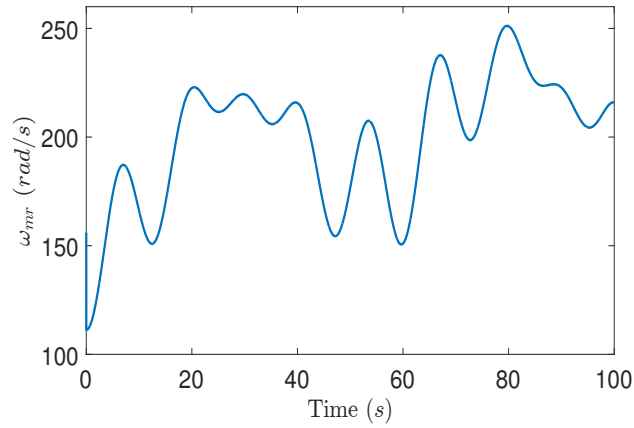


Figure 3.7. Controlled mechanic rotation speed ω_{mr}

The first test results shown in Fig. 3.5 and 3.6 are that of the d-axis rotor current $i_{rd}(t)$ and the q-axis rotor current $i_{rq}(t)$. As can be seen by Fig. 3.5 and 3.6, the $i_{rd}(t)$ and $i_{rq}(t)$ curves controlled by the proposed algorithm are stable and clear. The mechanic rotation speed ω_{mr} in Fig. 3.7 is presented in the same environment, and the controller depicts good performance in transient process during system tuning. It is clear from the figures that the proposed controller is robust against wind speed variations.

Fig. 3.8 to Fig. 3.13 show the performance of the two sliding controllers. Fig. 3.8 and Fig. 3.9 show the controllers u_{rd} and u_{rq} . Fig. 3.10 and Fig. 3.11 depict the adaptive gain K_d and K_q of u_{rd} and u_{rq} . The gain linearly increases before 0.3 sec. Until the errors converge

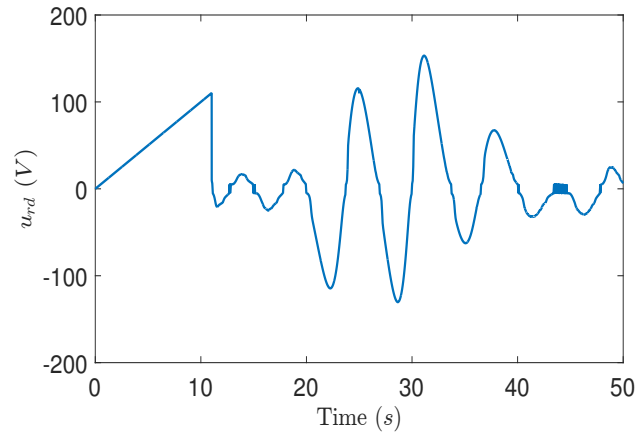


Figure 3.8. Direct-axis controller u_{rd}

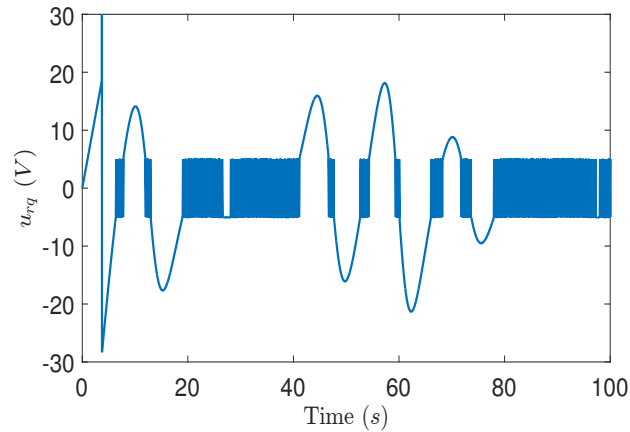


Figure 3.9. Quadrature-axis controller u_{rq}

to the region predefined by ε , the algorithm is changed to the second part. The zoom-in pictures of Fig. 3.12 and Fig. 3.13 show that the errors will never exceed the predefined limit $\varepsilon_d = 10 \text{ var}$ and $\varepsilon_q = 0.1 \text{ Nm}$, which are sufficiently small errors for WECS control. Fig. 3.12 and Fig. 3.13 are curves of the sliding variables s_d and s_q , which stands for the error of torque and the error of the reactive power. The errors of the sliding variables are extremely small compared with the work in [25], where the vibration of the system is greater than $3Nm$.

The second simulation results of a comparison work are shown in Fig. 3.14 and Fig. 3.15. The sliding variables with another adaptive controller of Plestan et al.[1] method

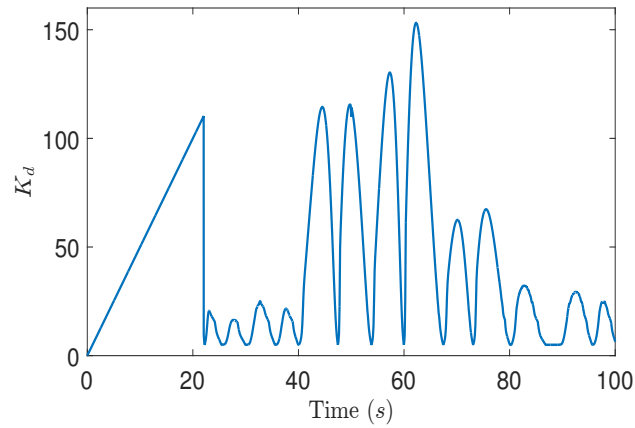


Figure 3.10. Adaptive gain K_d of direct-axis controller u_{rd}

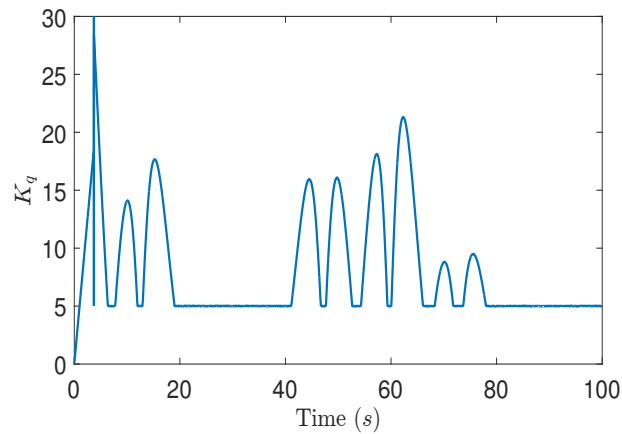


Figure 3.11. Adaptive gain K_q of quadrature-axis controller u_{rq}

are applied in the same WECS, for the same control objective as well. It should be noted that, the errors of the compared controller of Plestan et al. exceed the convergence neighborhood $\varepsilon_d = 10 \text{ var}$ and $\varepsilon_q = 5 \text{ Nm}$. The simulations depict that the proposed controller can constrain the tracking error in the predefined neighborhood ε without any overshooting, and for this reason we obtain better control performance from the proposed controller.

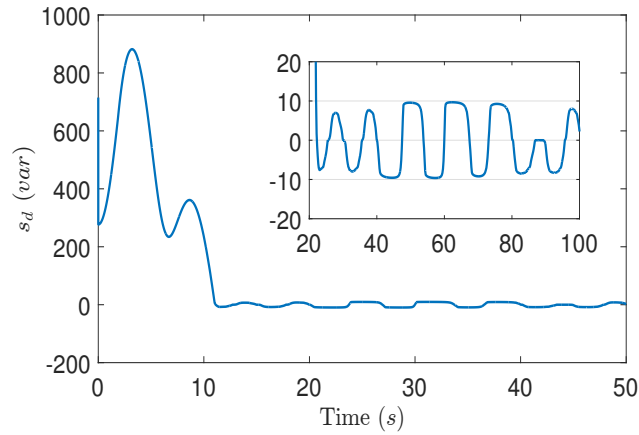


Figure 3.12. Sliding variable s_d in case of the proposed algorithm

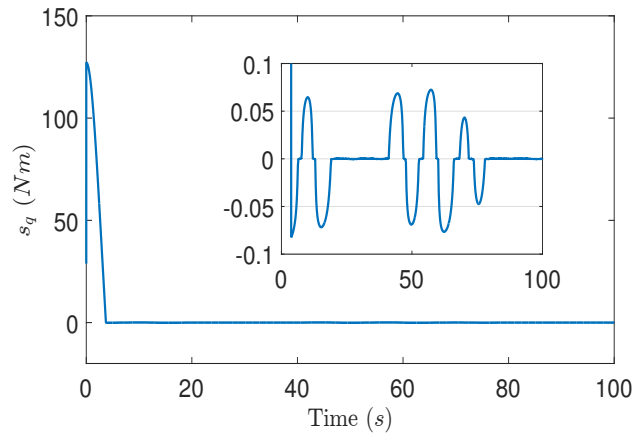


Figure 3.13. Sliding variable s_q in case of the proposed algorithm

3.4 Conclusion

This chapter presents a novel first order Lyapunov based adaptive controller. It allows the sliding variable to converge to a predefined neighborhood without any over-estimation. Then we apply the proposed controller to the wind energy system. Finally, we compared another adaptive controller adopting the method of Plestan et al. [1] with our algorithm. The simulation results show that the tracking error controlled by the proposed algorithm will never escape from the convergence region predefined. It means the proposed controller has a better control character.

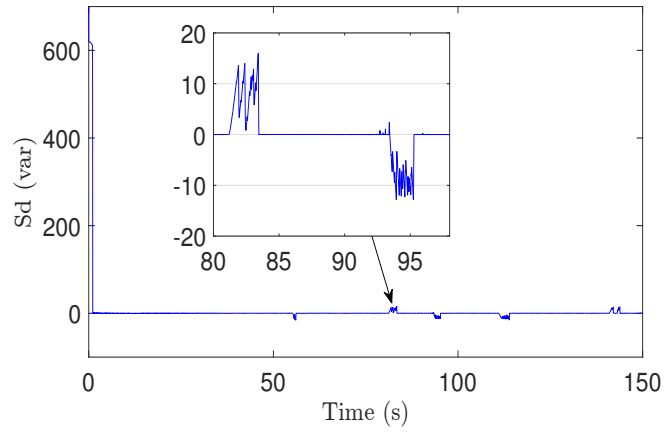


Figure 3.14. Sliding variable s_d in case of Plestan et al. [1] algorithm

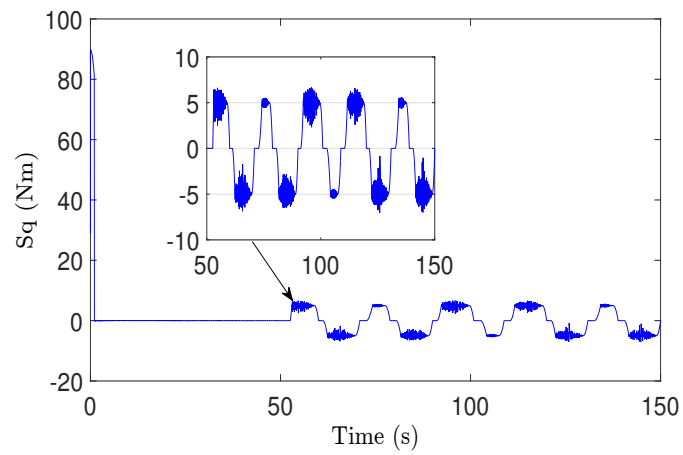


Figure 3.15. Sliding variable s_q in case of Plestan et al. [1] algorithm

Chapter 4

Adaptive HOSM Control for Uncertain System and Application on WECS

4.1 Introduction

Control under uncertainty condition, including parameter variation, unmodeled dynamic and external disturbance, has attracted much attention of modern control theory [80].

Sliding mode control (SMC) is one of the most powerful control strategy for its robustness against internal and external perturbances [21]. Due to the use of discontinuous function, the chattering phenomenon occurs, which is the main disadvantage of the conventional SMC for its implementation in a wide range of applications [42]. High order sliding mode (HOSM) controllers have been presented, in [81, 82, 83, 84], which allow to attenuate the chattering. In addition, HOSM control can remove the conventional relative degree restrictions [57]. However, those controllers do not have constructive algorithm for the gain tuning, and they require the knowledge of uncertainties bound which are usually overestimated.

[?, 85, 2] present adaptive sliding mode (ASM) controllers which do not require the knowledge of uncertainties bound. The dynamical adaptation of the control law design focuses on tuning a large gain to conquer the perturbations. However, in those works, their dynamic adaptation laws only have increasing gains, which inevitably arise gain overestimation leading to undesirable chattering. [38, 1] present ASM controllers using dynamic control

law with a decreasing gain after convergence which solve the gain overestimation problem. However, the gain decreases very slowly, in some approach it needs large time for the controller to be adjusted to a proper value. Also the control law does not guarantee that the sliding variable remains inside the neighborhood after convergence. [30, ?] present a controller to converge the states to a neighborhood of the origin, but the states may overshoot this neighborhood. [35, 86] present adaptive HOSM controllers, and [28, 87, 37, 88] presents discrete time ASMC. However, their states are not able to converge to a neighborhood rigidly. To our best knowledge, there is no contemporary work can ensure the convergence to a predefined neighborhood of origin.

In this chapter, we present a new Lyapunov-based adaptive HOSM controller for nonlinear systems. The problem has been formulated as the stabilization of a perturbed integral chain with unknown bounded uncertainties. Our main contribution is that the proposed controller can converge the sliding variables to a predefined neighborhood of origin without any overshooting. Additionally, the controller has been applied on a wind energy conversion system (WECS) to prove its advantages. A variable speed WECS is a high nonlinear system with unknown but physically bounded uncertainties. The controller of WECS is designed to maximize the active power and regulate the reactive power, which is so-called maximum power point tracking (MPPT) technique [13, 22, 24, 89]. And owing to the main attractive advantage of the controller, the controlled states have an exact convergence to the predefined neighborhoods. It helps alleviate the mechanical stress without chattering problem by generating continuous control input.

The chapter is organized as follows. Section II briefly discusses the problem formulation and the assumptions. Section III shows the design of the high order sliding mode controller with a $r - th$ order integral chain approach. The application on a wind energy conversion system example is carried out in Section VI with simulation results. Section V concludes the work.

4.2 Problem Formulation and Control Objective

Consider a nonlinear system

$$\begin{cases} \dot{x} = f(x) + g(x)u \\ y = \sigma(x) \end{cases} \quad (4.1)$$

where $x \in \mathbb{R}^n$ is the state vector, and $u \in \mathbb{R}$ is the control input. $y \in \mathbb{R}$ is the measured output function. $\sigma \in \mathbb{R}$ is known as the sliding variable. $f(x)$ and $g(x)$ are uncertain bounded smooth functions, and $g(x) \neq 0$.

Assumption 2. - *The relative degree of the system assumed to be constant and equal to r . This means that the controller will appear for the first time in the r -th time derivative.*

Assumption 3. - *The r -th order derivative of σ satisfies the following equation*

$$\sigma^r = \varphi(\cdot) + \gamma(\cdot)u \quad (4.2)$$

where, the functions $\varphi(\cdot) = L_f^r \sigma$ and $\gamma(\cdot) = L_g L_f^{r-1} \sigma$.

Assumption 4. *Functions $\varphi(\cdot)$ and $\gamma(\cdot)$ are supposed to be bounded. There exist unknown positive constants $\gamma_m, \gamma_M, \varphi_M$ that*

$$0 < \gamma_m \leq \gamma(\cdot) \leq \gamma_M, \quad |\varphi(\cdot)| \leq \varphi_M \quad (4.3)$$

Represent the system by a r -th order integral chain as:

$$\left\{ \begin{array}{l} \dot{z}_1 = z_2 \\ \dot{z}_2 = z_3 \\ \vdots \\ \dot{z}_{r-1} = z_r \\ \dot{z}_r = \varphi(\cdot) + \gamma(\cdot)u \end{array} \right. \quad (4.4)$$

where $(\sigma, \dot{\sigma}, \dots, \sigma^{r-1}) = (z_1, z_2, \dots, z_r)$.

The control objective consists of forcing the states z_1 and its first $(r-2)$ -th time derivatives $(z_1, z_2, \dots, z_{r-1})$ to an arbitrary predefined neighborhood of zero with the respect of the states z_i in (4.4). This means

$$\limsup_{z \rightarrow \infty} |z_i| \leq \Delta_i, \quad i = 1, \dots, (r-1) \quad (4.5)$$

where, the positive parameters $\Delta_1, \Delta_2, \dots, \Delta_{r-1}$ are predefined.

Before the control design, we recall the boundary layer definition.

Definition 1. In a μ -vicinity of the origin, the so-called boundary layer $sat_\mu(\cdot)$ is defined as follows [90]. For $|s| > \mu$, $sat_\mu(s)$ is just equal to $sign(s)$. For $|s| \leq \mu$, $sat_\mu(s)$ is continuous shown in Fig. 4.1.

$$sat_\mu(s) = \begin{cases} sign(s), & \text{for } |s| > \mu \\ \frac{s}{\mu}, & \text{for } |s| \leq \mu \end{cases} \quad (4.6)$$

where μ is arbitrary positive constant.

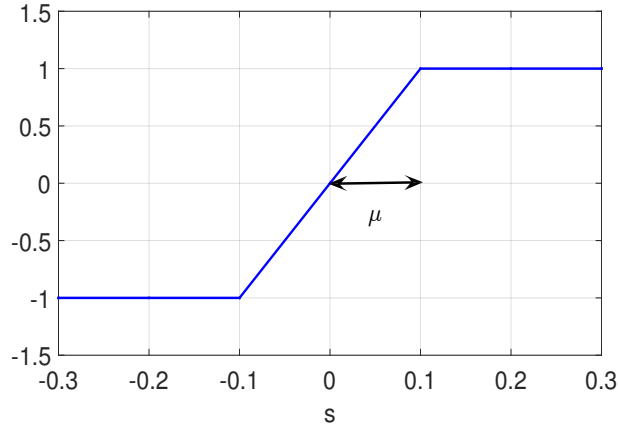


Figure 4.1. Function $sat_\mu(s)$

4.3 Control design

In this section, we design the controller in two steps. Firstly, the new adaptation algorithm for the first order system has been introduced. The continuous controller forces one integrator system converge to a predefined neighborhood of zero. Secondly, we cope the recalled the first order controller with a linear controller ω_{nom} which can stabilize a $(r-1)$ -th order integral chain. The controller converges $(r-1)$ -th order integrators to a predefined neighborhood.

4.3.1 First order controller

Consider the perturbed one integrator system

$$\dot{s} = \Phi(\cdot) + \Gamma(\cdot)u \quad (4.7)$$

with the bounded functions $\Gamma(\cdot), \Phi(\cdot)$ that

$$0 < \Gamma_m \leq \Gamma(\cdot) \leq \Gamma_M, \quad |\Phi(\cdot)| \leq \Phi_M \bar{\Phi}(x, t) \quad (4.8)$$

where $\Gamma_m, \Gamma_M, \Phi_M$ are unknown positive constants, and $\bar{\Phi}(x, t)$ is a known positive function which depends on state and time.

Theorem 2. *Consider the following controller*

$$u = \begin{cases} u_1 = -(k_1 t + k_2 \bar{\Phi}^2) \text{sat}_{\frac{\varepsilon}{2}}(s) & \text{until } |s| < \frac{\varepsilon}{2}, \\ u_2 = -\left(\frac{k_3}{1 - \frac{|s|}{\varepsilon}} + k_2 \bar{\Phi}^2\right) \text{sat}_{\frac{\varepsilon}{2}}(s) & \text{later,} \end{cases} \quad (4.9)$$

where k_1, k_2, k_3 are arbitrary positive constants. Then there exist a finite time t_T and constant $\bar{\varepsilon} < \varepsilon$, such that

$$\begin{aligned} (i) \quad & \forall t \geq t_T, \limsup |s| \leq \max\left(\frac{\varepsilon}{2}, \bar{\varepsilon}\right), \\ (ii) \quad & \limsup |u_2| \leq \max\left(k_3 + k_2 \bar{\Phi}^2, k_2 \left(\frac{\Phi_M^2}{4\Gamma_m^2 k_2^2} + \bar{\Phi}^2\right)\right). \end{aligned} \quad (4.10)$$

The function $\frac{k_3}{1 - \frac{|s|}{\varepsilon}}$ is depicted in Fig. 4.2. The proof of (4.10) is given as follows. Item

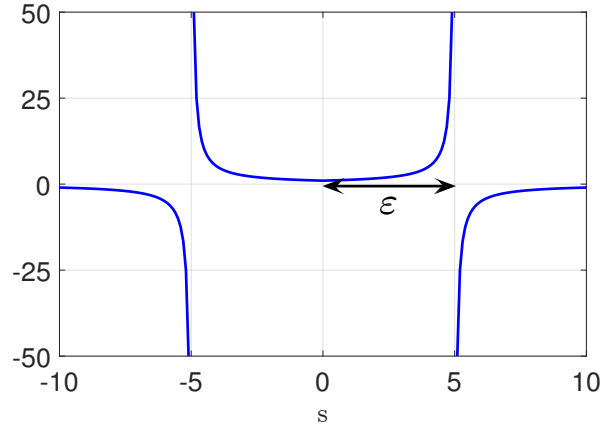


Figure 4.2. Function $\frac{k_3}{1 - \frac{|s|}{\varepsilon}}$

(4.10 (i)) and item (4.10 (ii)) are proved separately. For the attraction condition $s\dot{s} < 0$, interested reader could refer to Khalil's book [41].

Proof. The proof of item (4.10 (i)) is split into two steps. For the first step, we show that u_1 yield for the attraction condition $s\dot{s} < 0$ after t_T , where $|s| > \frac{\varepsilon}{2}$. We provide the proof that s will converge to the neighborhood $|s| < \frac{\varepsilon}{2}$ in finite time. For the second step of the proof (4.10 (i)), once the sliding variable reaches the neighborhood of $|s| \leq \frac{\varepsilon}{2}$, the u_2 works for the finite time convergence, and forces the sliding variable stay in the neighborhood ε .

Suppose that $|s| > \frac{\varepsilon}{2}$ at the beginning,

$$\begin{aligned} s\dot{s} &= s(\Phi + \Gamma u) \\ &= s[\Phi - \Gamma(k_1 t + k_2 \bar{\Phi}^2)] \text{sat}_{\frac{\varepsilon}{2}}(s) \\ &\leq |s| \left(\Phi_M \bar{\Phi} - \Gamma_m k_2 \bar{\Phi}^2 \left| \text{sat}_{\frac{\varepsilon}{2}}(s) \right| - \Gamma_m k_1 t \left| \text{sat}_{\frac{\varepsilon}{2}}(s) \right| \right) \end{aligned} \quad (4.11)$$

for $|s| > \frac{\varepsilon}{2}$ we have $\text{sat}_{\frac{\varepsilon}{2}}(s) = \text{sign}(s)$

$$\begin{aligned} s\dot{s} &\leq |s| (\Phi_M \bar{\Phi} - \Gamma_m k_2 \bar{\Phi}^2 - \Gamma_m k_1 t) \\ &= -|s| \Gamma_m k_2 \left(\bar{\Phi}^2 - \frac{\Phi_M \bar{\Phi}}{\Gamma_m k_2} + \frac{k_1}{k_2} t \right) \\ &= -|s| \Gamma_m k_2 \left[\left(\bar{\Phi} - \frac{\Phi_M}{2\Gamma_m k_2} \right)^2 - \frac{\Phi_M^2}{4\Gamma_m^2 k_2^2} + \frac{k_1}{k_2} t \right] \\ &= -|s| \Gamma_m k_2 \left[\left(\bar{\Phi} - \frac{\Phi_M}{2\Gamma_m k_2} \right)^2 + \frac{k_1}{k_2} \left(t - \frac{\Phi_M^2}{4\Gamma_m^2 k_2 k_1} \right) \right] \end{aligned} \quad (4.12)$$

Thus, after a finite time, $t_T = \frac{\Phi_M^2}{4\Gamma_m^2 k_2 k_1}$, we get $s\dot{s} < 0$. $|s|$ is decreasing to reach $|s| \leq \frac{\varepsilon}{2}$ in finite time. Then u_2 begins to work for forcing the sliding variable inside the neighborhood $|s| \leq \bar{\varepsilon}$.

Then, suppose that once $|s| \leq \frac{\varepsilon}{2}$,

$$\begin{aligned} s\dot{s} &= s(\Phi + \Gamma u) \\ &= s \left[\Phi - \Gamma \left(\frac{k_3}{1 - \frac{|s|}{\varepsilon}} + k_2 \bar{\Phi}^2 \right) \right] \text{sat}_{\frac{\varepsilon}{2}}(s) \\ &\leq |s| \left(\Phi_M \bar{\Phi} - \Gamma_m k_2 \bar{\Phi}^2 \left| \text{sat}_{\frac{\varepsilon}{2}}(s) \right| - \frac{\Gamma_m k_3}{1 - \frac{|s|}{\varepsilon}} \left| \text{sat}_{\frac{\varepsilon}{2}}(s) \right| \right) \end{aligned} \quad (4.13)$$

The worst case is to take consideration of $|s| > \frac{\varepsilon}{2}$. We have $\text{sat}_{\frac{\varepsilon}{2}}(s) = \text{sign}(s)$

$$\begin{aligned}
s\dot{s} &\leq |s| \left(\Phi_M \bar{\Phi} - \Gamma_m k_2 \bar{\Phi}^2 \left| \text{sat}_{\frac{\varepsilon}{2}}(s) \right| - \frac{\Gamma_m k_3}{1 - \frac{|s|}{\varepsilon}} \left| \text{sat}_{\frac{\varepsilon}{2}}(s) \right| \right) \\
&= -|s| \left(\Gamma_m k_2 \bar{\Phi}^2 - \Phi_M \bar{\Phi} + \frac{\Gamma_m k_3}{1 - \frac{|s|}{\varepsilon}} \right) \\
&= -|s| \Gamma_m k_2 \left(\bar{\Phi}^2 - \frac{\Phi_M}{\Gamma_m k_2} \bar{\Phi} + \frac{k_3}{k_2 \left(1 - \frac{|s|}{\varepsilon}\right)} \right) \\
&= -|s| \Gamma_m k_2 \left[\left(\bar{\Phi} - \frac{\Phi_M}{2\Gamma_m k_2} \right)^2 - \frac{\Phi_M^2}{4\Gamma_m^2 k_2^2} + \frac{k_3}{k_2 \left(1 - \frac{|s|}{\varepsilon}\right)} \right]
\end{aligned} \tag{4.14}$$

As a result, the upper bound of the sliding variable is given that

$$\limsup |s| \leq \max\left(\frac{\varepsilon}{2}, \bar{\varepsilon}\right) < \varepsilon$$

where, $\bar{\varepsilon} = \varepsilon \left(1 - \frac{4\Gamma_m^2 k_2 k_3}{\Phi_M^2}\right) < \varepsilon$.

This proves item (4.10 (i)).

□

Then we provide the proof of (4.10 (ii)). The upper bound of the controller has been ensured.

Proof. For $|s| \in (0, \bar{\varepsilon})$, the adaptive gain is monotonous. We estimate a bound of u_2

$$\begin{aligned}
|u_2| &= \left| - \left(\frac{k_3}{1 - \frac{|s|}{\varepsilon}} + k_2 \bar{\Phi}^2 \right) \right| \left| \text{sat}_{\frac{\varepsilon}{2}}(s) \right| \\
&= k_2 \left(\frac{k_3}{k_2 \left(1 - \frac{|s|}{\varepsilon}\right)} + \bar{\Phi}^2 \right)
\end{aligned} \tag{4.15}$$

When $|s| \leq \bar{\varepsilon}$, (4.15) becomes

$$\begin{aligned}
|u_2| &\leq k_2 \left(\frac{k_3}{k_2 \left(1 - \frac{\varepsilon \left(1 - \frac{4\Gamma_m^2 k_2 k_3}{\Phi_M^2}\right)}{\varepsilon}\right)} + \bar{\Phi}^2 \right) \\
&= k_2 \left(\frac{\Phi_M^2}{4\Gamma_m^2 k_2^2} + \bar{\Phi}^2 \right)
\end{aligned} \tag{4.16}$$

From (4.15) with $|s| = 0$, we get

$$|u_2| = k_3 + k_2 \bar{\Phi}^2 \quad (4.17)$$

As a result, the upper bound of u_2 is

$$\limsup |u_2| \leq \max \left(k_2 \left(\frac{\Phi_M^2}{4\Gamma_m^2 k_2^2} + \bar{\Phi}^2 \right), k_3 + k_2 \bar{\Phi}^2 \right)$$

This proves item (4.10 (ii)). □

4.3.2 Stabilization of the $(r-1)$ -th integral chain

Consider the following system which is represented by the pure integrator chain as

$$\begin{cases} \dot{z}_1 = z_2 \\ \dot{z}_2 = z_3 \\ \vdots \\ \dot{z}_{r-1} = \omega_{nom} \end{cases} \quad (4.18)$$

We recall a linear controller ω_{nom} to stabilize the $(r-1)$ -th order integral chain, interested reader could refer to Khalil's book [41].

Theorem 3. *Let $a_1, a_2, \dots, a_{r-1} > 0$ be such that the polynomial $\omega_{nom} = a_1 z_1 + a_2 z_2 + \dots + a_{r-1} z_{r-1}$ is Hurwitz. For the system (4.18), the origin is an exponential stable equilibrium under the feedback ω_{nom} [41].*

There exists a positive definite matrix P for all positive definite matrix Q , such that,

$$PA + A^T P = -Q. \quad (4.19)$$

Let $z = [z_1, z_2, \dots, z_{r-1}]^T$. A Lyapunov function is selected as $V = z^T P z$, then its time derivative can be given as follows

$$\begin{aligned} \dot{V} &= \dot{z}^T P z + z^T P \dot{z} \\ &= z^T A^T P z + z^T P A z \\ &= z^T (A^T P + P A) z \\ &= -z^T Q z \\ &\leq -\lambda_{\min} \|z\|^2 \end{aligned} \quad (4.20)$$

where, $A = \begin{bmatrix} 0 & 1 & & & \\ & 0 & 1 & & \\ & & 0 & \ddots & \\ & & & \ddots & 1 \\ a_1 & a_2 & \cdots & a_{r-2} & a_{r-1} \end{bmatrix}$,

λ_{\min} is the minimum eigenvalue of P .

Then consider the system with perturbation g , which is represented as

$$\dot{z} = Az + g \quad (4.21)$$

where, $A = \begin{bmatrix} 0 & 1 & & & \\ & 0 & 1 & & \\ & & 0 & \ddots & \\ & & & \ddots & 1 \\ a_1 & a_2 & \cdots & a_{r-2} & a_{r-1} \end{bmatrix}$,

and $g = [0, \dots, 0, \Psi]^T$. Ψ is unknown and bounded perturbation, $|\Psi| < \varepsilon$ with ε predefined. The same Lyapunov function is selected as $V = z^T P z$, then its time derivative can be given as follows

$$\begin{aligned} \dot{V} &= \dot{z}^T P z + z^T P \dot{z} \\ &= (z^T A^T + g^T) P z + z^T P (Az + g) \\ &= z^T A^T P z + g^T P z + z^T P A z + z^T P g \\ &= z^T (A^T P + P A) z + g^T P z + z^T P g \\ &= -z^T Q z + g^T P z + z^T P g \\ &\leq -\lambda_{\min} \|z\|^2 + 2 \|g\| \lambda_{\max} \|z\| \\ &\leq -\lambda_{\min} \|z\| \left(\|z\| - \frac{2\varepsilon \lambda_{\max}}{\lambda_{\min}} \right) \end{aligned} \quad (4.22)$$

where, λ_{\min} and λ_{\max} are the minimum and maximum eigenvalue of matrix P . This implies

$$\limsup_{z \rightarrow \infty} \|z\| \leq \frac{2\varepsilon \lambda_{\max}}{\lambda_{\min}} \quad (4.23)$$

Finally we get

$$\begin{aligned} \limsup_{z \rightarrow \infty} z_i &< \Delta_i \text{ with} \\ \Delta_i &\leq \frac{2\varepsilon \lambda_{\max}}{\lambda_{\min}}, \quad i = 1, \dots, r-1. \end{aligned} \quad (4.24)$$

4.3.3 Main Controller

Consider the sliding surface

$$s = z_r - \omega_{nom} \quad (4.25)$$

The first time derivative of s is

$$\begin{aligned} \dot{s} &= \dot{z}_r - \dot{\omega}_{nom} \\ &= \varphi + \gamma u - \dot{\omega}_{nom} \end{aligned} \quad (4.26)$$

The system is represented as

$$\dot{s} = \Phi + \Gamma u \quad (4.27)$$

with $\Phi = \varphi - \dot{\omega}_{nom}$, and $\Gamma = \gamma$.

For Φ_M is the maximum parameter of the polynomial controller, $\bar{\Phi}(x, t)$ is a function of the states, the bound of Φ is

$$\begin{aligned} \bar{\Phi} &= \varphi - \dot{\omega}_{nom} \\ &= -a_1 z_2 - a_2 z_3 - \dots - a_{r-1} z_r + \bar{\Phi} \\ &\leq \underbrace{\max(1, a_1, a_2, \dots, a_{r-1})}_{\Phi_M} \underbrace{(1 + |z_2| + |z_3| + \dots + |z_r|)}_{\bar{\Phi}(x,t)}, \end{aligned} \quad (4.28)$$

The bound of Γ is $0 < \gamma_m < \gamma \leq \gamma_M$, where γ_m and γ_M are unknown.

Replacing the control law (4.9) to system (4.27), the sliding variable s is forced to converge to the predefined neighborhood of zero with $|s| < \varepsilon$, which implies $|z_r - \omega_{nom}| < \varepsilon$. Then we have

$$\dot{z}_{r-1} = \omega_{nom} + \Psi, \quad (4.29)$$

$$\text{with } |\Psi| < \varepsilon \quad (4.30)$$

From (4.22) (4.23) (4.24), we know that

$$\limsup_{z \rightarrow \infty} z_i < \Delta_i \text{ with} \quad (4.31)$$

$$\Delta_i \leq \frac{2\varepsilon \lambda_{\max}}{\lambda_{\min}}, \quad i = 1, \dots, r-1, \quad (4.32)$$

It is easy to get the parameter ε from (4.32) $\varepsilon \leq \frac{\lambda_{\min}}{2\lambda_{\max}} \Delta$, if we want to force the sliding variable z_i in the range of Δ .

4.3.4 Academic Example

In order to illustrate the theory, the proposed controller is applied to a triple integrator uncertain system as the academic example. Consider a three integral chains system that

$$\begin{cases} \dot{z}_1 = z_2 \\ \dot{z}_2 = z_3 \\ \dot{z}_3 = \varphi + \gamma u \end{cases} \quad (4.33)$$

where $\varphi = \sin(t), \gamma = 3 + \sin(2t)$.

Using the nominal controller $\omega_{nom} = -4z_1 - 2z_2$, we have

$$\dot{z}_2 = \omega_{nom} + \Psi \text{ with } |\Psi| < \varepsilon \quad (4.34)$$

Then, a sliding surface can be defined as

$$s = z_3 - \omega_{nom} \quad (4.35)$$

$$= 4z_1 + 2z_2 + z_3 \quad (4.36)$$

First time derivative of s is

$$\dot{s} = 2\varphi + 2\gamma u + 4z_2 \quad (4.37)$$

Using the proposed ASM control law in (4.9), where k_1, k_2 and k_3 are given to be 1, 0.2, and 1. For system (4.33), we have $z = [z_1, z_2]^T$, $A = \begin{bmatrix} 0 & 1 \\ -4 & -2 \end{bmatrix}$, $g = [0, \varepsilon]^T$. Consider a

Lyapunov function $V = z^T P z$, $P = \begin{bmatrix} \frac{3}{2} & \frac{1}{8} \\ \frac{1}{8} & \frac{5}{16} \end{bmatrix}$, we have

$$\dot{V} = z^T (A^T P + P A) z + g^T P z + z^T P g \quad (4.38)$$

$$= -z^T Q z + g^T P z + z^T P g \quad (4.39)$$

$$\leq -\|z\|^2 + 2\lambda_{max}(P)\varepsilon\|z\| \quad (4.40)$$

where $Q = A^T P + P A = \begin{bmatrix} 1 & 0 \\ 0 & 1 \end{bmatrix}$.

We fix the control objective that $|z_1| < 0.2, |z_2| < 0.3$ as the converge region predefined. Solving the inequality $\varepsilon < \frac{\min(0.2, 0.3) \cdot \lambda_{max}(P)}{2} = 0.1513$, finally, we choose $\varepsilon = 0.15$.

Simulation has been made by MATLAB SIMULINK. Choose that $z_1(0) = 2$, $z_2(0) = 1$, $z_3(0) = -3$. The results are shown from Fig. 4.3 to Fig. 4.6.

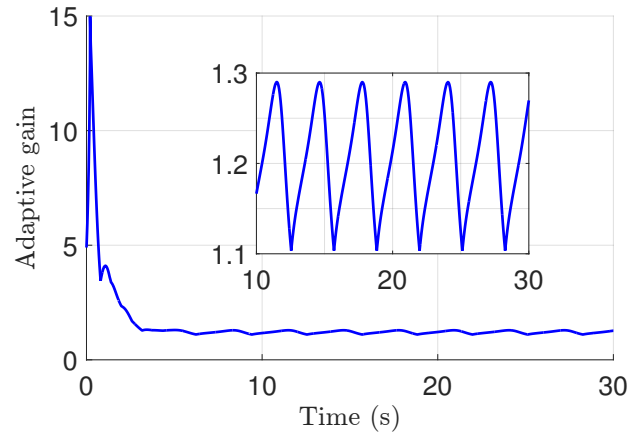


Figure 4.3. Adaptive gain K

The adaptive gain $K(t)$ is shown in Fig. 4.3. The adaptive gain K is increasing at the beginning to eliminate the perturbation, and decreasing rapidly when the gain is too high. After the sliding surface is reached, the adaptive gain is varying during a small region to compensate the perturbation and never overestimated.

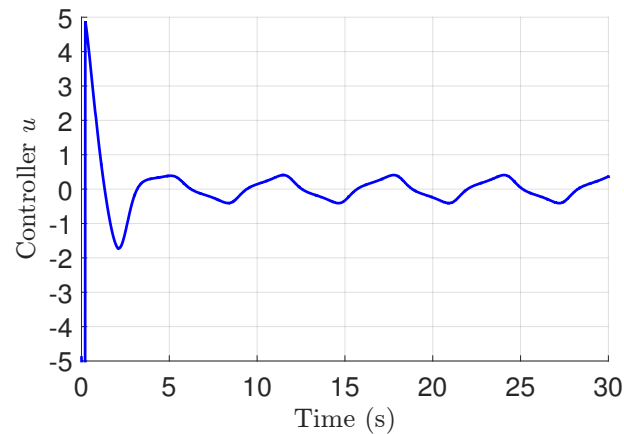


Figure 4.4. Controller u

The behavior of proposed controller is given in Fig. 4.4. Attribute to the $\text{sat}(\cdot)$ function,

the controller is continuous to avoid the chattering phenomenon. In the adaptive first order SM controller, we use a discontinuous controller. However, the chattering happens when the sliding variable is approximately equal to zero.

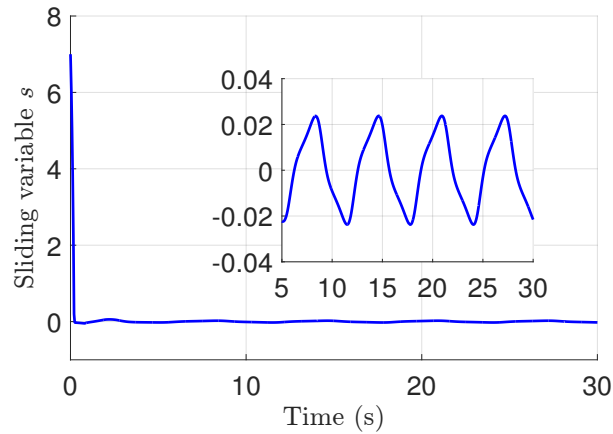


Figure 4.5. *Sliding variable s*

To illustrate the theory, the sliding variable s is pictured in Fig. 4.5. The zoom of Fig. 4.5 shows that the sliding variable s never escapes from the predefined value $\varepsilon < 0.15$ after the sliding surface reached.

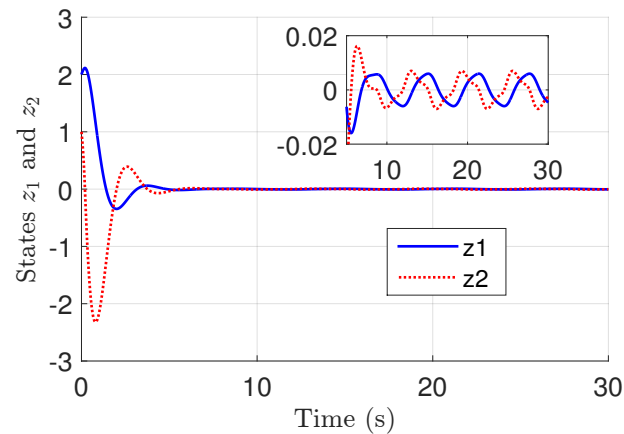


Figure 4.6. *States z_1 and z_2*

Additionally, the state z_1 and z_2 are zoomed in Fig. 4.6. For the control objective, we

predefine a neighborhood of zero to converge $|z_1| < 0.2$, $|z_2| < 0.3$. It is clearly depicted that the blue line z_1 and the red line z_2 are less than 0.2. The integral chains z_1 and z_2 are limited in the predefined region.

4.4 Adaptive HOSM controller for WECS

The system of variable speed wind generator with the back-to-back power converters is a high order, high nonlinear system [22] [78] [24]. The variable speed structure can operate at its optimal working point according to the various wind speed, which is so-called maximum power point tracking (MPPT) technique allowing the power generation maximize [26] [91] [89] [92]. The main control objective is to control the turbine torque to follow the optimal value, and to regulate the reactive power as command at the meanwhile with predefined errors. The proposed controller has been applied to the system to realize the control objective with the goodness of mechanical stress alleviation.

4.4.1 System Configuration

A Grid-connected variable speed wind system based on a double fed induction machine is considered in Fig. 4.7, consisting of the following parts [93] [13] [75] [94]:

- Turbine is the most important device to capture wind energy by its blades, and converting the wind kinetic power to mechanical torque.
- Gearbox and shaft increase the rotation speed given by the turbine, to suit the generator speed, assumed to be perfectly stiff in our study.
- Double fed induction generator (DFIG), which converts the power from mechanical form into electricity form. The stator of DFIG is connected to the grid directly, and the rotor is connected to the power converters.
- Converters are connected with the rotor of DFIG and the grid, adopting the famous back-to-back configuration.

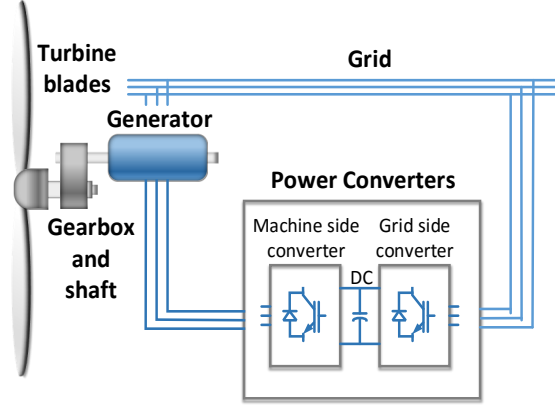


Figure 4.7. System configuration

4.4.2 Model of WECS

4.4.2.1 Aerodynamics

The aerodynamic power P_a in watt can be extracted from the wind turbine is

$$P_a = 0.5\pi r^2 C_p(\lambda, \beta) v^3 \quad (4.41)$$

where, r is the blade radius of turbine blades (m), v is the wind velocity (m/s), ρ is the air density of the area (kg/m^3). πr^2 is the area swept by the turbine blades. As a result, $\pi r^2 v \rho$ is the mass of the air passing through the turbine swept area in a unit time. Consequently, $0.5\pi r^2 v^3 \rho$ is the kinetic energy of the wind at the velocity v in a unit time.

As a matter of fact, it is impossible to obtain all the kinetic energy from the wind. Therefore a power coefficient C_p can be represented to describe the percentage of the wind power utilizing

$$C_p(\lambda, \beta) = c_1 \left(\frac{c_2}{\lambda_i} - c_3 \beta - c_4 \right) e^{-\frac{c_5}{\lambda_i}} + c_6 \lambda \quad (4.42)$$

$$\lambda = \frac{v_{tip}}{v} = \frac{\omega_t r}{v} \quad (4.43)$$

$$\frac{1}{\lambda_i} = \frac{1}{\lambda + 0.08\beta} - \frac{0.035}{\beta^3 + 1} \quad (4.44)$$

where, c_1 to c_6 are parameters designed by the turbine installation, ω_t is the angular speed of the turbine blades (rad/s), λ is the tip-speed ratio defined as the ratio between the turbine blades tip speed $v_{tip} = \omega_t r$ and wind speed v in (4.43). β is the pitch angle (deg).

4.4.2.2 Gearbox and Shaft

The torque produced by the turbine and the mechanic torque delivered by the gearbox is

$$\tau_t = \frac{P_a}{\omega_t} = \frac{\pi \rho r^2 C_p(\lambda, \beta) v^3}{2\omega_t} \quad (4.45)$$

$$\tau_t = k_{gb} \tau_m, \omega_{mr} = k_{gb} \omega_t \quad (4.46)$$

where, k_{gb} is the gearbox ratio. τ_t represents the aerodynamic torque in the turbine side. τ_m and ω_{mr} are the mechanic torque and mechanical speed of the generator in the machine side, respectively.

4.4.2.3 Double Fed Induction Generator

The dynamic and steady-state models of the double fed induction generator (DFIG) is introduced, which consists of the differential equations to describe the electromagnetic dynamic of the stator and rotor in synchronous frame as follows:

$$\dot{\psi}_{sd} = -R_s i_{rd} + \omega_L \psi_{sq} + v_{sd} \quad (4.47)$$

$$\dot{\psi}_{sq} = -R_s i_{rq} - \omega_L \psi_{sd} + v_{sq} \quad (4.48)$$

$$\dot{\psi}_{rd} = -R_r i_{rd} + (\omega_L - \omega_r) \psi_{rq} + v_{rd} \quad (4.49)$$

$$\dot{\psi}_{rq} = -R_r i_{rq} - (\omega_L - \omega_r) \psi_{rd} + v_{rq} \quad (4.50)$$

$$\psi_{sd} = L_s i_{sd} + L_m i_{rd} \quad (4.51)$$

$$\psi_{sq} = L_s i_{sq} + L_m i_{rq} \quad (4.52)$$

$$\psi_{rd} = L_r i_{rd} + L_m i_{sd} \quad (4.53)$$

$$\psi_{rq} = L_r i_{rq} + L_m i_{sq} \quad (4.54)$$

where the variables, the direct components and quadrature components are represented as d and q for short. The i_{sd} and i_{sq} are stator current viewed from rotating reference of d-q parts. Similarly, i_{rd} and i_{rq} are rotor currents. ψ_{sd} and ψ_{sq} are stator flux linkages. ψ_{rd} and ψ_{rq} are rotor flux linkages. L_s , L_r and L_m are the stator, the rotor and the mutual inductance. R_s and R_r are the resistance of the stator and rotor. ω_L is the frequency of the grid. The generator rotor electrical angular speed ω_r equals $\omega_r = p_r \omega_{rm}$, p_r is the number of the pole pairs of the generator. $L_{eq}^2 = L_r L_s - L_m^2$.

4.4.2.4 Reduced Order Model

As it is shown in Fig. 4.7, both the stator and rotor of DFIG provide electricity to the power grid. However the former is directly connected to the grid, while the latter is partially through a back-to-back converter. As a result, the flux of the stator is synchronous with the grid flux, and the voltage is fixed by the grid as well. The dynamic equations of the WECS are given below, with $x = \begin{bmatrix} i_{rd} & i_{rq} & \omega_r \end{bmatrix}$, $u = \begin{bmatrix} u_{rd} & u_{rq} \end{bmatrix}$,

$$\dot{x}_1 = -\frac{L_s R_r}{L_{eq}^2} x_1 + (\omega_L - x_3) x_2 + \frac{L_s}{L_{eq}^2} u_1 \quad (4.55)$$

$$\dot{x}_2 = -\left(\frac{L_m V_L}{\omega_L L_{eq}^2} + x_1\right)(\omega_L - x_3) - \frac{L_s R_r}{L_{eq}^2} x_2 + \frac{L_s}{L_{eq}^2} u_2 \quad (4.56)$$

$$\dot{x}_3 = \frac{\rho \pi r^3 C_p v^2 k_{gb} p_r^2}{2J\lambda} + \frac{3L_m V_L p_r^2}{2JL_s \omega_L} x_2 \quad (4.57)$$

4.4.3 Control Objective and Controller Design

There are two main control objectives:

- **Reactive power control:** The real reactive power Q tracks a given signal Q^* , with a predefined and acceptable error. The reference value Q^* is given by a superior command.
- **Torque control:** The real turbine torque T tracks an optimal signal T^* , with a predefined and acceptable error. The torque should be regulated by the controller with a small error of T^* . It would help to protect the actuator of controller from mechanic worn-off.

The tracking errors of the torque and the reactive power are:

$$\begin{aligned} e_Q &= Q - Q^*(t) \\ e_T &= T - T^*(t) \end{aligned} \quad (4.58)$$

Our control objective is defined as

$$\begin{aligned} |e_Q| &< \Delta_d \\ |e_T| &< \Delta_q \end{aligned} \quad (4.59)$$

where, Δ_d and Δ_q are chosen to be a predefined region of the errors, which are tolerable for the system.

The reactive power Q injected by the system into the grid and the torque T developed by the turbine and can be written as

$$Q = \frac{3}{2} V_L \left(\frac{L_m}{L_s} x_1 - \frac{V_L}{L_s \omega_L} \right) \quad (4.60)$$

$$T = -\frac{3}{2} \frac{L_m V_L}{L_s \omega_L} p_r x_2 \quad (4.61)$$

With the MPPT control technique, the optimal torque T^* could be rewritten as:

$$T^*(t) = \frac{k_{opt} p_r^2}{k_{gb}^3} x_3^2 \quad (4.62)$$

Define two sliding variables $[\sigma_d, \sigma_q]$ equal to the tracking errors of the control variables $[e_Q, e_T]$, we have two sliding surfaces that

$$\sigma_d(x) = \frac{3}{2} V_L \left(\frac{L_m}{L_s} x_1 - \frac{V_L}{L_s \omega_L} \right) - Q^*(t) \quad (4.63)$$

$$\sigma_q(x) = -\frac{3}{2} \frac{L_m V_L}{L_s \omega_L} p_r x_2 - \frac{k_{opt}}{p_r^2 k_{gb}^3} x_3^2 \quad (4.64)$$

The first order derivative of sliding variables $\dot{\sigma}_d$ and $\dot{\sigma}_q$ are:

$$\begin{aligned} \dot{\sigma}_d = & \underbrace{-\frac{3}{2} \frac{L_m R_r V_L}{L_{eq}^2} x_1 + \frac{3}{2} \frac{L_m V_L}{L_s} (\omega_L - x_3) x_2}_{\varphi_d} \\ & \underbrace{-\frac{\partial}{\partial x} Q_{ref}}_{\varphi_d} + \underbrace{\frac{3}{2} \frac{L_m V_L}{L_{eq}^2} u_1}_{\gamma_d} \end{aligned} \quad (4.65)$$

$$\begin{aligned} \dot{\sigma}_q = & \underbrace{\frac{3}{2} \left(\frac{L_m^2 V_L^2 p_r}{L_s \omega_L^2 L_{eq}^2} + \frac{L_m V_L p_r}{L_s \omega_L} x_1 \right) (\omega_L - x_3)}_{\varphi_q} \\ & \underbrace{-\frac{k_{opt}}{k_{gb}^3} \left(\frac{\rho \pi r^3 C_p v^2 k_{gb}}{J \lambda} + \frac{3 L_m V_L}{J L_s \omega_L} x_2 \right) x_3}_{\varphi_q} \\ & \underbrace{+\frac{3}{2} \frac{L_m V_L R_r p_r}{L_{eq}^2 \omega_L} x_2 - \frac{3}{2} \frac{L_m V_L p_r}{L_{eq}^2 \omega_L} u_2}_{\gamma_q} \end{aligned} \quad (4.66)$$

where, φ_d , φ_q , γ_d , and γ_q are systematic uncertainties. Then rewrite the σ_d and σ_q as σ_{d1} and σ_{q1} , we have two second order integral chains

$$\begin{aligned} \dot{\sigma}_{d1} &= \sigma_{d2} \\ \dot{\sigma}_{d2} &= \dot{\varphi}_d + \dot{\gamma}_d u_1 + \gamma_d \dot{u}_1 \end{aligned} \quad (4.67)$$

and

$$\begin{aligned}\dot{\sigma}_{q1} &= \sigma_{q2} \\ \dot{\sigma}_{q2} &= \dot{\varphi}_q + \dot{\gamma}_q u_2 + \gamma_q \dot{u}_2\end{aligned}\quad (4.68)$$

To apply ASM control law in (4.9), we define two new second order integral chain such as

$$\begin{aligned}\dot{z}_{d1} &= z_{d2} \\ \dot{z}_{d2} &= \Phi_d + \Gamma_d U_d\end{aligned}\quad (4.69)$$

and

$$\begin{aligned}\dot{z}_{q1} &= z_{q2} \\ \dot{z}_{q2} &= \Phi_q + \Gamma_q U_q\end{aligned}\quad (4.70)$$

where, $\Phi_d = \dot{\varphi}_d + \dot{\gamma}_d u_1$, $\Gamma_d = \gamma_d$, and the parallel definition, $\Phi_q = \dot{\varphi}_q + \dot{\gamma}_q u_2$, $\Gamma_q = \gamma_q$ and the new controller $U_1 = \dot{u}_1$ $U_2 = \dot{u}_2$. Finally, the control objective is represented as

$$\begin{aligned}|z_{d1}| &< \Delta_d \\ |z_{q1}| &< \Delta_q\end{aligned}\quad (4.71)$$

4.4.4 Simulation Results

To demonstrate the promised behavior of the controller, simulation has been carried out using MATLAB. To show the robustness of the motion with unknown parameter variations, unmodeled dynamics, and external disturbances in the sliding mode, perturbations are introduced to the nominal systems with a variation amplitude of 10%.

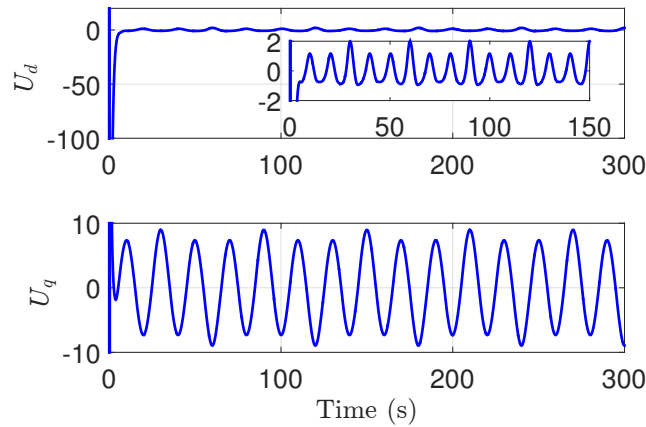


Figure 4.8. The controller U_d and U_q

And two external variables wind speed and superior reactive power command are simulated by test functions. The wind emulator generates wind speed ν using an approximate function $\nu(t) = \nu_{av}(1 - 0.18\cos(2\pi t) - 0.18\cos(2\pi t/60))$, where $\nu_{av} = 10\text{m/s}$ is the average wind speed. The superior reactive power command signal $Q^*(t)$ is given as a step signal after a low pass filter.

To assess the ability of the controller which is able to force the error inside a predefined region, great but acceptable errors $\Delta_d = 10\text{var}$ and $\Delta_q = 5\text{Nm}$ have been chosen. As we have two cascaded control loops of the direct axis and quadrature axis, the label d and q are related to the parameters of U_d and U_q . Consequently, the parameters of the controller $\varepsilon_d = 10$, $\varepsilon_q = 5$, $k_1 = k_3 = 5$, $k_2 = 0.1$ are chosen.

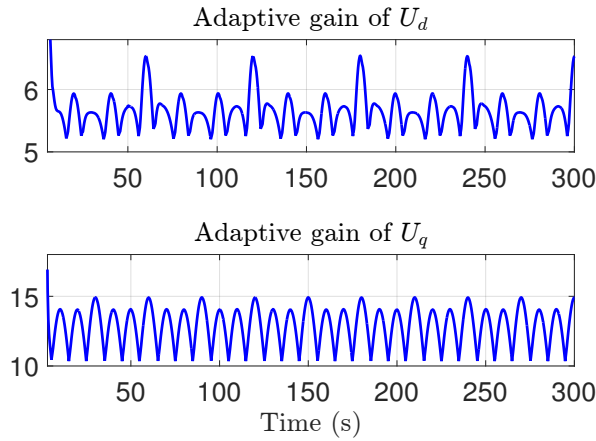


Figure 4.9. The adaptive gain of U_d and U_q

The controllers U_d and U_q are designed in (4.69) (4.70) with an adapted algorithm according to (4.9).

Fig. 4.8 to Fig. 4.13 show the good characters of the proposed controller. The two continuous controllers U_d and U_q are shown in Fig. 4.8. U_d and U_q have a transient vibration at the beginning seconds, which is largely due to the start-up procedure of the system. U_d and U_q are increased fast by the first part of the adaptation algorithm. After the control large enough to force the system to converge, U_d and U_q begin to fall down during a very short period of time. Fig. 4.9 shows the adaptive gains of the controllers U_d

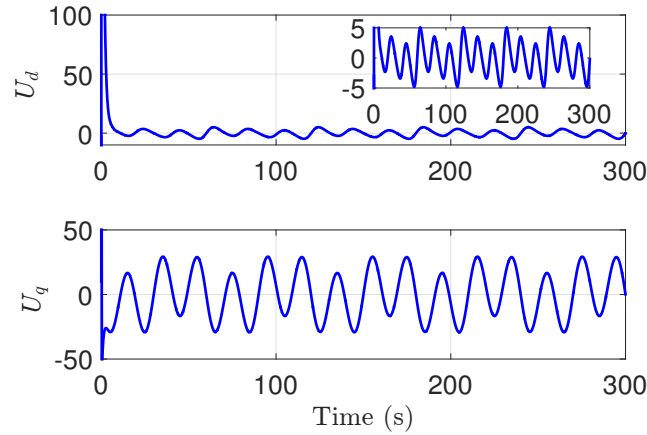


Figure 4.10. The controller u_d and u_q

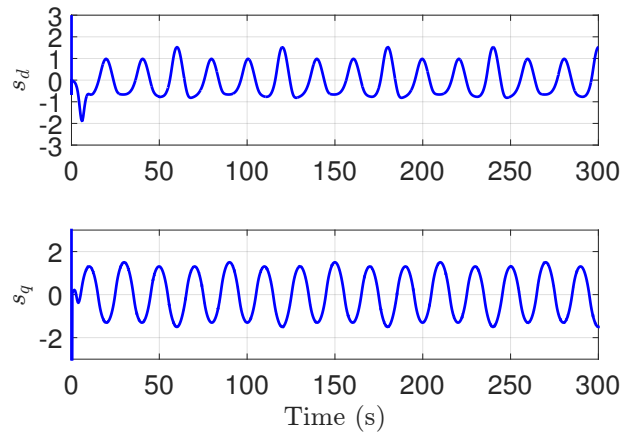


Figure 4.11. Sliding variable s_d and s_q

and U_q . The gains are estimated effectively by the adaptation law without prior knowledge of the uncertainties bounds. It should be noted that the proposed controller can adapt to a proper value very quickly, because the gain can decrease very fast according to the unknown perturbation of the system without any over estimation. And u_d and u_q are given in Fig. 4.10 as the output of ASMC module. Continuous control input do not have harmful chattering on the actuators.

Two sliding variables s_d and s_q are shown in Fig. 4.11. In order to converge the sliding variables to a predefined neighborhood of zero, Fig. 4.12 and Fig. 4.13 shows the integral

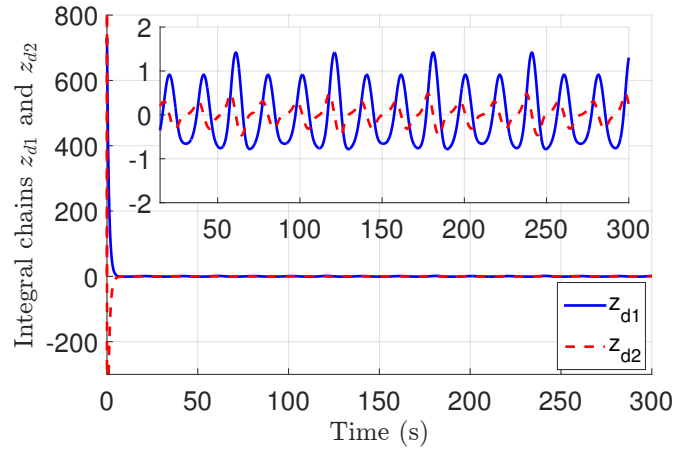


Figure 4.12. Integral chains of direct axis z_{d1} and z_{d2}

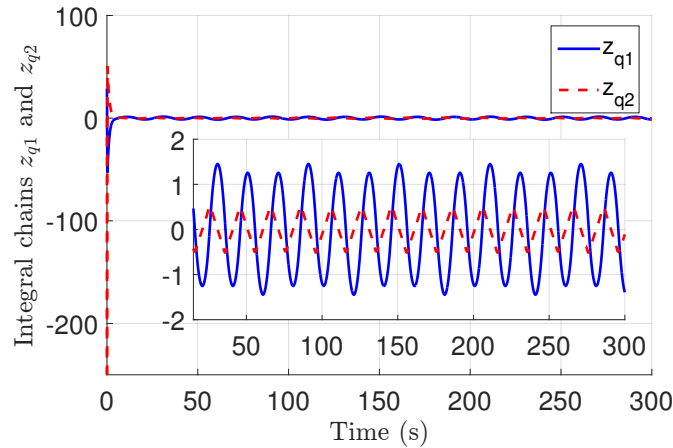


Figure 4.13. Integral chains of quadrature axis z_{q1} and z_{q2}

chains of the direct control loop z_{d1} , z_{d2} , and the integral chains of the quadrature control loop z_{q1} , z_{q2} . Physically, z_{d1} is the tracking error of the reactive power, and z_{q1} represents the tracking error of the torque in blue solid line. Their first derivatives are depicted in red dash lines. As the control objective is forcing z_{d1} , z_{q1} , and their first derivative z_{d2} , z_{q2} to converge to the predefined neighborhood $\Delta_d = 10\text{var}$ and $\Delta_q = 5\text{Nm}$, it is clearly from Fig. 4.12 and Fig. 4.13 that $|z_{d1}|$ and $|z_{q1}|$ are restricted in the predefined neighborhood $|z_{d1}| < 10$ and $|z_{q1}| < 5$. Moreover, these states never exceed the predefined neighborhood after their first convergence to the neighborhood. The curves are smooth and continuous, without any overshooting the restricted region in the zoom pictures of Fig. 4.12 and Fig. 4.13. This result is quite different with other ASM controllers.

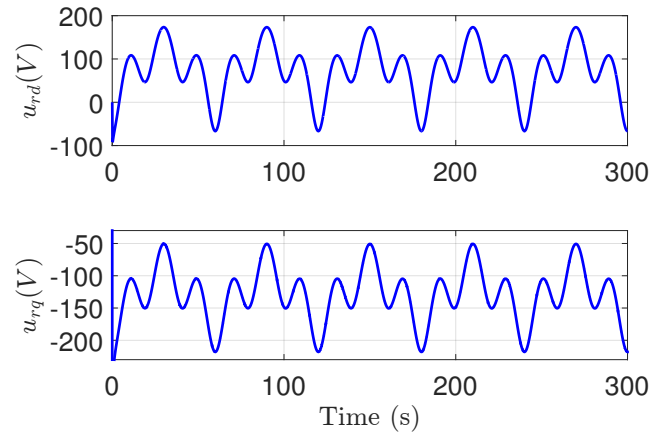


Figure 4.14. Rotor voltages u_{rd} and u_{rq}

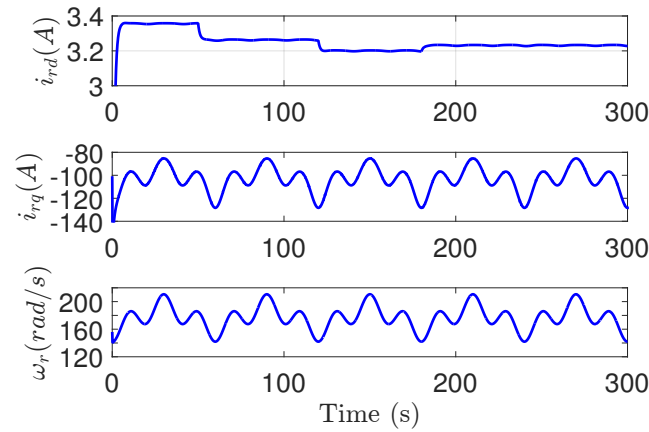


Figure 4.15. Rotor currents i_{rd} and i_{rq} and rotor speed ω_r

Fig. 4.14 to Fig. 4.17 show the performance of the controlled WECS. Fig. 4.14 shows the final input voltages u_{rd} and u_{rq} of the DFIG rotor. It is clearly that input voltage is smooth and continuous. This chattering-free character is attractive because it will alleviate the mechanical stress of the WECS actuators. The states of WECS, such as rotor currents i_{rd} , i_{rq} and rotor speed ω_r , are shown in Fig. 4.15. It can be observed that the curves of the states are very smooth. Fig. 4.16 and Fig. 4.17 show the tracking performance of the reactive power Q and torque T_a . The real value in blue solid line responds to the variation of the reference value in red dash line very fast. The WECS, initially working in

turn-off state, has been given at time 0 s a step Q^* variation from 0 to 40 *var*. And in the consequent simulation, Q tracks the reference signal composed of a set of transitions from high to low Q^* vice and versa. As expected, the error of Q is limited in a predefined region shown in the zoom of Fig. 4.16 and never exceeds after its first convergence. Meanwhile, T converges properly to T^* too.

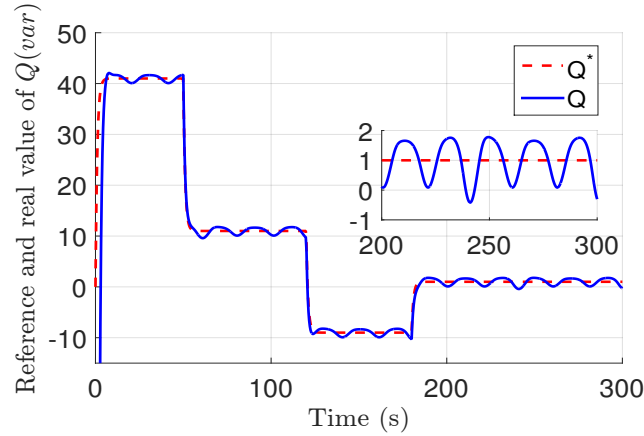


Figure 4.16. Tracking performance of Q

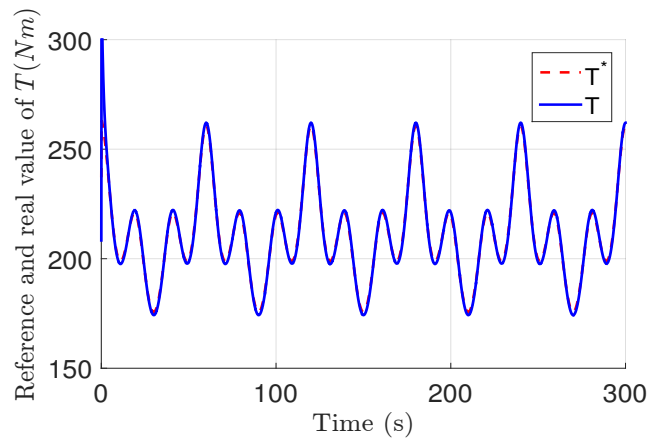


Figure 4.17. Tracking performance of T

4.5 Conclusion

A new adaptive HOSM controller for uncertain systems has been presented in this chapter. The controller has been designed in the control scheme to deal with the unknown bounded uncertainty of the arbitrary order integral chains system. The proposed controller promises that once the sliding variable is forced into a predefined neighborhood, its trajectory would never get out of the neighborhood. The proposed control law is continuous, and can reduce the chattering phenomenon of sliding mode, for which is suitable for practical application. The stability is proved by Lyapunov analysis. Academic simulation result is given to show the controller performance. Additionally, the proposed controller is applied to a WECS for practical applications. The simulation result shows that the error of the torque and the error of the reactive power converge to a predefined value, which could help reducing mechanic worn out of the practical system. It can be expected for a wide range of application on arbitrary high-order complex nonlinear model in practice.

Chapter 5

Fault Tolerant Control with On-line Allocation for Linear Time Varying Systems

In the previous chapter, we have designed adaptive HOSM control for wind energy conversion system. We now turn attention towards the fault tolerant control with online allocation. A FTC with a fixed control allocation for LTV systems using only output information is going to be proposed. The designed controller compensates theoretically exactly just after the initial time the fault effects in the critical input channels while minimize the effects in the non-critical ones. A hierarchical observer using only the fault-free outputs is given assuring theoretical exact reconstruction of the state vector right after the initial time.

This chapter is organized as follows. Section 5.2 presents the problem formulation and the necessary assumptions. Section 5.3 gives the design procedure for the OISM controller. The hierarchical observer methodology is explained in Section 5.4. While Section 5.5 discusses the issues of a bad reconstruction of the control input and states. Moreover, sufficient stability conditions are developed. In Section 5.6 the wind turbine case of study is presented, together with a brief discussion of the issues that can arise in the application of the methodology. Finally, Section 5.7 summaries the chapter.

5.1 Introduction

Several control allocation schemes have been developed. [95] design a family of controllers for control allocation identifying the faults by solving a minimization problem. [96] gives a control allocation approach based on the solution of a system of linear equations subject to constraints. [97] proposes a real time adaptive scheme for a high performance aircraft based on a linear control allocation problem and a weighted pseudo-inverse for fault reconstruction, while [98] uses a sequential quadratic programming approach. In [99] a fault tolerant sliding mode for systems with actuator faults is proposed. The fault identification is made by using a test control input.

In [100] an on-line control allocation is proposed based on an optimization procedure. This methodology allows that once the fault has been identified, the controller can be reconfigured automatically assuring the control objective is fulfilled. Based on this idea [101] uses a sliding mode controller for fault tolerant control and on-line allocation by seeing the additive faults as perturbations of a linear time invariant system, allowing the identification of the faults, and to redistribute the control in the available actuators without external information. Following this same idea, [102] uses an integral sliding mode controller for on-line control allocation. However, this techniques were developed for linear time invariant systems and require the knowledge of the system's states.

To avoid the necessity of the states, it is possible to use observers based on sliding modes. In specific in [103] an output integral sliding mode (OISM) technique is proposed for linear time invariant systems. This technique allows to make the system insensitive to matched uncertainties/perturbations and to reconstruct its states theoretically exactly just after the initial time. Recently, [104] broaden this result to linear time varying systems (LTV).

The objective of the chapter is to design a fault tolerant controller with on-line control allocation for LTV systems using an OISM methodology and a control allocation scheme similar to the one proposed in [100, 101]. This algorithm will allow on-line identification of the faults by using any fault detection and identification (FDI) schemes available in the literature [4, 19, 105, 101]. Moreover, sufficient conditions to assure the stability remains even when the states or the faults are not well reconstructed will be presented.

Wind energy is the fastest growing renewable power source around the world, but the increasing number and size of turbines have raised the necessity of compensate the effects of the faults to reduce the damage and to increase the efficiency[106, 107, 108]. In [108, 109] different kind of faults and its relevance for wind turbine are presented. In this benchmark papers the actuators are subject to abrupt or slow changes in its dynamics, besides torque offsets and stuck actuators. In [110, 106, 111, 107, 109, 112, 113] different approaches to deal with actuator faults have been presented, from fault tolerant architectures, compensation of identified faults, reconfiguration of controllers and control allocation schemes. But at the best of our knowledge, there is not any control scheme based in a sliding mode technique applied for fault tolerant control and on-line allocation of the wind turbine.

The proposed FTC and control allocation scheme will be applied to a linear parameter varying model of a wind turbine subject to partial and total faults in the actuators. Redundancy will be assumed as well as controllability restrictions. The system will be studied in two different scenarios, when the faults are completely reconstructed by a suitable FDI scheme and when the reconstruction is deficient.

5.2 Problem Formulation

Assume a LTV system subject to actuator faults,

$$\begin{aligned}\dot{x}(t) &= A(t)x(t) + B_u(t)(I - K(t))u(t), \\ y(t) &= C(t)x(t),\end{aligned}\tag{5.1}$$

where $x(t) \in \mathbb{R}^n$, $u(t) \in \mathbb{R}^m$, $y(t) \in \mathbb{R}^p$ represent the states, inputs and outputs respectively. $A(t) \in \mathbb{R}^{n \times n}$, $B_u(t) \in \mathbb{R}^{n \times m}$, $C(t) \in \mathbb{R}^{p \times n}$ are known matrices. $K(t) = \text{diag}(k_1, k_2, \dots, k_m(t))$, denotes the possible actuators faults, where $0 \leq k_i(t) \leq 1$, if $k_i(t) = 0$ there is no fault in the i -actuator, and $k_i(t) = 1$ denotes a complete one.

Assumption 1. *The matrices $A(t), B_u(t), C(t)$ are $\bar{n}-2, \bar{n}-1, \bar{n}-1$ times continuously differentiable. This matrices and its derivatives are bounded and known.*

Assumption 2. *Assume the redundancy in actuators is such that $\text{rank}(B_u(t)) = l < m$.*

Using rank factorization it is always possible to represent the control matrix as $B_u(t) = B_v(t)B(t)$, where $B_v(t) \in \mathbb{R}^{n \times l}$ and $B(t) \in \mathbb{R}^{l \times m}$ (see [114, Section 5.4, pp 144]). Let $\bar{v}(t) =$

$B(t)u(t)$ then $u(t) = B^+(t)\bar{v}(t)$, where

$$B^+(t) = W(t)B^T(t)(B(t)W(t)B^T(t))^{-1},$$

with $W = (I - K)$ [100, 101]. Then the system takes the form

$$\dot{x}(t) = A(t)x(t) + B_v(t)B(t)W(t)B^+(t)\bar{v}(t). \quad (5.2)$$

Considering $\tilde{v}(t) = (B(t)W(t)B^T(t))^{-1}\bar{v}(t)$ the system can be rewritten as

$$\dot{x}(t) = A(t)x(t) + B_v(t)B(t)W(t)^2B^T(t)\tilde{v}(t). \quad (5.3)$$

Finally, defining a "virtual control" $v(t)$ such that $\tilde{v}(t) = (B(t)B^T(t))^{-1}v(t)$,

$$\phi(t) = (B(t)W(t)^2B^T(t)(B(t)B^T(t))^{-1} - I)v(t)$$

as the unknown input, and adding and subtracting $B_v(t)v(t)$ the system (5.1) can be rewritten as

$$\begin{aligned} \dot{x}(t) &= A(t)x(t) + B_v(t)v(t) - B_v(t)\phi(t), \\ y(t) &= C(t)x(t). \end{aligned} \quad (5.4)$$

It is logic to assume the control effort $v(t)$ is bounded. Hence, since $k_{\mathbf{i}} \in [0, 1]$, and the matrices $B(t)$ are assumed bounded, it is possible to assure $\|\phi(t)\| \leq \phi_{max}$.

OUR AIM IS TO ASSURE ON-LINE CONTROL ALLOCATION AND FAULT TOLERANT CONTROL FOR LTV SYSTEMS USING AN OUTPUT INTEGRAL SLIDING MODE CONTROLLER ALLOWING ON-LINE DETECTION AND ISOLATION OF THE CONSIDERED FAULTS

In order to achieve the above objectives the matrices $A(t), B_v(t), C(t)$ must fulfil the following usual conditions.

Assumption 3. *The pair $(A(t), B_v(t))$ is uniformly completely controllable with controllability index n_c .*

Assumption 4. *The pair $(A(t), C(t))$ is uniformly completely observable with observability index n_o .*

Assumption 5. *The pair $(A(t), B_v(t), C(t))$ is strongly observable.*

Assumption 6. $\bar{n} = \max\{n_c, n_o\}$.

Since we want to construct an output based fault tolerant control consider:

Assumption 7. *The value of $x(t)$ and $K(t)$ for all $t \geq t_0$ are unknown.*

Assumption 8. *The initial condition is unknown but bounded.*

$$\|x(0)\| \leq \mu.$$

Assumption 9. *Assume $\text{rank}(C(t)B_v(t)) = l$ and $p > l$.*

5.2.1 Nominal System

Assuming the system does not have actuator faults, i.e. $W(t) = I$, a nominal system is proposed

$$\begin{aligned} \dot{x}_N(t) &= A(t)x_N(t) + B_v(t)v_N(t), \\ y_N(t) &= C(t)x_N(t). \end{aligned} \tag{5.5}$$

Without loss of generality assume $v_N(t) = -\mathcal{K}(t)x_N(t)$, where $\mathcal{K}(t)$ is a bounded matrix designed such that the closed loop system

$$\dot{x}_N(t) = (A(t) - B_v(t)\mathcal{K}(t))x_N(t)$$

is exponentially stable. Then, for all $t \geq t_0$ there exist a matrix $P(t) \in \mathbb{R}^{n \times n}$ and positive constants c_1, c_2, c_3 such that

$$c_1 I \leq P(t) \leq c_2 I$$

satisfies

$$-\dot{P}(t) = P(t)(A(t) - B_v(t)\mathcal{K}(t)) + (A(t) - B_v(t)\mathcal{K}(t))^T P(t) + Q(t), \tag{5.6}$$

with

$$Q(t) \geq c_3 I.$$

5.3 Output Integral Sliding Mode Controller

In order to assure the effects of the additive faults do not affect the behaviour of the system an OISM "virtual controller" is proposed. First, assume $v(t) = v_N(t) + v_I(t)$, where $v_I(t)$ is a sliding mode controller assuring the compensation of the additive faults. To design v_I define a sliding surface

$$s(y, t) = G(t)(y(t) - y(t_0)) - \int_{t_0}^t (\mathcal{G}(\tau)\hat{x}(\tau) + D(\tau)v_N(\tau)) d\tau, \tag{5.7}$$

where the vector $\hat{x}(t)$ is the observed state given by a hierarchical observer [104],

$$\mathcal{G}(t) = \dot{G}(t)C(t) + G(t)\dot{C}(t) + G(t)C(t)A(t),$$

$D(t) = G(t)C(t)B(t)$ and $G(t)$ is a design projection matrix, such that

$$\det(D(t)) \neq 0 \text{ and } \frac{dG(t)C(t)}{dt} \neq 0.$$

Sufficient conditions assuring the existence of a first order sliding mode are given in the next theorem.

Theorem 4. *If $\det(D(t)) \neq 0$ and $v_I(t)$ is designed as a first order sliding mode controller of the form*

$$v_I(t) = -\beta \frac{D(t)^T s(y, t)}{\|D(t)^T s(y, t)\|}, \quad (5.8)$$

where

$$\beta > \phi_{max} + \|D(t)^{-1}\mathcal{G}(t)\| \|x(t) - \hat{x}(t)\|.$$

The trajectory of (5.4) converges right after the initial time to the surface $s(y, t)$ and the control $v_I(t)$ is capable to compensate theoretically exactly the additive fault $\phi(t)$ for all $t \in (t_0, t_f]$, $i = 1, 2, \dots, r$.

Proof. The proof of this statement comes directly from [104, Theorem 5] □

Without loss of generality, assume $G(t)$ is designed such that $D(t) = I$. During the sliding phase the equivalent control [115]

$$v_{I,eq}(t) = -\mathcal{G}(t)(x(t) - \hat{x}(t)) - \phi(t)$$

is achieved and (5.4) takes the form

$$\begin{aligned} \dot{x}(t) &= \tilde{A}(t)x(t) + B_v(t)v_N(t) + B_v(t)\mathcal{G}(t)\hat{x}(t), \\ y(t) &= C(t)x(t), \end{aligned} \quad (5.9)$$

where $\tilde{A}(t) = A(t) - B_v(t)\mathcal{G}(t)$.

Remark 2. *Under the assumptions of this work the sliding mode dynamics are observable.**

*For a bigger discussion about this result see [104, Theorem 4].

The dimension of the controller $v_I(t)$ and the sliding variable $s(y, t)$ will depend on B_u 's rank. Note that since we assure the system is in the sliding mode for all $t \geq t_0$, the control $v_I(t)$ contains the equivalent control since the first moment. With this information and with a FDI scheme the value of $K(t)$ can be obtained and the real control $u(t)$ reconstructed (see [19, Chapter 6],[4, 105] and the reference there in).

5.4 States Reconstruction

To fulfil the objective of the chapter it is necessary to reconstruct the states of the system. For the sliding mode dynamics (5.9), design a hierarchical observer on the time interval $[t_0, t_f]$ [†].

$$\dot{\tilde{x}}(t) = \tilde{A}(t)\tilde{x}(t) + B_v(t)v_N(t) + B_v(t)\mathcal{G}(t)\hat{x}(t) - K_O(t)(y(t) - C(t)\tilde{x}(t)), \quad (5.10a)$$

$$\begin{aligned} \dot{x}_{a_k} = & \tilde{A}(t)\tilde{x}(t) + B_v(t)v_N(t) + B_v(t)\mathcal{G}(t)\hat{x}(t) \\ & - L_k(N_{k-1}(t)L_k)^{-1}(v_{O,k}(t) + \dot{N}_{k-1}(t)(\tilde{x}(t) - x_{a_k})), \end{aligned} \quad (5.10b)$$

$$\hat{x}(t) = \tilde{x}(t) + \mathcal{O}_{\bar{n}}^+ v_{O_{av}}(t); \quad (5.10c)$$

where

$$v_{O_{av}}(t) = \begin{bmatrix} C(t)x_{a1}(t) - C(t)\tilde{x}(t) \\ v_{O,1_{av}}(t) \\ v_{O,2_{av}}(t) \\ \vdots \\ v_{O,(\bar{n}-1)_{av}}(t) \end{bmatrix} \in \mathbb{R}^p \quad (5.11)$$

and

$$\mathcal{O}_{\bar{n}} = \begin{bmatrix} N_0(t) \\ N_1(t) \\ \vdots \\ N_{\bar{n}-1}(t) \end{bmatrix}, \quad (5.12)$$

with $N_0(t) = C(t)$ and $N_k(t) = N_{k-1}(t)A(t) + \frac{dN_{k-1}(t)}{dt}$ for $k = 1, \dots, \bar{n}$.

This observer is composed by three parts. The first part (5.10a) is a Kalman-Bucy type stabilizer, the matrix $K_O(t)$ should be designed such that it assure exponential stability

[†]Here we just present a brief explanation of the observer, for a deep discussion see [104].

of the error dynamics. (5.10b) conforms a sliding mode observer that will reconstruct theoretically exactly just after the initial time the output and its derivatives. The next theorem gives the guideline for its design.

Theorem 5. [104] *If the auxiliary state vectors x_{ak} , for all $k = 1, \dots, \bar{n} - 1$ are designed as (5.10b) where $L_k \in \mathbb{R}^{n \times p}$ is a design matrix such that $\det(N_i(t)L_k) \neq 0$, and the initial conditions should satisfy*

$$C(t_0)x_{a1}(t_0) = y(t_0),$$

and

$$N_k(t_0)\tilde{x}(t_0) + v_{O,k-1}(t_0) = N_k(t_0)x_{ak}(t_0).$$

Moreover, the variables s_k are designed as

$$s_1(y(t), x_{a1}(t)) = y(t) - C(t)x_{a1}(t) \quad (5.13)$$

and

$$s_k(y(t), x_{ak}(t)) = N_{k-1}(t)\tilde{x}(t) + v_{k-1}(t) - N_{k-1}(t)x_{ak}, \quad (5.14)$$

for $1 < k < \bar{n} - 1$. The control input $v_{O,k}(t)$ is designed as a first order sliding mode

$$v_{O,k}(t) = M_k(t) \frac{s_k(y(t), x_{ak}(t))}{\|s_k(y(t), x_{ak}(t))\|},$$

where the scalar gain $M_k(t)$ should satisfy the condition

$$\|N_k(t)\| \|x(t) - \tilde{x}(t)\| < M_k(t).$$

Then, for all $t \in [t_0, t_f]$

$$v_{O,k_{eq}}(t) = N_k(t)(x(t) - \tilde{x}(t)) \quad \text{and } k = 1 \dots \bar{n} - 1,$$

and it is possible to reconstruct completely all the vector functions $N_k(t)x(t)$, $k = 1, \dots, \bar{n} - 1$.

Finally, (5.10c) reconstructs theoretically exactly just after the initial time the states of the system if $v_{O,k_{av}}(t) = v_{O,k_{eq}}(t)$. The values $v_{O,k_{av}}(t)$ are approximations of the equivalent control $v_{k_{eq}}(t)$, obtained from $v_{O,k}(t)$ with a first order low-pass filter:

$$\tau \dot{v}_{O,k_{av}}(t) + v_{O,k_{av}}(t) = v_{O,k}(t).$$

Due to the approximation process the state cannot be exactly reconstructed, but the lower the filter gain τ is the lower the error will be.

5.5 Discussion: $u(t)$ reconstruction

The state is reconstructed using a hierarchical observer that is capable to reconstruct theoretically exactly the state just after the initial moment [104] and the control input $v_I(t)$ is capable to reconstruct in the same manner the additive faults $\phi(t)$. However, in order to reconstruct the control it is necessary to first identify the unknown matrix $K(t)$.

The additive fault $v_{I,eq}(t)$ contains $K(t)$ and can be reconstructed from $v_I(t)$ by using a first order filter

$$\tau \dot{v}_{I,ap}(t) + v_{I,ap}(t) = v_I(t), \quad (5.15)$$

with a time constant τ sufficiently small [115]. Under the assumption that the state is full reconstructed, i.e. $\|x(t) - \hat{x}(t)\| = 0$.

$$v_{I,ap}(t) \approx -\phi(t).$$

To reconstruct $K(t)$ a FDI scheme can be used. But this schemes normally cannot reconstruct exactly the faults. This combine with the filtration errors introduces unwanted dynamics to the system. Moreover, the reconstruction of $u(t)$ depends on the approximate values k_i and $\hat{x}(t)$. Taking all this into account, the next theorem will gives sufficient conditions to assure stability of the system.

Theorem 6. *Let $\bar{W}(t) = W(t) + \Delta W(t)$ and $\hat{x}(t) = x(t) + \Delta x(t)$ the reconstructed values of the additive faults $W(t)$ and the states $x(t)$. If*

$$\|\Delta W(t)\| \leq \alpha_W < \frac{c_1 c_3}{2c_2^2 \kappa_1 \kappa_2^2 \kappa_3 \kappa_4}$$

and $\|\Delta x(t)\| \leq \alpha_x$. Then, (5.4) is stable and its states are ultimately bounded with an ultimate bound

$$x_{ub} = \frac{c_2 \gamma}{\Upsilon c_1 \theta}.$$

Proof. The proof of this fact is made using the comparison method [116, Chapter 9]. First let us analysed the nominal case, i.e. $\Delta W(t) = 0$, $\Delta x(t) = 0$. Under this conditions, $v_{I,eq}(t) = -\phi(t)$, $u(t) = W(t)B^T(t)(B(t)B^T(t))^{-1}v(t)$ and

$$\begin{aligned} \dot{x}(t) &= A(t)x(t) + B_v(t)v_N(t) \\ &= (A(t) - B_v(t)\mathcal{K}(t))x(t). \end{aligned}$$

Let

$$V(x(t)) = x(t)^T P(t)x(t)$$

be the nominal candidate Lyapunov function, with $P(t)$ satisfying the time varying Lyapunov equation (5.6). This Lyapunov equation is bounded by

$$c_1 \|x(t)\|^2 \leq V(x(t)) \leq c_2 \|x(t)\|^2$$

and its time derivative along the trajectories of (5.4) is negative definite:

$$\dot{V}(x(t)) \leq -c_3 \|x(t)\|^2.$$

For the general case, $v_{I,eq}(t) = -\phi(t) - \mathcal{G}(t)(x(t) - \hat{x}(t)) = -\phi(t) - \mathcal{G}(t)\Delta x(t)$, $u(t) = \bar{W}(t)B^T(t)(B(t)B^T(t))^{-1}v(t)$ and (5.4) conforms a perturbed linear system

$$\begin{aligned} \dot{x}(t) &= A(t)x(t) + B_v(t)v_N(t) + B_v(t)\Xi(t)v(t) \\ &= (A(t) - B_v(t)\mathcal{K}(t))x(t) + g(x(t), t); \end{aligned}$$

where $\Xi(t) = B(t)W(t)\Delta W(t)B^T(t)(B(t)B^T(t))^{-1}$, and

$$g(x(t), t) = B_v(t)(-\Xi(t)\mathcal{K}(t)x - (\Xi(t) + I)\mathcal{K}(t)\Delta x + \Xi(t)v_I(t)).$$

This term constitutes a bounded perturbation with a vanishing at the origin part and a non-vanishing one. Recall that $\|W(t)\| \leq 1$ and $\|v_I(t)\| \leq \sqrt{l}\beta$. By assumption 2 $B_v(t), B(t)$ are bounded and by design $\mathcal{K}(t)$ is also bounded. Let the positive constants κ_1 , κ_2 and κ_3 be its respective bounds. Note that since $\text{rank}(B(t)) = l$ it is possible to assure $\|(B(t)B^T(t))^{-1}\| \leq \kappa_4$. Then,

$$\|\Xi(t)\| \leq \alpha_W \kappa_2^2 \kappa_4$$

and

$$\|g(x(t), t)\| \leq \delta \|x(t)\| + \gamma;$$

where $\delta = \alpha_W \kappa_1 \kappa_2^2 \kappa_3 \kappa_4$ and $\gamma = \sqrt{l}\beta \alpha_W \kappa_1 \kappa_2^2 \kappa_4 + \alpha_W \alpha_x \kappa_1 \kappa_2^2 \kappa_3 \kappa_4 + \alpha_x \kappa_1 \kappa_3$. It is easy to see that if

$$\alpha_W < \frac{c_1 c_3}{2c_2^2 \kappa_1 \kappa_2^2 \kappa_3 \kappa_4},$$

then

$$\delta < \frac{c_1 c_3}{2c_2^2}.$$

The time derivative of the nominal Lyapunov function along the trajectories of the perturbed system is bounded by

$$\begin{aligned}\dot{V}(x(t)) &\leq -c_3\|x(t)\|^2 + 2c_2\delta\|x(t)\|^2 + 2c_2\gamma\|x\| \\ &\leq -\left[\frac{c_3}{c_2} - \frac{2c_2}{c_1}\delta\right]V(x(t)) + 2c_2\gamma\sqrt{\frac{V(x(t))}{c_1}}.\end{aligned}\quad (5.16)$$

Hence, by [116, Lemma 9.4], it is possible to assure

$$\|x(t)\| \leq \sqrt{\frac{c_2}{c_1}}\mu e^{-\Upsilon(t-t_0)} + \frac{c_2\gamma}{c_1\Upsilon}(1 - e^{-\varepsilon(t-t_0)}),$$

with $\Upsilon = \frac{1}{2}\left[\frac{c_3}{c_2} - \delta\frac{2c_2}{c_1}\right]$. Observe that if the bounds α_W and α_x became sufficiently small, we can assure exponential stability of (5.4). Now, since γ is a constant, the state $x(t)$ is ultimately bounded with the ultimate bound

$$x_{ub} = \frac{c_2\gamma}{\Upsilon c_1\theta},$$

with $\theta \in (0, 1)$ an arbitrary constant (see [116, Lemma 9.6]). \square

5.5.1 Academic Example

Let's apply the proposed methodology to a LTV model (5.1) with $x(t) = \begin{bmatrix} x_1 & x_2 & x_3 & x_4 \end{bmatrix}^T$,

$$A(t) = A_0 + A_1\rho_1(t) + A_2\rho_2(t), \quad B_u(t) = B_0(1 + \rho_1(t) + \rho_2(t))$$

and $y(t) = \begin{bmatrix} x_1 & x_2 & x_4 \end{bmatrix}^T$, where

$$A_0 = \begin{bmatrix} 0 & 1 & 0 & 0 \\ 0 & 0 & 1 & 0 \\ 0 & 0 & 0 & 1 \\ 1 & 2 & 3 & 4 \end{bmatrix}, \quad A_1 = \begin{bmatrix} 0 & 1 & 0 & 1 \\ 1 & 0 & 0 & 1 \\ 0 & 0 & 1 & 0 \\ 1 & 1 & 1 & 1 \end{bmatrix},$$

$$A_2 = \begin{bmatrix} 0 & -1 & 0 & -1 \\ -1 & 0 & 0 & 0 \\ 0 & 0 & 0 & -1 \\ -7 & 0 & -2 & 0 \end{bmatrix}, \quad B_0 = \begin{bmatrix} 0 & 0 & 0 \\ 0 & 0 & 0 \\ 0 & 0 & 0 \\ 1 & 1 & 1 \end{bmatrix},$$

$\rho_1(t) = 1 + 0.3\sin(\pi t)$ and $\rho_2(t) = -1 - 0.6\cos(\pi t)$. The rank decomposition of $B_u(t)$ is composed by

$$B_v(t) = \begin{bmatrix} 0 \\ 0 \\ 0 \\ \rho_1(t) + \rho_2(t) + 1 \end{bmatrix}, \quad \text{and} \quad B = \begin{bmatrix} 1 & 1 & 1 \end{bmatrix}.$$

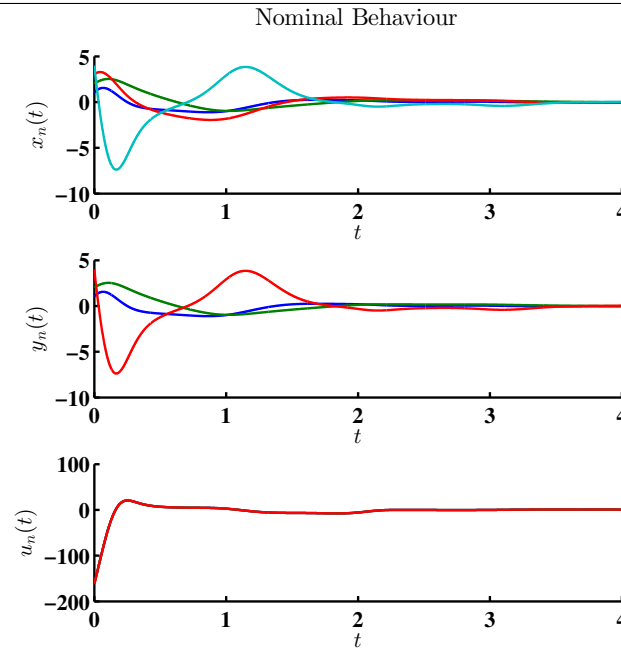


Figure 5.1. *Nominal Behaviour of the Academic System*

The proposed nominal controller is a simple feedback control law with a gain scheduling scheme. The nominal behaviour of the system is shown in Fig. 5.1.

It is assumed that the system is affected by actuator faults, that conform a continuous functions guaranteeing the system remains controllable (see the first graphic of Fig 5.2). Note that the proposed faults assure the non-existence of a complete fault in every actuator at the same time. The behaviour of the system in the absence of a fault tolerant control scheme is presented in Fig. 5.3.

Now applying the OISM fault tolerant control to the academic system[‡]. The additive faults are rejected completely for the system and the stability remains (see Fig. 5.4). The control allocation is done assuming the value K can be completely reconstructed since the initial time, i.e. $\Delta W = 0$ and with a controller gain $\beta = 600$. However, it is very difficult to reconstruct completely the K vector and normally it is only possible to identified the average of the active faults. The K vector was identified using the reconstructed value of

[‡]The present simulation was done with a step size $\Delta t = 1e-6$ since as it was shown in [104] the observation error $\|x(t) - \hat{x}(t)\|$ will be lower with a small step size.

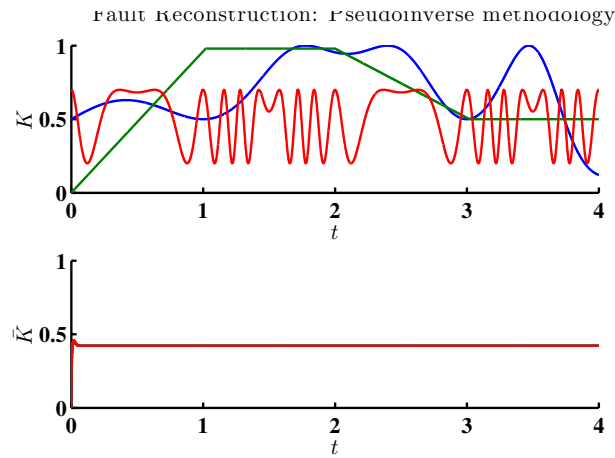


Figure 5.2. Additive Faults Reconstruction using a pseudoinverse methodology for the identified perturbation $v_{I,ap}(t)$

Faulty System Behaviour: Only Nominal Controller

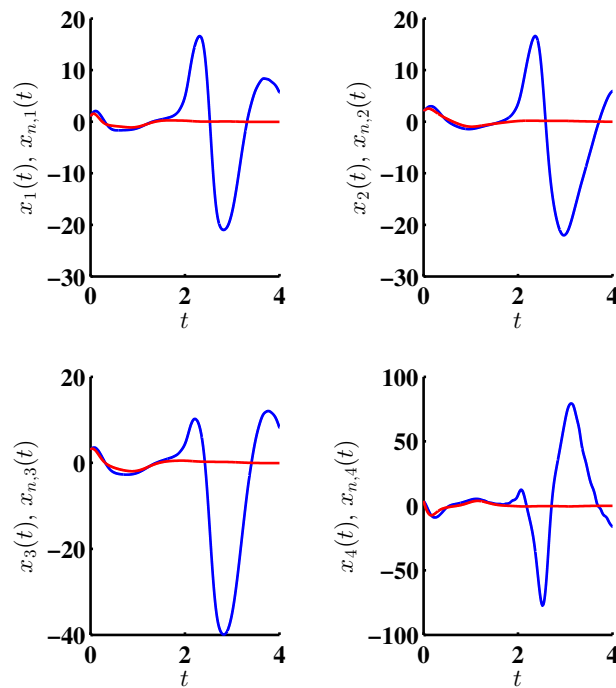


Figure 5.3. Behaviour of the Academic System subject to additive faults in the absence of a fault tolerant control scheme: Nominal Behavior (red line), Faulty System (blue line)

the equivalent control $v_{I,ap}(t)$ and a pseudo-inverse approach (see Fig. 5.2). As it can be seen the reconstructed value is the average of the original signal K . Fig. 5.5 shows the states of the system when the control allocation is done with the obtained \bar{K} value and with $\beta = 2100$. Observe that the objective of the fault tolerant control is not significantly affected and the states remains ultimately bounded, but in order to assure the sliding motion the controller gain should be increased.

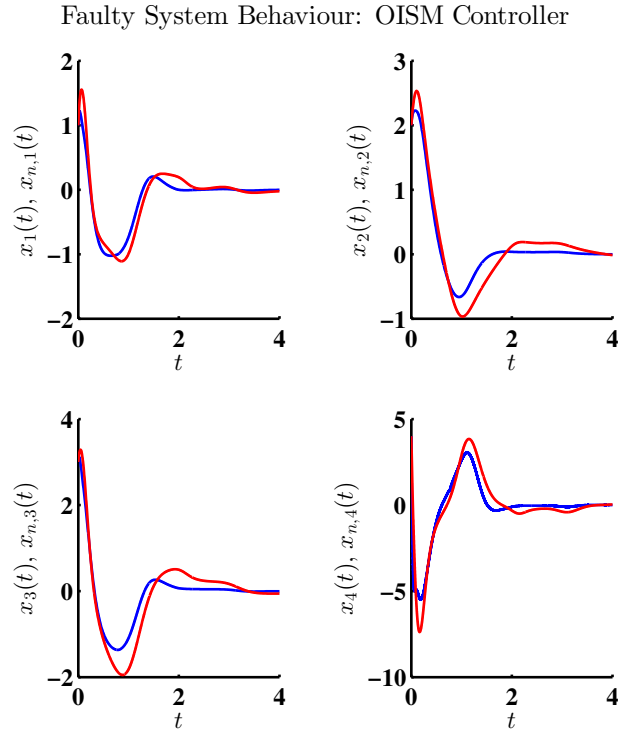


Figure 5.4. Behaviour of the Academic System subject to additive faults. OISM fault tolerant control scheme assuming the K value is completely reconstructed since the initial time: Nominal Behavior (red line), Faulty System (blue line)

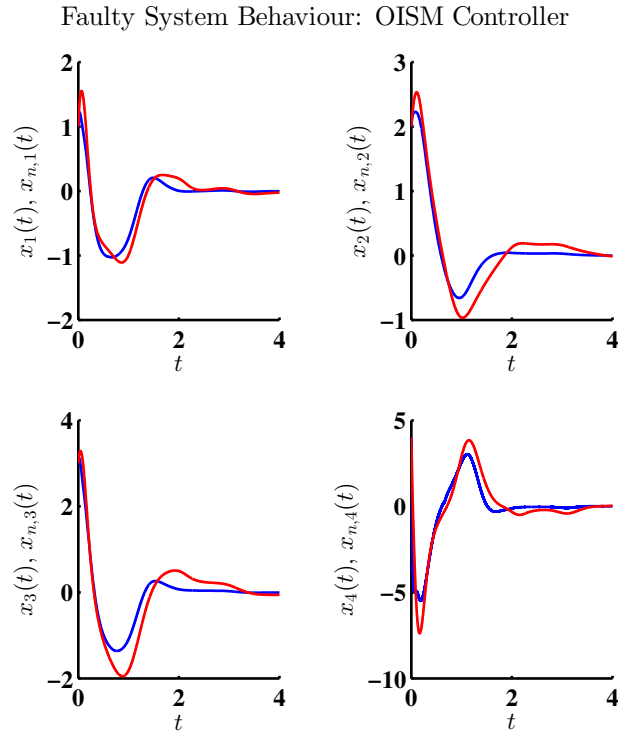


Figure 5.5. Behaviour of the Academic System subject to additive faults. OISM fault tolerant control scheme, K reconstructed with a pseudoinverse methodology: Nominal Behavior (red line), Faulty System (blue line)

5.6 FTC with on-line allocation of Wind Energy Conversion System

Wind power generating system based on a doubly fed induction generator (DFIG) has been considered as one of the most widely used industrial configurations that shown in Fig.(5.6). We here consider the WECS as a LTV system. The model of wind turbine generally has two parts. The first part is the aerodynamic model with the turbine blade, which extracts the kinetic energy from the wind. And the second part is the electrical model with DFIG, which converts the mechanical energy into electrical power.

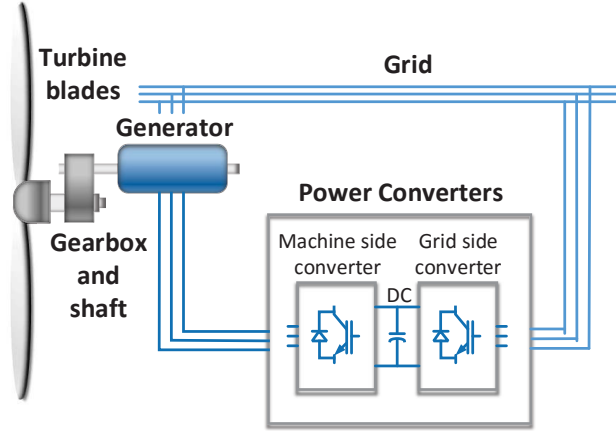


Figure 5.6. The configuration of the wind generation system

5.6.1 LPV Model of the Wind turbine system

The wind energy captured by the turbine blades is

$$\begin{aligned}
 P_a &= 0.5\rho\pi R^2 V^3 C_p(\lambda), \\
 \lambda &= \frac{\omega_t R}{V},
 \end{aligned}
 \tag{5.17}$$

where R is the length of the turbine blades, V is the speed of wind, ω_t is the turbine rotation speed, λ is the tip-speed ratio and C_p is the power coefficient that describes how much kinetic energy the turbine extracts from the wind. C_p is a function of λ , which has a unique maximum point.

Consider a drive train system which is stiff and could change the turbine torque from a large scale into a suitable working region of the generator

$$\begin{aligned}
 \omega_m &= n_g \omega_t, \\
 \omega_r &= p \omega_m,
 \end{aligned}
 \tag{5.18}$$

where n_g is the ratio of gearbox, p is the pole pair of the generator and ω_m and ω_r denote the mechanical speed and the electrical speed of the generator.

The wind turbine system adopts a DFIG generator. The advantage of DFIG is to reduce the converter costs, for the stator of DFIG connecting to the power grid directly. The

model of DFIG system is defined in the stator flux reference frame. The direct and quadrature component of the synchronous frame are represented as d and q in short.

$$\begin{aligned}
\dot{\lambda}_{sd} &= -R_s i_{sd} + \omega_s \lambda_{sq} + v_{sd}, \\
\dot{\lambda}_{sq} &= -R_s i_{sq} + \omega_s \lambda_{sd} + v_{sq}, \\
\dot{\lambda}_{rd} &= -R_r i_{rd} + (\omega_r - \omega_s) \lambda_{rq} + v_{rd}, \\
\dot{\lambda}_{rq} &= -R_r i_{rq} - (\omega_r - \omega_s) \lambda_{rd} + v_{rq}, \\
\lambda_{sd} &= L_s i_{sd} + M_{sr} i_{rd}, \\
\lambda_{sq} &= L_s i_{sq} + M_{sr} i_{rq}, \\
\lambda_{rd} &= L_r i_{rd} + M_{sr} i_{sd}, \\
\lambda_{rq} &= L_r i_{rq} + M_{sr} i_{sq};
\end{aligned} \tag{5.19}$$

where L_s, L_r, M_{sr} are the stator inductance, rotor inductance and mutual inductance, respectively. R_s and R_r are the stator resistance and rotor resistance. The motion dynamic equation of DFIG is

$$\dot{\omega}_m = p \frac{M_{sr}}{J L_s} (\lambda_{sq} i_{rd} - \lambda_{sd} i_{rq}) - \frac{T_L}{J} - \frac{F}{J} \omega_m. \tag{5.20}$$

The rest parameters are defined as follows

$$\gamma_1 = \frac{R_r L_s^2 + R_s M_{sr}^2}{\sigma L_s L_r}, \quad \gamma_2 = \frac{M_{sr}}{\sigma L_s L_r}, \quad \gamma_3 = \frac{1}{\sigma L_r}, \quad \sigma = 1 - \frac{M_{sr}^2}{L_s L_r}, \quad \tau_s = \frac{L_s}{R_r}.$$

Assume a linear parameter varying model (5.19) with

$$x(t) = \begin{bmatrix} x_1 & x_2 & x_3 & x_4 \end{bmatrix}^T = \begin{bmatrix} \lambda_{sd} & \lambda_{sq} & i_{rd} & i_{rq} \end{bmatrix}^T,$$

and consider the rotation speed $\omega_r(t)$ as the time varying parameter. For each controller, we have three same voltage actuators working together to support the inputs v_d and v_q to the system. We assume the system has an external known input $u_0 = [v_{sd}, v_{sq}]^T$ and redundancy in actuators, so the control input has the form

$$u = \begin{bmatrix} u_{d1} & u_{q1} & u_{d2} & u_{q2} & u_{d3} & u_{q3} \end{bmatrix}^T.$$

Finally, the system is represented as a LPV model

$$\dot{x} = Ax + B_0 u_0 + B_1(1 - K)u$$

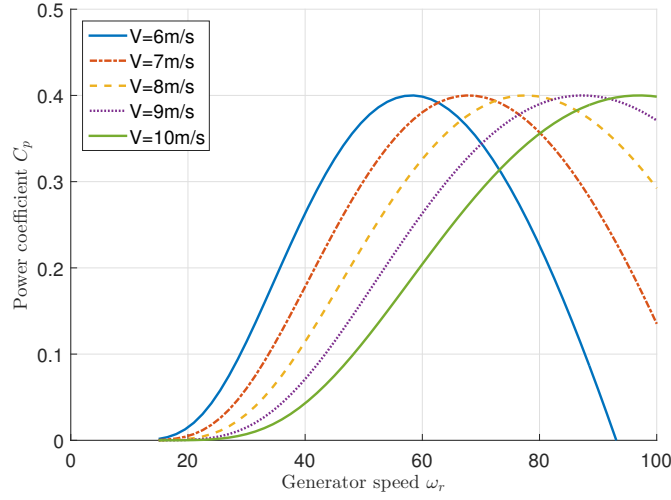


Figure 5.7. The power coefficient C_p versus generator speed ω_r under different wind speed V

and $y(t) = \begin{bmatrix} x_2 & x_3 & x_4 \end{bmatrix}^T = Cx$ as the outputs, where

$$A = \begin{bmatrix} -\frac{1}{\tau_s} & \omega_s & \frac{M_{sr}}{\tau_s} & 0 \\ -\omega_s & -\frac{1}{\tau_s} & 0 & \frac{M_{sr}}{\tau_s} \\ \frac{\gamma_2}{\tau_s} & -\gamma_2\omega_s & -\gamma_1 & \omega_s - \omega_r \\ \gamma_2\omega_r & \frac{\gamma_2}{\tau_s} & -(\omega_s - \omega_r) & -\gamma_1 \end{bmatrix}, \quad B_0 = \begin{bmatrix} 1 & 0 \\ 0 & 1 \\ -\gamma_2 & 0 \\ 0 & -\gamma_2 \end{bmatrix},$$

$$B_1 = \begin{bmatrix} 0 & 0 & 0 & 0 & 0 & 0 \\ 0 & 0 & 0 & 0 & 0 & 0 \\ \gamma_3 & 0 & \gamma_3 & 0 & \gamma_3 & 0 \\ 0 & \gamma_3 & 0 & \gamma_3 & 0 & \gamma_3 \end{bmatrix}, \quad C = \begin{bmatrix} 0 & 1 & 0 & 0 \\ 0 & 0 & 1 & 0 \\ 0 & 0 & 0 & 1 \end{bmatrix}.$$

5.6.2 Control Objective

It is impossible that the turbine obtain all the kinetic energy from the wind in reality. C_p is an uni-modal function with the variation of the generator speed ω_r and wind speed V , as Fig.(5.7) shown. As a result, the nominal controller of the wind system is designed to maximize the power generation. According to[22], the limitation of C_p is 0.4. Then $C_p(\lambda_{opt}) = 0.4$, when λ equals to its optimal value $\lambda_{opt} = 7.2$. From (5.17) and (5.18), the optimal generator speed $\omega_{r_{opt}}$ is given as

$$\omega_{ropt} = \frac{pn_g \lambda_{opt} V}{R} \quad (5.21)$$

The maximum value of C_p is available when the generator speed is tracking the reference ω_{ropt} , which is so-called maximum power point tracking (MPPT) technique [13]. The final control objective is to force the generator speed $\omega_r = \omega_{ropt}$, even in the presence of faults in the actuator.

5.6.3 Simulation Results

The simulations have been carried out using MATLAB/SIMULINK. In our work, the emulator of wind turbine uses this equation to approximate the wind speed V with $V = V_{av}(1 - 0.18\cos(2\pi t) - 0.18\cos(2\pi t/60))$, where V_{av} is the average wind speed. The simulation results are shown in Fig.5.8 to Fig.5.16 from 0sec to 2sec. We assume the system has not any fault during the first 0.05sec. To avoid the transient stage that increase the size of the controller gain, the observer starts working since initial time while the sliding mode controller does it until the 0.05sec. The results presented in the images are restricted to the period of time 0.05sec to 2sec.

The proposed nominal controller of system is composed by two cascade PI control laws based on field-oriented-control (FOC) [117]. On the d-axis, a flux control loop commands the inner direct current loop. While on the q-axis, a speed loop rules the inner quadrature current loop. The behavior of the system with the nominal controller is shown in Fig.5.8. Note that when the system works without perturbation, the generator speed tracks the optimal value.

The faults in the actuators are considered to be partial fault between [0,1] (see Fig.5.9).

Fig.5.10 shows the tracking performance of the nominal PI controller in the presence of faults. Clearly, the speed (blue solid line) could not follow the varying reference value (red dash line). And the current references have changed due to the faults.

After that, we adopt an OISM controller to compensate the faults in the actuators. Fig.5.11 shows the tracking performance of the proposed methodology under the assumption that the value of the faults is available from the initial time. Note that the speed, d-axis cur-

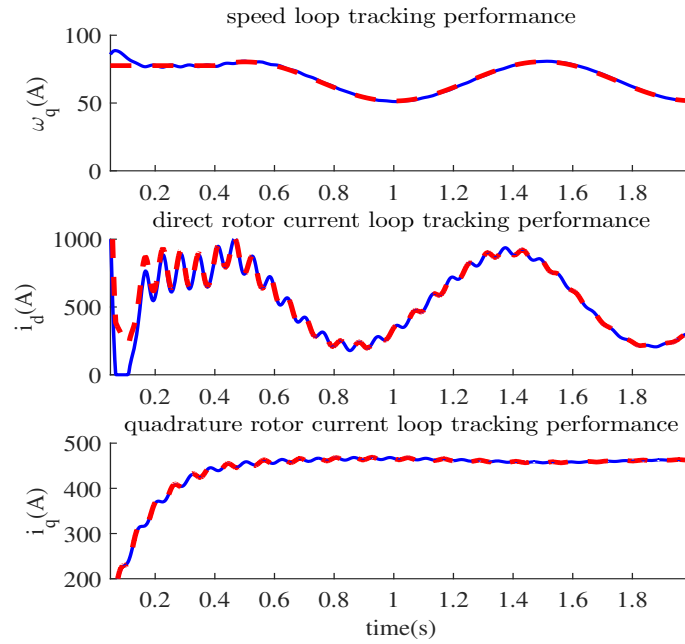


Figure 5.8. The tracking performance of nominal PI controller without perturbation. The red dash lines are the reference values, and the blue solid lines are the real signals of speed and d/q currents.

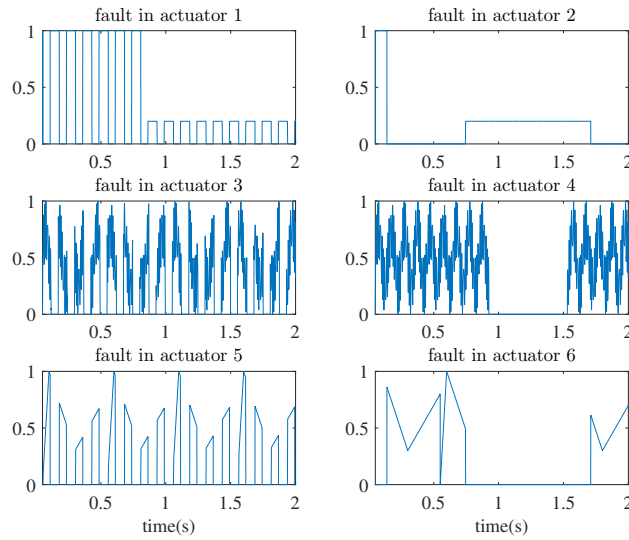


Figure 5.9. The faults in the actuators

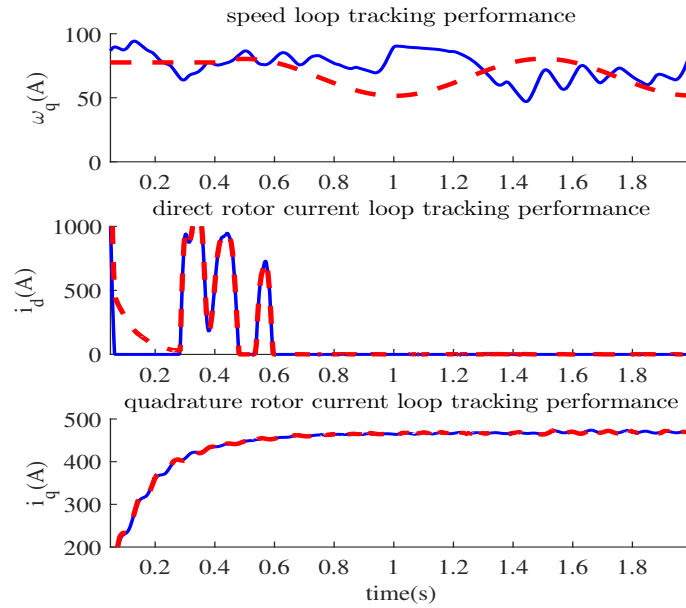


Figure 5.10. The tracking performance of nominal PI controller with perturbation. The red dash lines are the reference values, and the blue solid lines are the real signals of speed and d/q currents.

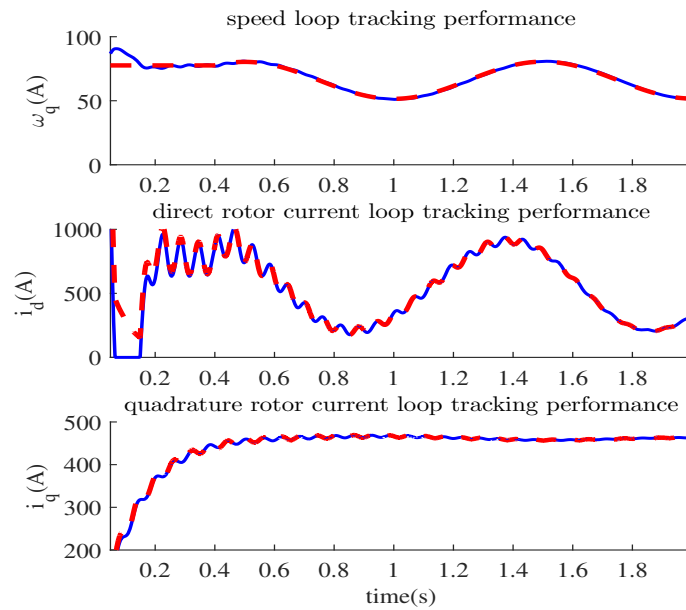


Figure 5.11. The tracking performance of proposed controller with perturbation. The red dash lines are the reference values, and the blue solid lines are the real signals of speed and d/q currents.

rent and q-axis current performances are similar to the nominal ones. The additive faults reconstruction is presented in Fig5.13.

Fig.5.12 shows the observed states and the real states of the system. The observed states converge to the real states theoretically, exactly just after initial time.

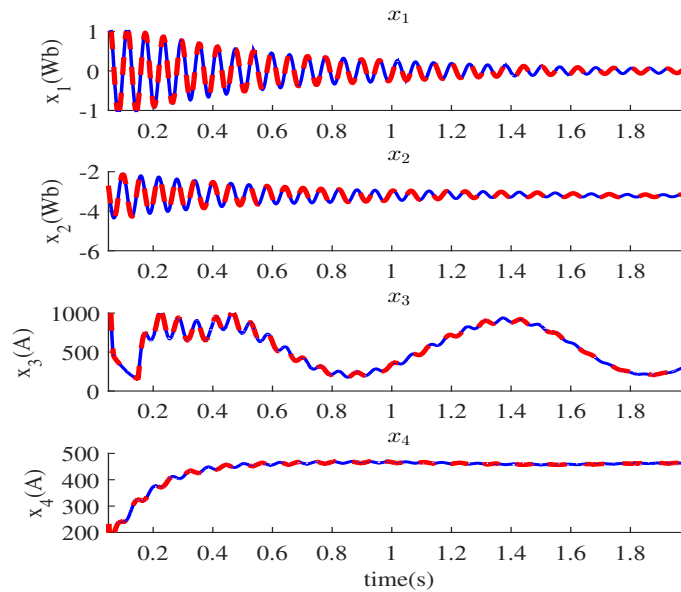


Figure 5.12. The observer performance of proposed structure. The red dash line are the real states, the blue solid line are the observed states

Then, the faults in actuators were reconstructed using a Pseudo-inverse methodology (see Fig.5.14). Under this assumption the proposed OISM controller can work in a quite good manner. The reconstruction of ϕ is shown in Fig5.15. But note that, the size of the faults is increased, making necessary to increase the gain of OISM controller. The speed loop and current loops are given in Fig.5.16 and are almost equal as the nominal ones.

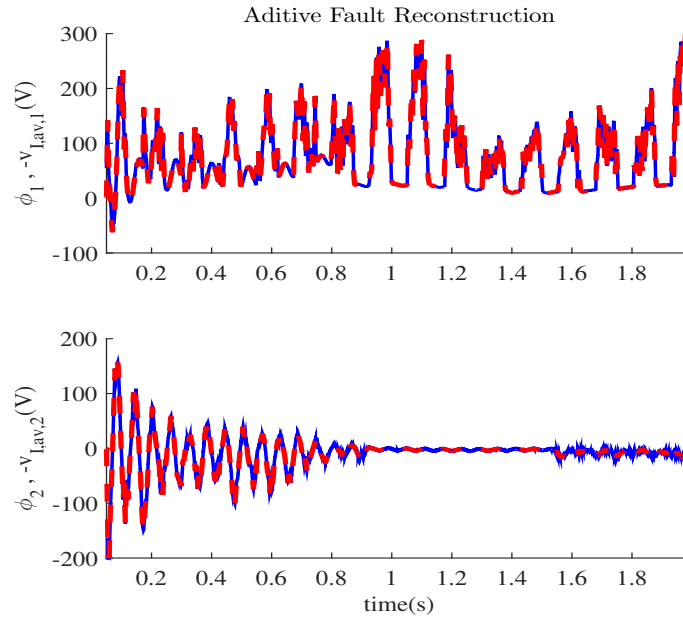


Figure 5.13. *The reconstructed perturbation ϕ_1 and ϕ_2*

5.7 Conclusion

A fault tolerant control with on-line control allocation using only output information was proposed. The designed control makes the system insensitive to partial and complete faults in the actuators theoretically exactly just after the initial time. The controller gain needs to be increased when all the available actuators have significant faults. The effects of possible errors in the reconstructed states and faults was studied, and sufficient conditions to assure stability of the system was found.

The proposed methodology was applied to a wind turbine assuring the maximum power can be achieved even when the actuators are faulty. Two sceneries were studied: when the real value of the faults is available and when the faults are reconstructed using a very simple empirical methodology that is only capable to reconstruct the average of the faults. This shows that it is possible to assure the stability of the system and the control objective when the faults are not well reconstructed but it is necessary to increase the controller gain.

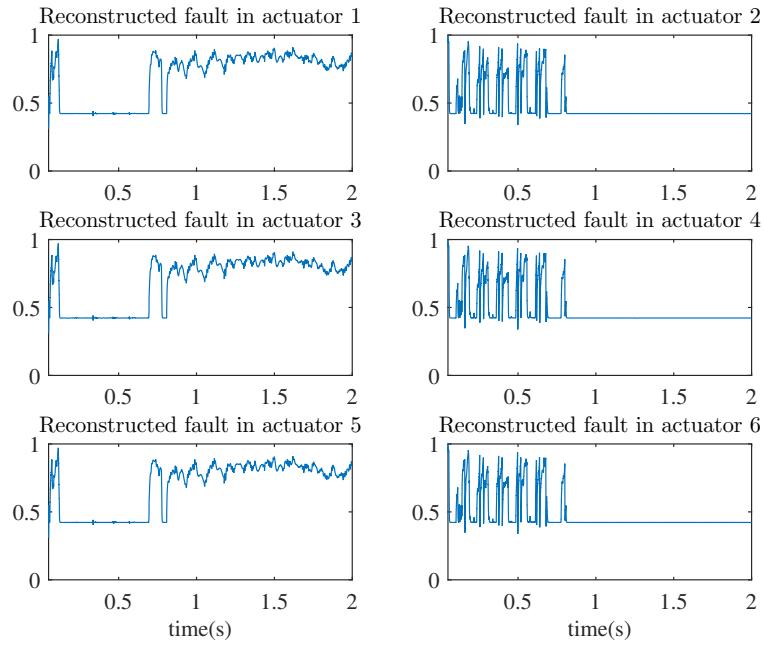


Figure 5.14. The reconstructed faults K

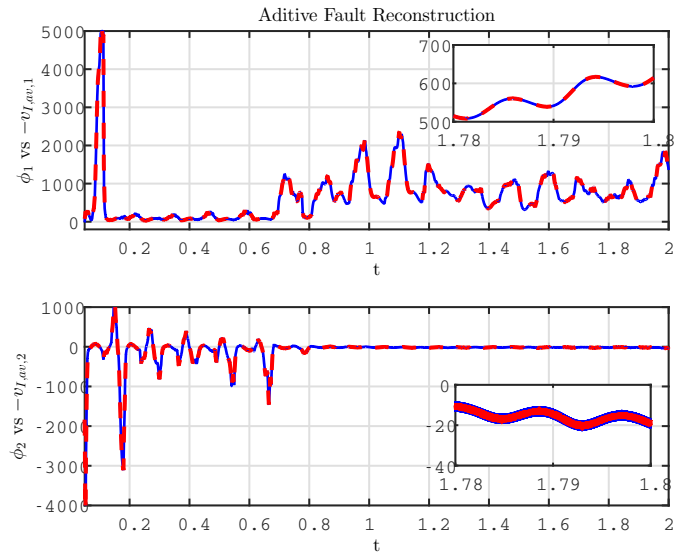


Figure 5.15. The reconstructed perturbation ϕ_1 and ϕ_2

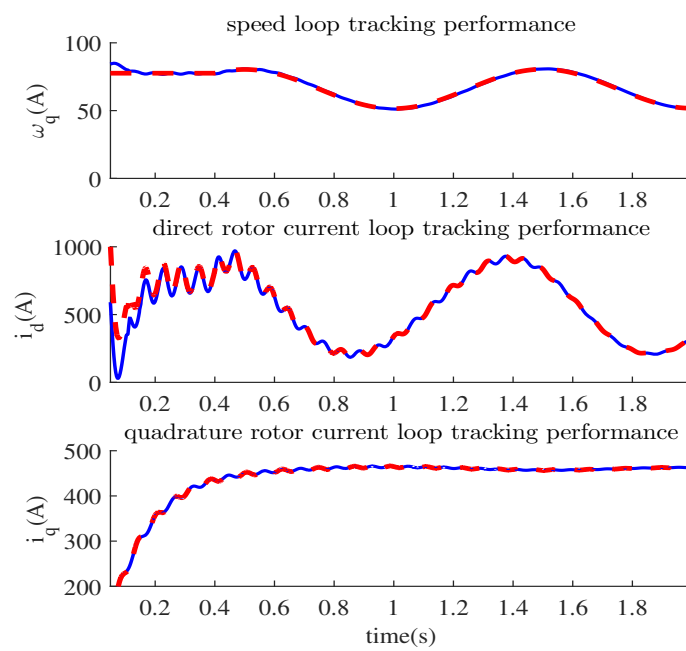


Figure 5.16. The tracking performance of proposed controller with reconstructed faults. The red dash lines are the reference values, and the blue solid lines are the real signals of speed and d/q currents.

Conclusion and Perspectives

Overview

The efficiency of wind energy conversion system (WECS) is highly dependent on the operating conditions, environmental disturbances and varying parameters, such as wind speed, pitch angle, tip-speed ratio, sensitive resistor and inductance. The uncertainties of WECS is hard to obtain exactly while it affects the stability. In the aim to assure optimal operating conditions, maximum power point tracking (MPPT), on-line control allocation, robust control and fault tolerant control are going to play an important role. The thesis work concerns the establishment of an adaptive controller solution of wind energy conversion system with a doubly fed induction generator. After a literature review, the thesis mainly includes these components:

Firstly, we discuss the adaptive sliding mode (ASM) control design for uncertain nonlinear systems. Traditional first order sliding mode design has been introduced for uncertain systems. Then the first order design strategies were extended to a class of high order systems.

The nonlinear model of the wind energy conversion system has been studied. Variable speed WECS with a double-fed induction generator (DFIG) has been controlled. The works offer a current controller for the wind power system. The control objective is to maximize the total active power supplied by the system and to regulate the reactive power injected by the voltage source converters synchronized to the power grid.

A novel Lyapunov-based adaptive first order sliding mode and a novel Lyapunov-based adaptive high order sliding mode (HOSM) controller for uncertain system have been p-

resented. A continuous control input has been designed. Stability of arbitrary order integrator chains has been proved by Lyapunov function. The main contribution of the proposed controller is to force the sliding variables and their first time derivatives to a predefined neighborhood of zero. Additionally, the sliding variables and their first time derivatives will remain in the predefined neighborhood for all consequential time after the first convergence. Our Approach has been compared to the result of Plestan et al. [1]. Simulations have been made to demonstrate the advantage of the proposed algorithm. This algorithm computes efficiently and performs quite well on chattering elimination.

Then it is devoted to the application of an output integral sliding mode (OISM) methodology for fault tolerant control (FTC) and on-line control allocation of linear time varying (LTV) systems. The considered faults are restricted to actuators faults modelled as additive ones. A study of the effects of possible errors in the reconstruction of the faults and states is presented. Finally, an application to a wind turbine model is presented.

Future Research

This thesis may be extended in the future in the following aspects:

- This study validates the observer performance on a test bench with emulated wind energy conversion system. In the future, a real experimental platform can be set up by integrating real components of the wind energy conversion system, such as wind turbine, power converters and induction motor. By performing real experiments, we can further validate the performance of the proposed observer and control strategies in practical applications.
- The objective is to further research especially in the stability, even in actuators faults, to ensure better robust control and reduce chattering phenomenon. In further research, other faults affect dynamic performance and cause low voltage ride through (LVRT), which lead to significant voltage drop will be studied in future. The extension of proposed observer design for wind energy conversion system to the application fault-tolerant control designs will be considered for future.
- The wind energy conversion system is highly nonlinear and requires efficient control. In the future work, the proposed observer will be integrated into feedback control

design, such as control of tip speed ratio. The control design will be integrated with observers in order to reduce additional physical sensors.

- Power management control strategies for the wind energy conversion system, especially for wind farm, will be considered in future. Based on the technologies of intelligent algorithm, the autonomous energy management system could be studied on basis of the previous work. For example, with the advanced advisor, one or more sensor-less wind turbines are considered in the wind farm for this coordination. As for the energy management system, converters can approach the interface with wind turbine and synchronize with the power grid in an adaptive way as the sequence plan generated by MPPT algorithm.

Appendices

A1: NOMENCLATURE

ρ_s	Angle of the grid-voltage space vector.
u_g	Grid-side inverter phase voltages.
i_g	Grid-side inverter phase currents.
L and R	Interconnection series inductance and its parasitic resistance.
P and Q	Active and reactive powers, exchanged between the inverter and the grid.
ω_r	Pulsation of the electrical grid.
u_s	Motor-side inverter phase voltages.
i_s	Motor-side inverter phase currents.
τ_e	Electromagnetic torque.
ψ_r	Rotor-flux linkage space vector.
ρ_r	Angle of the rotor-flux linkage space vector.
p_r	Number of pole pairs.
ω_m	Machine speed (in mechanical angles).
ω_t	Wind-turbine speed.
p_t	Turbine mechanical power.
c_p	Performance power coefficient of the turbine.
c_t	Performance torque coefficient of the turbine.
ρ	Air density
v	Wind tangential speed.
λ	Tip speed ratio of the rotor blade tip speed.
β	Blade pitch angle.

A2: INDUCTION MOTOR PARAMETERS

Symbol	Parameter	Value
P_{rated}	Rated power [kW]	2.2
U_{rated}	Rated voltage [V]	220
	Pole-pairs	2
R_s	Stator resistance [Ω]	2.9
L_s	Stator inductance [mH]	223
R_r	Rotor resistance [Ω]	1.52
L_r	Stator inductance [mH]	229
L_m	3-phase magnetizing inductance [mH]	217
J	Moment of inertia [$\text{kg}\cdot\text{m}^2$]	0.0048

A3: WIND TURBINE PARAMETERS

Parameter	Value
R[m]	2.5
λ_{opt}	7
C_{pmax}	0.45
n	4.86
Generator rated power [kW]	5.5
Generator rated speed [rpm]	1500

Bibliography

- [1] F. Plestan, Y. Shtessel, V. Bregeault, and A. Poznyak, “New methodologies for adaptive sliding mode control,” *International journal of control*, vol. 83, no. 9, pp. 1907–1919, 2010.
- [2] S. Mondal and C. Mahanta, “Adaptive integral higher order sliding mode controller for uncertain systems,” *Journal of Control Theory and Applications*, vol. 11, no. 1, pp. 61–68, 2013.
- [3] M. Soltani, T. Knudsen, M. Svenstrup, R. Wisniewski, P. Brath, R. Ortega, and K. Johnson, “Estimation of rotor effective wind speed: A comparison,” *Control Systems Technology, IEEE Transactions on*, vol. 21, no. 4, pp. 1155–1167, July 2013.
- [4] C. Edwards, S. K. Spurgeon, and R. J. Patton, “Sliding mode observers for fault detection and isolation,” *Automatica*, vol. 36, no. 4, pp. 541 – 553, 2000. [Online]. Available: <http://www.sciencedirect.com/science/article/pii/S0005109899001776>
- [5] C. Tan and C. Edwards, “Sliding mode observers for detection and reconstruction of sensor faults,” *Automatica*, vol. 38, no. 10, pp. 1815–1821, 2002.
- [6] —, “Sliding mode observers for robust detection and reconstruction of actuator and sensor faults,” *International Journal of Robust and Nonlinear Control*, vol. 13, no. 5, pp. 443–463, 2003.
- [7] B. Jiang, M. Staroswiecki, and V. Cocquempot, “Fault estimation in nonlinear uncertain systems using robust/sliding-mode observers,” *IEE Proceedings-Control Theory and Applications*, vol. 151, no. 1, pp. 29–37, 2004.

- [8] X. Yan and C. Edwards, "Nonlinear robust fault reconstruction and estimation using a sliding mode observer," *Automatica*, vol. 43, no. 9, pp. 1605–1614, 2007.
- [9] —, "Adaptive Sliding-Mode-Observer-Based Fault Reconstruction for Nonlinear Systems With Parametric Uncertainties," *IEEE Transactions on Industrial Electronics*, vol. 55, no. 11, pp. 4029–4036, 2008.
- [10] D. Luenberger, "Observing the state of a linear system," *IEEE Transactions on Military Electronics*, vol. 8, no. 2, pp. 74–80, 1964.
- [11] V. Utkin, *Sliding Modes in Control and Optimization*. Springer-Verlag Berlin, 1992.
- [12] W. Perruquetti and J.-P. Barbot, *Sliding Mode Control in Engineering*. CRC Press, 2002.
- [13] Q.-C. Zhong and T. Hornik, *Control of power inverters in renewable energy and smart grid integration*. John Wiley & Sons, 2012.
- [14] S. Heier, *Grid integration of wind energy conversion systems*. Wiley, 1998.
- [15] M. Karrari, W. Rosehart, and O. P. Malik, "Comprehensive control strategy for a variable speed cage machine wind generation unit," *Energy Conversion, IEEE Transactions on*, vol. 20, no. 2, pp. 415–423, June 2005.
- [16] E. Koutroulis and K. Kalaitzakis, "Design of a maximum power tracking system for wind-energy-conversion applications," *Industrial Electronics, IEEE Transactions on*, vol. 53, no. 2, pp. 486–494, April 2006.
- [17] Z. Xu, Q. Hu, and M. Ehsani, "Estimation of effective wind speed for fixed-speed wind turbines based on frequency domain data fusion," *Sustainable Energy, IEEE Transactions on*, vol. 3, no. 1, pp. 57–64, Jan 2012.
- [18] R. Isermann, "Model-based fault-detection and diagnosis — status and applications," *Annual Reviews in Control*, vol. 29, no. 1, pp. 71 – 85, 2005. [Online]. Available: <http://www.sciencedirect.com/science/article/pii/S1367578805000052>
- [19] M. Blanke and J. Schröder, *Diagnosis and fault-tolerant control*. Springer, 2006, vol. 691.

- [20] Y. Zhang and J. Jiang, "Bibliographical review on reconfigurable fault-tolerant control systems," *Annual Reviews in Control*, vol. 32, no. 2, pp. 229 – 252, 2008. [Online]. Available: <http://www.sciencedirect.com/science/article/pii/S1367578808000345>
- [21] V. I. Utkin, *Sliding modes and their application in variable structure systems*. Mir Publishers, 1978.
- [22] S. Heier, *Grid integration of wind energy*. John Wiley & Sons, 2014.
- [23] D. Dang, Y. Wang, and W. Cai, "A multi-objective optimal nonlinear control of variable speed wind turbine," in *IEEE International Conference on Control and Automation*, 2009, pp. 17–22.
- [24] M. Cirrincione, M. Pucci, and G. Vitale, *Power Converters and AC Electrical Drives with Linear Neural Networks*. CRC Press, 2012.
- [25] B. Beltran, M. El Hachemi Benbouzid, and T. Ahmed-Ali, "Second-order sliding mode control of a doubly fed induction generator driven wind turbine," *IEEE Transactions on Energy Conversion*, vol. 27, no. 2, pp. 261–269, 2012.
- [26] N. Bolouki, S. Roozbehani, and K. Abbaszadeh, "Second order sliding mode control of permanent-magnet synchronous wind generator for direct active and reactive power control," in *The 5th Power Electronics, Drive Systems and Technologies Conference (PEDSTC)*. IEEE, 2014, pp. 434–439.
- [27] J.-J. E. Slotine and J. A. Coetsee, "Adaptive sliding controller synthesis for nonlinear systems," *International Journal of Control*, vol. 43, no. 6, pp. 1631–1651, 1986.
- [28] G. Bartolini, A. Ferrara, and V. I. Utkin, "Adaptive sliding mode control in discrete-time systems," *Automatica*, vol. 31, no. 5, pp. 769–773, 1995.
- [29] Y.-J. Huang, T.-C. Kuo, and S.-H. Chang, "Adaptive sliding-mode control for nonlinear systems with uncertain parameters," *IEEE Transactions on Systems, Man, and Cybernetics, Part B: Cybernetics*, vol. 38, no. 2, pp. 534–539, 2008.
- [30] M. Harmouche, S. Laghrouche, and Y. Chitour, "Robust and adaptive higher order sliding mode controllers," in *Proceedings of the 51st IEEE Annual Conference on Decision and Control (CDC)*, 2012, pp. 6436–6441.

- [31] Y. B. Shtessel, J. A. Moreno, F. Plestan, L. M. Fridman, and A. S. Poznyak, "Super-twisting adaptive sliding mode control: A lyapunov design," in *Proceedings of the 49th IEEE Conference on Decision and Control (CDC)*, 2010, pp. 5109–5113.
- [32] L. Fridman, J. Davila, and A. Levant, "High-order sliding-mode observation for linear systems with unknown inputs," *Nonlinear Analysis: Hybrid Systems*, vol. 5, no. 2, pp. 189–205, 2011.
- [33] M. Taleb, A. Levant, and F. Plestan, "Twisting algorithm adaptation for control of electropneumatic actuators," in *The 12th International Workshop on Variable Structure Systems (VSS)*, Jan 2012, pp. 178–183.
- [34] M. Harmouche, S. Laghrouche, and Y. Chitour, "A lyapunov approach to robust and adaptive finite time stabilization of integrator chains with bounded uncertainty," *arXiv preprint arXiv:1303.5117*, 2013.
- [35] D. Y. Negrete and J. A. Moreno, "Adaptive output feedback second order sliding mode control with unknown bound of perturbation," in *IFAC World Congress*, vol. 19, no. 1, 2014, pp. 10 832–10 837.
- [36] M. Taleb, F. Plestan, and B. Bououlid, "Higher order sliding mode control based on adaptive first order sliding mode controller," in *IFAC World Congress*, 2014, pp. 1–6.
- [37] X. Chen, "Adaptive sliding mode control for discrete-time multi-input multi-output systems," *Automatica*, vol. 42, no. 3, pp. 427–435, 2006.
- [38] F. Plestan, Y. Shtessel, V. Bregeault, and A. Poznyak, "Sliding mode control with gain adaptation application to an electropneumatic actuator," *Control Engineering Practice*, vol. 21, no. 5, pp. 679–688, 2013.
- [39] S. Laghrouche, M. Harmouche, F. S. Ahmed, and Y. Chitour, "Control of pemfc air-feed system using lyapunov-based robust and adaptive higher order sliding mode control," *IEEE Transactions on Control Systems Technology*, vol. 23, no. 4, pp. 1594–1601, 2015.
- [40] A. Isidori, *Nonlinear Control Systems*. Springer, 1995.
- [41] H. K. Khalil and J. Grizzle, *Nonlinear systems*. Prentice hall New Jersey, 1996, vol. 3.

- [42] V. I. Utkin, "Sliding modes in control and optimization, communications and control engineering series," 1992.
- [43] A. Levant, "Universal Single-Input-Single-Output (SISO) Sliding-Mode Controllers with Finite-Time Convergence," *IEEE Transactions on Automatic Control*, vol. 46, no. 9, pp. 1447–1451, 2001.
- [44] G. Bartolini, A. Ferrara, E. Usai, and V. I. Utkin, "On multi-input chattering-free second-order sliding mode control," *IEEE Transactions on Automatic control*, vol. 45, no. 9, pp. 1711–1717, 2000.
- [45] S. Laghrouche, M. Smaoui, M. Harmouche, F. Plestan, and X. Brun, "Higher order sliding mode control based on optimal approach of an electropneumatic actuator," *International journal of Control*, vol. 79, no. 2, pp. 119–131, 2006.
- [46] S. Laghrouche, F. Plestan, and A. Glumineau, "Higher order sliding mode control based on integral sliding mode," *Automatica*, vol. 43, no. 3, pp. 531–537, 2007.
- [47] S. Žak and S. Hui, "On variable structure output feedback controllers for uncertain dynamic systems," *IEEE Transactions on Automatic Control*, vol. 38, no. 10, pp. 1509–1512, 1993.
- [48] C. Edwards and S. K. Spurgeon, "Sliding mode stabilization of uncertain systems using only output information," *International Journal of Control*, vol. 62, no. 5, pp. 1129–1144, 1995.
- [49] A. Levant, "Sliding order and sliding accuracy in sliding mode control," *International Journal of Control*, vol. 58, no. 6, pp. 1247–1263, 1993.
- [50] A. TORNAMBÉ, "High-gain observers for non-linear systems," *International Journal of Systems Science*, vol. 23, no. 9, pp. 1475–1489, 1992.
- [51] A. Tornambé, "Output feedback stabilization of a class of non-minimum phase non-linear systems," *Systems & Control Letters*, vol. 19, no. 3, pp. 193–204, 1992.
- [52] A. N. Atassi and H. K. Khalil, "A separation principle for the stabilization of a class of nonlinear systems," *IEEE Transactions on Automatic Control*, vol. 44, no. 9, pp. 1672–1687, 1999.

- [53] A. J. Peixoto, L. Hsu, R. R. Costa, and F. Lizarralde, "Global Tracking Sliding Mode Control for Uncertain Nonlinear Systems Based on Variable High Gain Observer," in *46th IEEE Conference on Decision and Control*. IEEE, 2007, pp. 2041–2046.
- [54] A. Prasov and H. Khalil, "A nonlinear high-gain observer for systems with measurement noise in a feedback control framework," *Automatic Control, IEEE Transactions on*, vol. 58, no. 3, pp. 569–580, 2013.
- [55] A. J. Koshkouei and A. S. I. Zinober, "Sliding mode controller-observer design for SISO linear systems," *International Journal of Systems Science*, vol. 29, no. 12, pp. 1363–1373, 1998.
- [56] H. Sira-Ramirez, G. Escobar, and R. Ortega, "On Passivity-Based Sliding Mode Control of Switched DC-to-DC Power Converters," in *Proceedings of the 35th IEEE Decision and Control*, vol. 3. IEEE, 1996, pp. 2525–2526.
- [57] A. Levant, "Higher-order sliding modes, differentiation and output-feedback control," *International journal of Control*, vol. 76, no. 9-10, pp. 924–941, 2003.
- [58] ———, "Principles of 2-sliding mode design," *Automatica*, vol. 43, no. 4, pp. 576–586, 2007.
- [59] B. Subudhi and S. S. Ge, "Sliding-Mode-Observer-Based Adaptive Slip Ratio Control for Electric and Hybrid Vehicles," 2012.
- [60] J. Na, X. Ren, and D. Zheng, "Adaptive Control for Nonlinear Pure-Feedback Systems With High-Order Sliding Mode Observer," *Neural Networks and Learning Systems, IEEE Transactions on*, vol. 24, no. 3, pp. 370–382, 2013.
- [61] A. Levant, "Robust Exact Differentiation Via Sliding Mode Technique," *Automatica*, vol. 34, no. 3, pp. 379–384, 1998.
- [62] H. Sira-Ramirez, "Dynamic second-order sliding mode control of the hovercraft vessel," *IEEE Transactions on Control Systems Technology*, vol. 10, no. 6, pp. 860–865, 2002.
- [63] G. Bartolini, A. Pisano, E. Punta, and E. Usai, "A survey of applications of second-order sliding mode control to mechanical systems," *International Journal of Control*, vol. 76, no. 9-10, pp. 875–892, 2003.

- [64] A. Pisano and E. Usai, "Output-feedback control of an underwater vehicle prototype by higher-order sliding modes," *Automatica*, vol. 40, no. 9, pp. 1525–1531, 2004.
- [65] A. Filippov, *Differential Equations with Discontinuous Righthand Sides: Control Systems*. Springer, 1988, vol. 18.
- [66] A. Sabanovic, L. Fridman, and S. K. Spurgeon, *Variable Structure Systems: From Principles to Implementation*. IET, 2004, vol. 66.
- [67] A. Isidori, *Nonlinear Control Systems*. Springer Verlag, 1995, vol. 1.
- [68] G. Bartolini, A. Ferrara, and E. Usai, "Chattering avoidance by second-order sliding mode control," *IEEE Transactions on Automatic control*, vol. 43, no. 2, pp. 241–246, 1998.
- [69] J. A. Moreno, "Lyapunov analysis of non homogeneous super-twisting algorithms," in *11th International Workshop on Variable Structure Systems (VSS)*. IEEE, 2010, pp. 534–539.
- [70] M. Zhihong, A. Paplinski, and H. Wu, "A robust mimo terminal sliding mode control scheme for rigid robotic manipulators," *IEEE Transactions on Automatic Control*, vol. 39, no. 12, pp. 2464–2469, 1994.
- [71] H. Lee and V. I. Utkin, "Chattering suppression methods in sliding mode control systems," *Annual Reviews in Control*, vol. 31, no. 2, pp. 179–188, 2007.
- [72] C. E. Hall and Y. B. Shtessel, "Sliding mode disturbance observer-based control for a reusable launch vehicle," *Journal of guidance, control, and dynamics*, vol. 29, no. 6, pp. 1315–1328, 2006.
- [73] H.-J. Wagner and J. Mathur, *Introduction to wind energy systems: basics, technology and operation*. Springer, 2009.
- [74] M. Cirrincione, M. Pucci, and G. Vitale, "Growing neural gas-based mppt of variable pitch wind generators with induction machines," *Industry Applications, IEEE Transactions on*, vol. 48, no. 3, pp. 1006–1016, May 2012.
- [75] J. M. Carrasco, L. G. Franquelo, J. T. Bialasiewicz, E. Galván, R. P. Guisado, M. A. Prats, J. I. León, and N. Moreno-Alfonso, "Power-electronic systems for the grid

- integration of renewable energy sources: A survey,” *IEEE Transactions on Industrial Electronics*, vol. 53, no. 4, pp. 1002–1016, 2006.
- [76] M. Cirrincione, M. Pucci, and G. Vitale, “Growing neural gas-based mppt of variable pitch wind generators with induction machines,” *IEEE Transactions on Industry Applications*, vol. 48, no. 3, pp. 1006–1016, 2012.
- [77] Y. Daili, J.-P. Gaubert, and L. Rahmani, “Implementation of a new maximum power point tracking control strategy for small wind energy conversion systems without mechanical sensors,” *Energy Conversion and Management*, vol. 97, pp. 298–306, 2015.
- [78] M. Pucci and M. Cirrincione, “Neural mppt control of wind generators with induction machines without speed sensors,” *IEEE Transactions on Industrial Electronics*, vol. 58, no. 1, pp. 37–47, 2011.
- [79] A. Girin, F. Plestan, X. Brun, and A. Glumineau, “High-order sliding-mode controllers of an electropneumatic actuator: Application to an aeronautic benchmark,” *IEEE Transactions on Control Systems Technology*, vol. 17, no. 3, pp. 633–645, 2009.
- [80] I. U. VADIM, “Survey paper variable structure systems with sliding modes,” *IEEE Transactions on Automatic control*, vol. 22, no. 2, 1977.
- [81] S. Emel’Yanov, S. Korovin, and L. Levantovski, “Higher-order sliding modes in binary control systems,” in *Soviet Physics Doklady*, vol. 31, 1986, p. 291.
- [82] S. Emelyanov, S. Korovin, and A. Levant, “Higher-order sliding modes in control-systems,” *Differential equations*, vol. 29, no. 11, pp. 1627–1647, 1993.
- [83] S. Laghrouche, M. Smaoui, M. Harmouche, F. Plestan, and X. Brun, “Higher order sliding mode control based on optimal approach of an electropneumatic actuator,” *International journal of Control*, vol. 79, no. 2, pp. 119–131, 2006.
- [84] S. Laghrouche, F. Plestan, and A. Glumineau, “Higher order sliding mode control based on integral sliding mode,” *Automatica*, vol. 43, no. 3, pp. 531–537, 2007.
- [85] Y.-J. Huang, T.-C. Kuo, and S.-H. Chang, “Adaptive sliding-mode control for non-linear systems with uncertain parameters,” *Systems, Man, and Cybernetics, Part B: Cybernetics, IEEE Transactions on*, vol. 38, no. 2, pp. 534–539, 2008.

- [86] V. I. Utkin and A. S. Poznyak, "Adaptive sliding mode control with application to super-twist algorithm: Equivalent control method," *Automatica*, vol. 49, no. 1, pp. 39–47, 2013.
- [87] D. Munoz and D. Sbarbaro, "An adaptive sliding-mode controller for discrete nonlinear systems," *IEEE Transactions on Industrial Electronics*, vol. 47, no. 3, pp. 574–581, 2000.
- [88] I. Salgado, S. Kamal, I. Chairez, B. Bandyopadhyay, and L. Fridman, "Super-twisting-like algorithm in discrete time nonlinear systems," in *2011 International Conference on Advanced Mechatronic Systems (ICAMechS)*. IEEE, 2011, pp. 497–502.
- [89] C. Evangelista, P. Puleston, F. Valenciaga, and A. Dávila, "Variable gains super-twisting control for wind energy conversion optimization," in *Variable Structure Systems (VSS), 2010 11th International Workshop on*. IEEE, 2010, pp. 50–55.
- [90] J. Slotine and S. S. Sastry, "Tracking control of non-linear systems using sliding surfaces, with application to robot manipulators?" *International journal of control*, vol. 38, no. 2, pp. 465–492, 1983.
- [91] F. Akel, T. Ghennam, E. Berkouk, and M. Laour, "An improved sensorless decoupled power control scheme of grid connected variable speed wind turbine generator," *Energy Conversion and Management*, vol. 78, no. 0, pp. 584 – 594, 2014.
- [92] C. Evangelista, P. Puleston, F. Valenciaga, and L. M. Fridman, "Lyapunov-designed super-twisting sliding mode control for wind energy conversion optimization," *Industrial Electronics, IEEE Transactions on*, vol. 60, no. 2, pp. 538–545, 2013.
- [93] Z. Chen, J. M. Guerrero, and F. Blaabjerg, "A review of the state of the art of power electronics for wind turbines," *Power Electronics, IEEE Transactions on*, vol. 24, no. 8, pp. 1859–1875, 2009.
- [94] J. A. Baroudi, V. Dinavahi, and A. M. Knight, "A review of power converter topologies for wind generators," *Renewable Energy*, vol. 32, no. 14, pp. 2369–2385, 2007.
- [95] W. C. Durham, "Constrained control allocation," *Journal of Guidance, Control, and Dynamics*, vol. 16, no. 4, pp. 717–725, July 1993. [Online]. Available: <http://dx.doi.org/10.2514/3.21072>

- [96] D. Enns, "Control allocation approaches," in *Guidance, Navigation, and Control Conference and Exhibit*, ser. Guidance, Navigation, and Control and Co-located Conferences. American Institute of Aeronautics and Astronautics, Aug. 1998. [Online]. Available: <http://dx.doi.org/10.2514/6.1998-4109>
- [97] J. B. Davidson, F. J. Lallman, and W. T. Bundick, "Real-time adaptive control allocation applied to a high performance aircraft," in *5th SIAM Conference on Control & its Applications*, 2001.
- [98] T. Johansen, T. Fossen, and S. Berge, "Constrained nonlinear control allocation with singularity avoidance using sequential quadratic programming," *Control Systems Technology, IEEE Transactions on*, vol. 12, no. 1, pp. 211–216, Jan 2004.
- [99] M. Corradini, G. Orlando, and G. Parlangeli, "A fault tolerant sliding mode controller for accommodating actuator failures." in *Decision and Control, 2005 and 2005 European Control Conference. CDC-ECC '05. 44th IEEE Conference on*, Dec 2005, pp. 3091–3096.
- [100] O. Härkegård and S. T. Glad, "Resolving actuator redundancy - optimal control vs. control allocation," *Automatica*, vol. 41, no. 1, pp. 137 – 144, 2005. [Online]. Available: <http://www.sciencedirect.com/science/article/pii/S0005109804002559>
- [101] H. Alwi and C. Edwards, "Fault tolerant control using sliding modes with on-line control allocation," *Automatica*, vol. 44, no. 7, pp. 1859 – 1866, 2008. [Online]. Available: <http://www.sciencedirect.com/science/article/pii/S0005109807004803>
- [102] M. Hamayun, C. Edwards, and H. Alwi, "Integral sliding mode fault tolerant control incorporating on-line control allocation," in *Variable Structure Systems (VSS), 2010 11th International Workshop on*, June 2010, pp. 100–105.
- [103] F. J. Bejarano, L. Fridman, and A. S. Poznyak, "Output integral sliding mode control based on algebraic hierarchical observer," *International Journal of Control*, vol. 80, pp. 443 – 453, 2007.
- [104] R. Galván-Guerra and L. Fridman, "Robustification of time varying linear quadratic optimal control based on output integral sliding modes," *IET Control Theory & Applications*, vol. 9, pp. 563–572(9), February 2015. [Online]. Available: <http://digital-library.theiet.org/content/journals/10.1049/iet-cta.2014.0095>

- [105] A. Zolghadri, F. Castang, and D. Henry, "Design of robust fault detection filters for multivariable feedback systems," *International Journal of Modelling and Simulation*, vol. 26, no. 1, p. 17, 2006.
- [106] B. Boussaid, C. Aubrun, and N. Abdelkrim, "Active fault tolerant approach for wind turbines," in *Communications, Computing and Control Applications (CCCA), 2011 International Conference on*, March 2011, pp. 1–6.
- [107] J. Y. Kim and D. G. Lee, "Fault tolerant control of wind turbine with sensor and actuator faults," *Journal of Sensor Science and Technology*, vol. 22, no. 1, pp. 28–37, 2013. [Online]. Available: <http://dx.doi.org/10.5369/JSST.2013.22.1.28>
- [108] P. Odgaard and K. Johnson, "Wind turbine fault detection and fault tolerant control - an enhanced benchmark challenge," in *American Control Conference (ACC), 2013*, June 2013, pp. 4447–4452.
- [109] P. Odgaard, J. Stoustrup, and M. Kinnaert, "Fault-tolerant control of wind turbines: A benchmark model," *Control Systems Technology, IEEE Transactions on*, vol. 21, no. 4, pp. 1168–1182, July 2013.
- [110] P. Flannery and G. Venkataramanan, "A fault tolerant doubly fed induction generator wind turbine using a parallel grid side rectifier and series grid side converter," *Power Electronics, IEEE Transactions on*, vol. 23, no. 3, pp. 1126–1135, May 2008.
- [111] J. Kim, I. Yang, and D. Lee, "Control allocation based compensation for faulty blade actuator of wind turbine," in *8th IFAC Symposium on Fault Detection, Supervision and Safety of Technical Processes*, vol. 8, no. 1, 2012, pp. 355–360.
- [112] D. Rotondo, V. Puig, J. Acevedo Valle, and F. Nejjari, "Ftc of lpv systems using a bank of virtual sensors: application to wind turbines," in *Control and Fault-Tolerant Systems (SysTol), 2013 Conference on*, Oct 2013, pp. 492–497.
- [113] P. Odgaard and J. Stoustrup, "An evaluation of fault tolerant wind turbine control schemes applied to a benchmark model," in *Control Applications (CCA), 2014 IEEE Conference on*, Oct 2014, pp. 1366–1371.
- [114] S. Banerjee and A. Roy, *Linear Algebra and Matrix Analysis for Statistics*, ser. Chapman & Hall/CRC Texts in Statistical Science. CRC Press, 2015. [Online]. Available: <https://books.google.fr/books?id=WDTcBQAAQBAJ>

- [115] V. I. Utkin, *Sliding Modes in Control and Optimization*. Springer-Verlag, 1992.
- [116] H. K. Khalil, *Nonlinear Systems*, 3rd ed. Upper Saddle River, New Jersey 07458: Prentice Hall, 2002.
- [117] M. Pucci and M. Cirrincione, "Neural mppt control of wind generators with induction machines without speed sensors," *Industrial Electronics, IEEE Transactions on*, vol. 58, no. 1, pp. 37–47, Jan 2011.

Résumé :

Les principaux défis pour le déploiement de systèmes de conversion de l'énergie éolienne est de maximiser la puissance électrique produite, malgré les variations des conditions météorologiques, tout en minimisant les coûts de fabrication et de maintenance du système. L'efficacité de la turbine éolienne est fortement dépendante des perturbations de l'environnement et des paramètres variables du système, tels que la vitesse du vent et l'angle de tangage. Les incertitudes sur le système sont difficiles à modéliser avec précision alors qu'ils affectent sa stabilité. Afin d'assurer un état de fonctionnement optimal, malgré les perturbations, le commande adaptative peut jouer un rôle déterminant. D'autre part, la synthèse de commandes tolérantes aux défauts, capables de maintenir les éoliennes connectées au réseau après la survenance de certains défauts est indispensable pour le bon fonctionnement du réseau. Le travail de cette thèse porte sur la mise en place de lois de commande adaptatives et tolérantes aux défauts appliqués aux systèmes de conversion de l'énergie éolienne. Après un état de l'art, les contributions de la thèse sont:

Dans la première partie de la thèse, un modèle incertain non linéaire du système de conversion d'énergie éolienne avec un générateur à induction à double alimentation est proposé. Une nouvelles approches de commande adaptative par mode glissant est synthétisée et ensuite appliquée pour optimiser l'énergie issue de l'éolienne.

Dans la deuxième partie, une nouvelle commande par modes glissants tolérante aux défauts et basée sur les modes glissants intégrales est présentée. Puis, cette méthode est appliquée afin de forcer la vitesse de la turbine éolienne à sa valeur optimale en prenant en compte des défauts qui surviennent sur l'actionneur.

Mots clés: Commande adaptative par mode glissant, commande tolérantes au défauts, système de conversion de l'énergie éolienne, robustesse, optimisation de puissance.

Abstract:

The main challenges for the deployment of wind energy conversion systems (WECS) are to maximize the amount of good quality electrical power extracted from wind energy over a significantly wide range of weather conditions and minimize both manufacturing and maintenance costs. Wind turbine's efficiency is highly dependent on environmental disturbances and varying parameters for operating conditions, such as wind speed, pitch angle, tip-speed ratio, sensitive resistor and inductance. Uncertainties on the system are hard to model exactly while it affects the stability of the system. In order to ensure an optimal operating condition, with unknown perturbations, adaptive control can play an important role. On the other hand, a Fault Tolerant Control (FTC) with control allocation that is able to maintain the WECS connected after the occurrence of certain faults can avoid major economic losses. The thesis work concerns the establishment of an adaptive control and fault diagnosis and tolerant control of WECS. After a literature review, the contributions of the thesis are:

In the first part of the thesis, a nonlinear uncertain model of the wind energy conversion system with a doubly fed induction generator (DFIG) is proposed. A novel Lyapunov-based adaptive Sliding Mode (HOSM) controller is designed to optimize the generated power.

In the second part, a new output integral sliding mode methodology for fault tolerant control with control allocation of linear time varying systems is presented. Then, this methodology has been applied in order to force the wind turbine speed to its optimal value the presence of faults in the actuator.

Keywords: Adaptive Sliding Mode Control, Wind Energy Conversion System, Double-Fed Induction Generator, Maximum Power Point Tracking, Lyapunov Analysis, On-line Control Allocation, Fault Tolerant Control, Fault Diagnosis

The logo for SPIM (École doctorale SPIM) features a stylized white 'S' on a blue background, followed by the letters 'PIM' in a large, white, sans-serif font.

■ École doctorale SPIM - Université de Technologie Belfort-Montbéliard

F - 90010 Belfort Cedex ■ tél. +33 (0)3 84 58 31 39

■ ed-spim@univ-fcomte.fr ■ www.ed-spim.univ-fcomte.fr

